5-2018

Coupling of Vortex Flows with Control Jets for Enhanced Mixing and Flame Holding in Supersonic Flows

Thomas Paul Fetterhoff
University of Tennessee, tfetterh@vols.utk.edu

To the Graduate Council:

I am submitting herewith a dissertation written by Thomas Paul Fetterhoff entitled "Coupling of Vortex Flows with Control Jets for Enhanced Mixing and Flame Holding in Supersonic Flows." I have examined the final electronic copy of this dissertation for form and content and recommend that it be accepted in partial fulfillment of the requirements for the degree of Doctor of Philosophy, with a major in Aerospace Engineering.

Ahmad D. Vakili, Major Professor

We have read this dissertation and recommend its acceptance:

Reza Abedi, Trevor M. Moeller, Andrew Yu

Accepted for the Council:
Dixie L. Thompson

Vice Provost and Dean of the Graduate School

(Original signatures are on file with official student records.)

Coupling of Vortex Flows with Control Jets for Enhanced Mixing and Flame Holding in Supersonic Flows

A Dissertation Presented for the
Doctor of Philosophy
Degree
The University of Tennessee, Knoxville

Thomas Paul Fetterhoff
May 2018

Acknowledgements

I would like to thank my advisor, Dr. Vakili, for his guidance and patience throughout this endeavor. In addition, I would like to thank the members of my committee; Dr. Moeller, Dr. Abedi, and Dr. Yu for their advice during this research. I especially appreciate the efforts by Dr. Meganathan and Mahdi Boudaghi for their computational work in support of this effort. A special thanks to my friends and family who have patiently tolerated my inattentiveness during this undertaking.

Abstract

This study presents results of innovative integration of passive and active flow physics to accomplish effective supersonic mixing. The study is continuing cavity flow control research in the supersonic wind tunnel at the University of Tennessee Space Institute (UTSI). Initially numerical simulations were employed in support of choosing and refining the experimental configuration designs. Mixing enhancement was achieved through innovative coupling of aerodynamics of corner vortex flows and cavity flow control jets. The two geometries were chosen for their potential to generate strong streamwise vortices, weaker shock losses, low drag, and cavity recirculation zones. Another consideration was that the two physically different concepts would be studied to provide better understanding of the innovative mixing. Jets, simulating fuel injection, were used for flow control provided through penetrations in the front face and side walls of the cavity. Flow visualization, dynamic pressure (sound pressure level) data are measured and PIV measurements are presented and compared with computational predictions for several geometries. High frequency dynamic pressure data were recorded to determine the cavity flow acoustic patterns. Measurements were acquired by a digital data acquisition system from two dynamic pressure transducers, located at different locations on the floor of the cavity. PIV measurements of selected configurations were performed. Schlieren and PIV images, pressure spectra and 2-D PIV data obtained are used as a basis for understanding the flow processes involved and comparison for improving the overall mixing and penetration performance. Streamwise vortices were

generated using two different innovatively designed geometries, strategically located upstream of selected cavity configurations, including various jet arrangements, simulating fuel flow and control. Both configurations tested developed relatively strong streamwise vortex flows and weakened or lofted shear layers, indicating that mixing was enhanced. The two configurations exhibited flow changes with the simulated fuel injection. However, different injection arrangements by the simulated fuel jets resulted in different details in the flow fields and their resulting acoustic spectra. The resulting flow fields show improved potential for fuel flow mixing and increased penetration while amplifying or attenuating flow unsteadiness in the cavity.

Table of Contents

List of Tables

List of Figures

Chapter 1: Introduction

Background

The study of cavity flows is important in various industrial systems as a result of many aerodynamics engineering configurations and applications. The automotive and aerospace industries have a particular need to study these types of flows. In the automotive industry optimizing the flow over wheel wells, open windows of passenger cabins and tractor and trailer combinations is crucial to noise free, low-drag and efficient systems. For example, the sound levels produced by pressure oscillations (buffeting effects) caused by an open window in a moving vehicle can result in occupant fatigue and potential deafening. In the aircraft industry the flow over bomb bays, landing gear bays, and other doors and cavities is important to the aircraft's ability to perform its mission. Flow over weapons bays can drastically affect weapon separation, vehicle performance, and the structural life of aircraft components. A common problem in the flow over cavities is acoustic resonance generating large amplitude pressure fluctuations within the cavity. A number of researchers have studied various cavities [Heller & Bliss 1975, Vakili & Gauthier 1994, Fowler 2010, Milne 2012, Thiemann 2013, Plentovich et. al 1993, Rockwell and Naudascher 1978, Karamcheti 1955, Roshko 1955 and Rossiter 1966] and found that at resonance the cavity flow can have substantial effect on a system's health. Various studies have also been performed to develop attenuating the cavity flow oscillations, as discussed later. This study seeks to advance the state of the art by innovatively applying cavity flow control techniques to improve fuel flow mixing

and penetration in supersonic flows, while controlling acoustic unsteadiness in such cavity configurations.

Previously Investigated Suppression Techniques

In general, past supersonic studies at the University of Tennessee have been to understand these flows and develop active damping techniques which can be exploited over a broad operational envelope. Studies at UTSI have focused on flow controls which modify boundary layer and the shear layer flows over the cavity.

Vakili and Gauthier [Vakili & Gauthier 1994] applied steady distributed mass injection through porous plates upstream of the cavity and obtained near complete suppression of the cavity oscillations. A schematic of this concept, depicting upstream mass injection, is provided as Figure 1. Implementation of such a technique has not been readily suited for broad application most likely due to the added complexity and weight. Continued research has been motivated by the desire to develop better understandings and flow control techniques with comparable results, but with much simpler implementation.

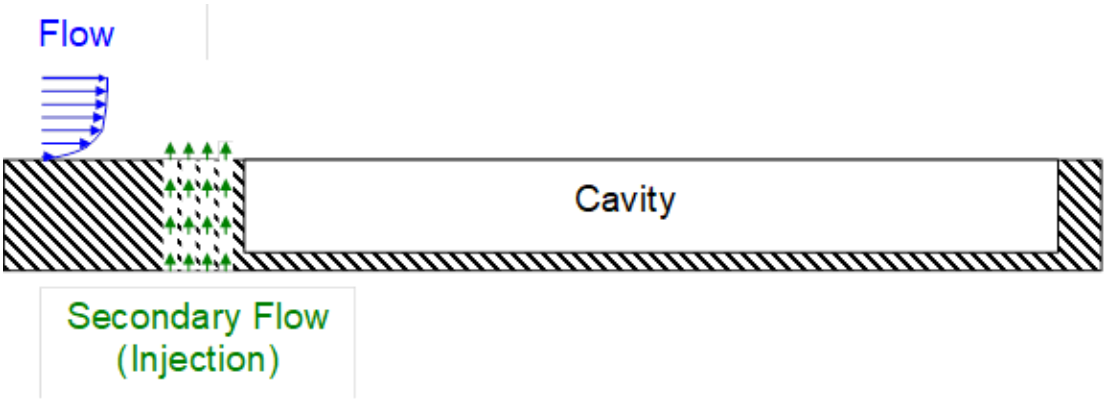

Figure 1. Upstream Mass Injection Schematic (Active Cavity Flow Control Technique) [Fowler 2010].

Passive suppression techniques offer less complexity. Early investigations include the use of upstream fences to attenuate the flow instabilities by modifying the shear layer. Figure 2 is a depiction of such a fence placed upstream of a cavity. Givogue et.. al [Givogue et. al 2011] investigated the use of two dimensional Cylinders to alter the resonant tones and shear layer. Figure 3 depicts the placement of a rod in the flow at the leading edge of the cavity. The shedding vortices interact with the cavity shear layer, altering the acoustic tones within the cavity. Figure 4 is a representation of an airfoil similarly placed within the flow field. In this study the horizontal rod provided the best performance. The airfoil produced separated flows and provided the best results at the highest negative angle of attack.

Milne [Milne 2010] and later Thiemann [Thiemann 2013] replaced distributed jets and two-dimensional cylinders with cylindrical rods placed vertically in the flow upstream of the cavity as shown in Figure 5. The height of rods could be adaptively

controlled to make the resulting flow control process adaptive. Furthermore, rods could transport fluids internally for expanded flow control and functionality, beyond cavity flow control.

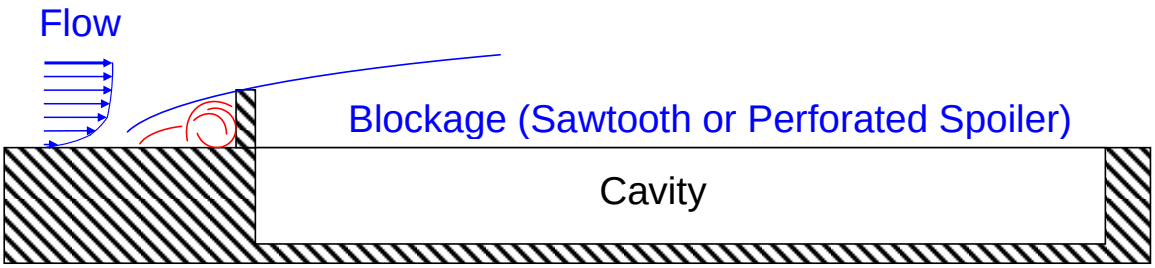

Figure 2. Blockage with Sawtooth or Perforated Spoiler Schematic (Passive Cavity Flow Control Technique) [Fowler 2010].

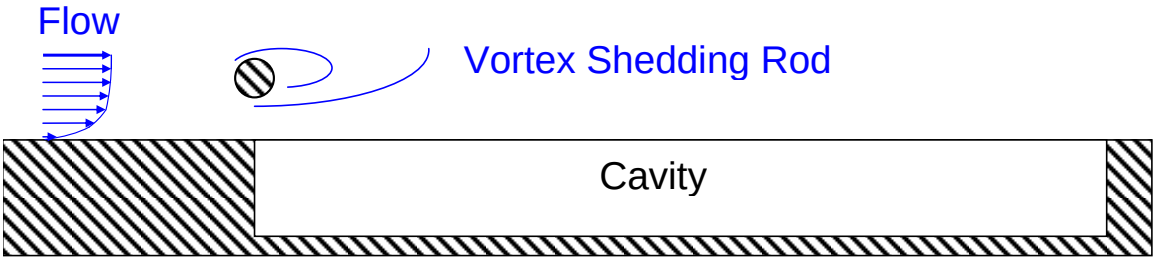

Figure 3. Rod in Crossflow Schematic (Passive Cavity Flow Control Technique) [Fowler 2010].

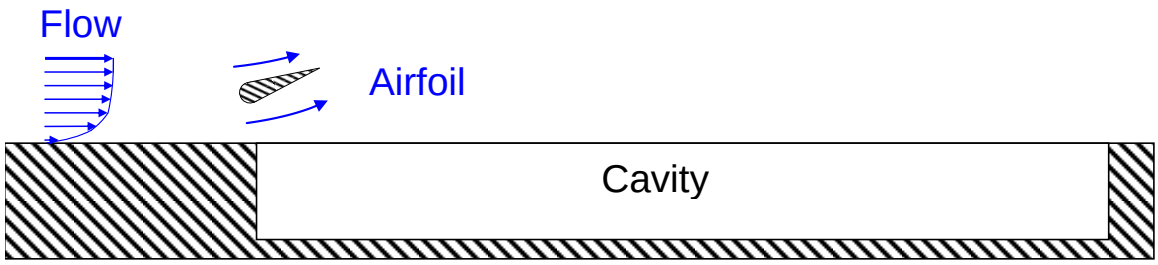

Figure 4. Airfoil in Crossflow Schematic (Passive Cavity Flow Control Technique) [Fowler 2010].

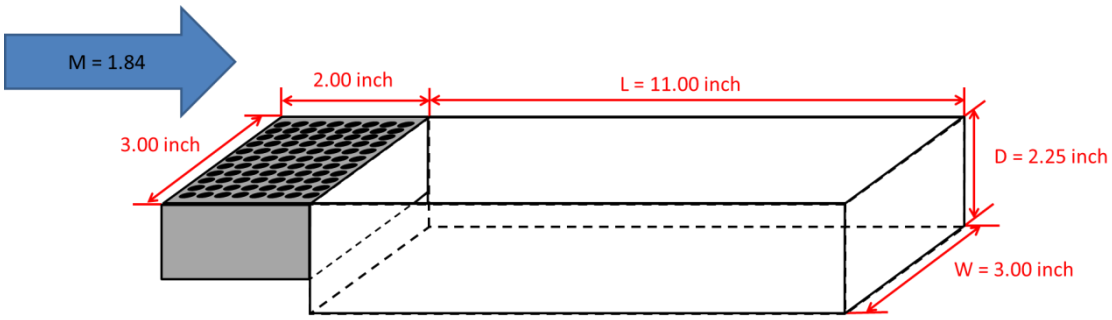

Figure 5. Upstream distributed jets and verticle rods flow control [Milne 2012].

Dissertation Scope

This research study performed in this dissertation seeks to extend the state of the art in cavity flow control and apply it to Supersonic Combustion Ramjet (SCRAMJET) combustor fuel injection and flame holding. SCRAMJETs are characterized by having supersonic flow inside the combustors. In supersonic flow, mixing for combustion is limited by slow shear layer growth. To accomplish combustion in practical streamwise distances in SCRAMJETs, innovative fuel injection, mixing and flame holding techniques are the focus of numerous research and development studies. This

dissertation seeks to advance the state of the art by innovatively applying active and passive flow control techniques to improve fuel flow mixing and penetration while controlling acoustic unsteadiness in the cavity, using low loss configurations. Leading edge shapes are investigated for the creation of corner flows and vortex creation. Cavity shaping and blowing are utilized to minimize cavity oscillations and improve fuel mixing and distribution. Complimentary numerical studies were performed as well as validation experiments in the UTSI supersonic wind tunnel, (M = 1.85), to help improve the geometry and flow path for better overall results. The author has conducted an exhaustive literature search for more contemporary literature, with limited success. This is believed to be an indicator that the subject of this study is highly current and relevant to supersonic mixing applications. It may also be that some of the relevant research results are either proprietary or are just not disseminated due to sensitivity of this topic. The author also believes and anticipates that results of this work would establish a fundamental milestone in supersonic mixing enhancements.

Chapter 2: Literature Review

Cavity Classifications

There have been traditionally three methods for classifying cavity types. The first is by geometry. Figure 6 outlines the layout of a simple cavity in a crossflow. Here, deep cavities are cavities that are deeper than they are long. Shallow cavities have their longest dimension as length.

The second method of classification is based upon where the shear layer reattaches [Plentovich et. al 1993]. In an open Cavity, shown in Figure 7, the shear layer separates at the leading edge and attaches again at the rear of the cavity. Closed cavities, Figure 8, are sufficiently shallow that the shear layer attaches to the bottom of the cavity floor before separating and exiting the cavity. Transitional cavities, Figure 9, lie in between these two and can be either open or closed.

The third method is based upon the type of oscillations that are maintained in the cavity. Rockwell and Naudascher [Rockwell & Naudascher 1978] classify these cavities as Fluid Dynamic, Fluid Resonant, and Fluid Elastic, see Figure 10. Fluid Dynamic oscillation are typical of flow that is unstable. Fluid Resonant cavity flows have strong resonant oscillations within the cavity. Fluid Elastic flows result from the coupling of the oscillations with a moving boundary within the cavity.

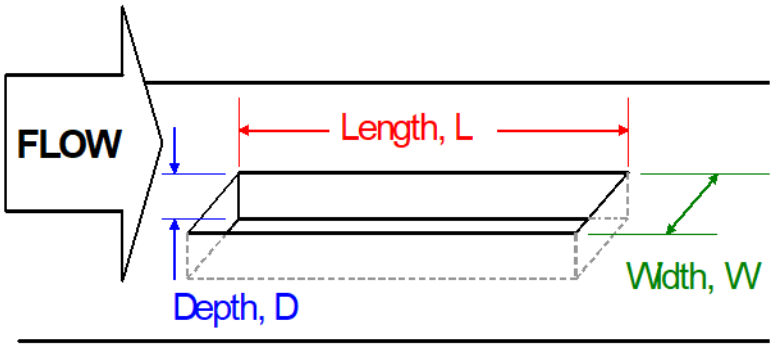

Figure 6. A Typical Rectangular Cavity with a Freestream Crossflow [Fowler 2010].

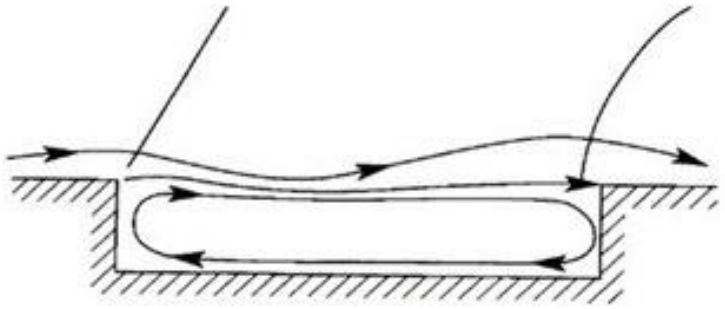

Figure 7. Open Cavity Flow, *L*/*D*<10. [Pentovich et. Al 1993].

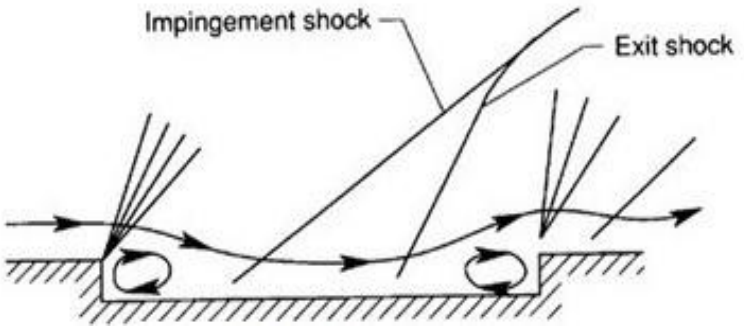

Figure 8. Closed Cavity Flow, *L*/*D*>13. [Pentovich et. Al 1993].

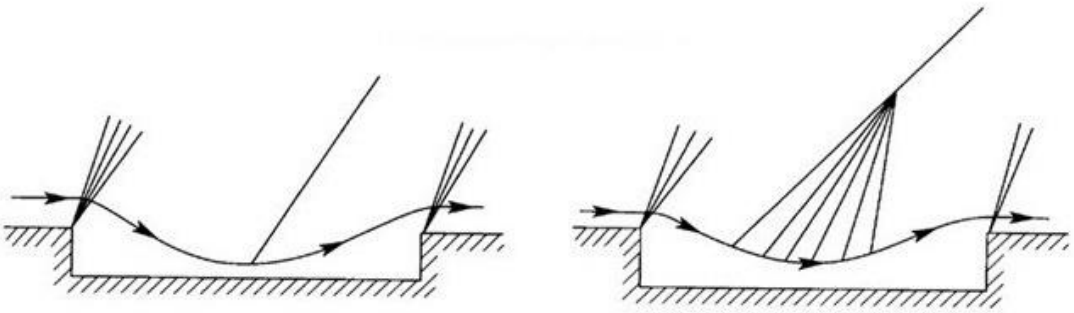

Figure 9. Transitional Cavity Flow, 10<*L*/*D*<13. [Pentovich et. Al 1993].

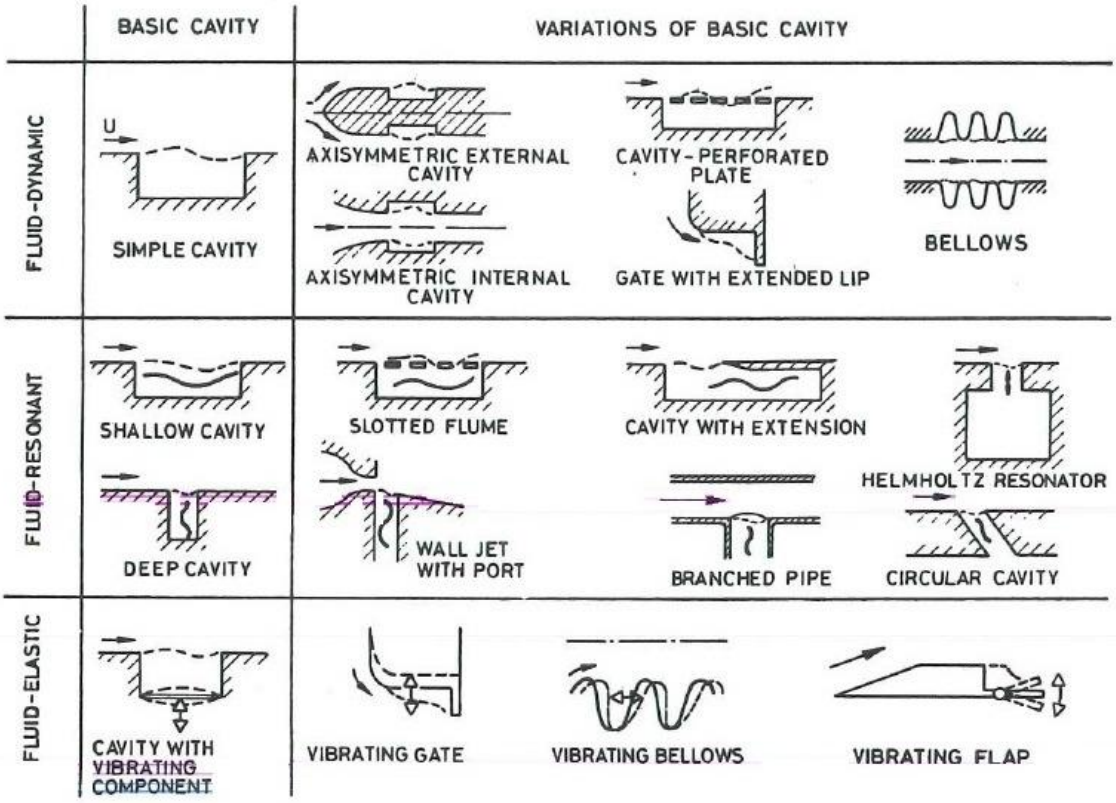

Figure 10. Categories of Fluid Cavities. [Rockwell & Naudascher 1978].

Cavity Oscillations

Cavity oscillations are pressure, density, and velocity fluctuations that occur as flow travels over the open side of a cavity. These flow oscillations occur as the free shear layer develops unsteady interactions with the rear wall of the cavity which may develop resonance with the cavity acoustics.

In the 1950's Karamcheti [Karamcheti 1955] studied flow over a wide variety of shallow cavities at Mach numbers up to 1.5. Karamcheti observed that flows with laminar upstream boundary layers emitted more intense sound levels than those with turbulent boundary layers. He also noted that when the length of the cavity was small enough that the shear layer transverses the cavity there was no sound emission from the cavity flow.

Roshko [Roshko 1955], while studying drag effects of various length to depth ratio cavities, noted the formation of vortices forming from the separated boundary layer impinging on the trailing edge causing a high-pressure zone.

Rossiter [Rossiter 1966] developed an empirical model for calculating the periodic cavity frequency (f).

$$(1) \qquad f = \frac{U_\infty\,(m-n)}{L(\frac{1}{K_v}+M)}$$

Where L is the cavity length, U_∞ is the freestream velocity, M is the freestream Mach number, K_v is the ratio of convective velocity of vortices to freestream velocity, n is

the phase delay between acoustic wave and new vortex, and *m* is the mode number for the cavity oscillations.

Rossiter's equation was suitable for Mach numbers up to 1.5. Above Mach 1.5 there was an increasing error in the prediction. This error was due to the assumption that the cavity speed of sound was the same as the freestream speed of sound. Heller, Holmes and Covert [Heller et. al 1971] modified Rossiter's Equation (1) to improve its accuracy above Mach 1.5 by assuming that the cavity speed of sound was the freestream recovery speed of sound. They introduced the non-dimensional cavity frequency, Strouhal number (*St)* [Heller et. al 1971],

$$(2) \qquad St = \frac{fL}{U_\infty} = \frac{(m-n)}{\left\{ \frac{M}{\left[1+\frac{\gamma-1}{2}M^2\right]^{\frac{1}{2}}} + \frac{1}{K_v} \right\}}$$

where γ is the ratio of specific heats. This equation shows good agreement up to Mach number 3.2.

Bilanin and Covert [Bilanin & Covert 1993] modeled supersonic flow over a cavity using a vortex sheet and a noise source. Their model related the inflow and outflow at the rear of the cavity to fluctuations of the free shear layer that was approximated by a vortex sheet. The interaction of the vortex sheet, the cavity trailing edge, the resulting inflow and outflow from the cavity excited the shear layer at the

leading edge. They modeled these interactions by a noise source at the trailing edge of the cavity. These fluctuations are the source of the acoustic radiation.

Heller and Bliss [Heller & Bliss 1975] observed, in a water tunnel, a six-step oscillation process resulting in inflow and outflow at the trailing edge caused by unsteady oscillations of the shear layer. Figure 11 outlines the progression of these unsteady oscillations.

From [Heller & Bliss 1975]

A. *"The pressure wave from the previous trailing-edge disturbance reaches the front of the cavity and reflects. Another such wave, already reflected of the front wall, approaches the rear of the cavity. The shear layer is above the trailing edge, so the external flow cannot interact with the trailing edge to produce disturbances. Some fluid leaves the cavity."*

B. *"The shear layer waveform travels rearward, reducing the height of the shear layer above the trailing edge. A new compression wave begins to flow from the rear as the flow interacts with the trailing edge and fluid is added to the cavity. The front compression wave has reflected off the front wall and moves rearward nearly in phase with the shear layer displacement. The previous rearward wave has reached the training edge."*

C. *"The wave reflected off the front wall continues to move rearward in phase with the shear layer displacement. The shear layer, which is now below the trailing edge*

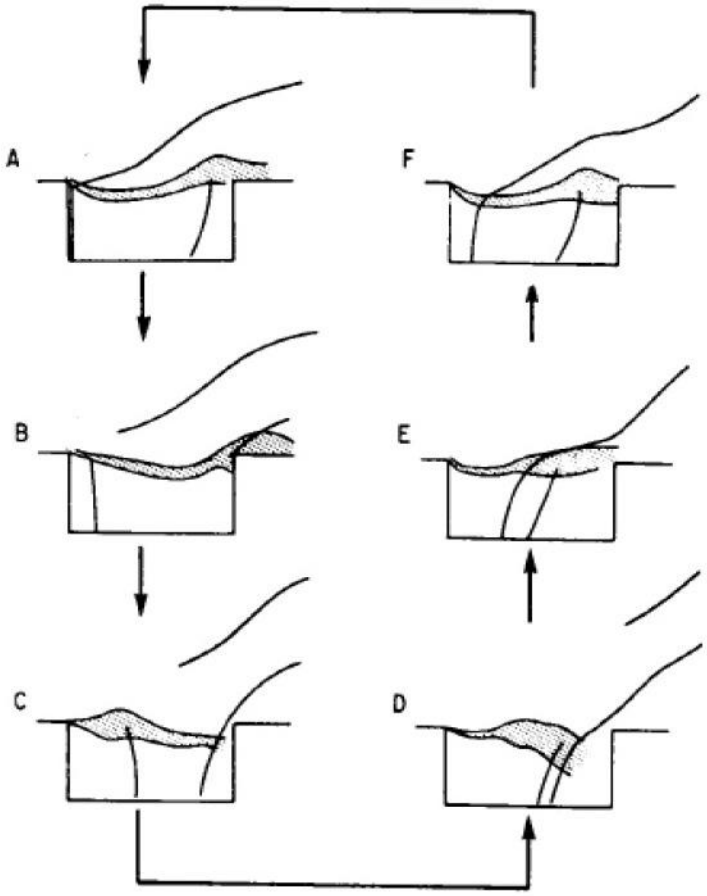

Figure 11. Cavity Pseudo-Piston Oscillation Cycle. [Heller & Bliss 1975].

at the rear of the cavity, forms a new forward traveling compression wave as the external flow impinges on the back of the cavity."

D. *"the newly generated forward traveling compression wave and the reflected, rearward traveling compression wave meet and interact near the cavity center."*

E. *"After the interaction, the waves continue in their receptive directions. The external part of the forward traveling wave moves into the supersonic flow, thus causing it to be tipped more than the external flow Mach angle. The rearward wave moves in the same direction as the external flow and travels at subsonic speed relative to it. This subsonic relative speed explains why the rearward traveling wave stops at the shear layer. At the rear, the shear layer reaches the trailing-edge height."*

F. *"The shear layer is now above the trailing edge height. The wave generated at the trailing edge approaches the front of the cavity, and the reflected wave nears the rear of the cavity. The next step is the same as A, and the oscillation cycle repeats."*

The inflow and outflow at the trailing edge can be modeled by a replacing the rear wall of the cavity with a pseudo piston as depicted in Figure 12.

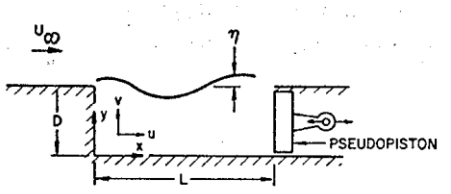

Figure 12. Simple analytical cavity model. [Heller & Bliss 1975].

Cavity Flow Control Techniques

Both active and passive cavity flow control techniques have been utilized to minimize the drag and acoustic oscillations found in cavity flows. Techniques that have been investigated are typically employed to affect the shear layer or the boundary layer upstream of the cavity. Passive methods that have been investigated are shaping of the leading and trailing walls of the cavity, or by placing objects like vortex generators, pins, rods, or airfoils upstream of the cavity. Active methods for suppression include blowing and suction techniques as well as movable upstream devices placed in the flow or boundary layer.

Passive Cavity Flow Control

After concluding that the different sound spectrums from two geometrically different size cavities with a common length over depth ratio was the result of upstream boundary layer differences, Rossiter [Rossiter 1966] investigated spoilers located at the leading edge of a cavity to alter the boundary layer. The largest spoiler had the largest effect on attenuating the larger scales of flow unsteadiness.

Heller and Bliss [Heller & Bliss 1975] and Zhang et.al [Zhang et. al 1998] investigated slanting the training edge of the cavity. Heller and Bliss [Heller & Bliss 1975] discovered that the slanting the trailing edge of the cavity allowed the shear layer to remain straight over the cavity and for the proper impingement angle at the trailing edge. Heller and Bliss [Heller & Bliss 1975] also investigated adding a detached cowl. The position of the detached cowl is critical. Placed properly the cowl creates a low-

pressure area between the cowl and the trailing edge of the cavity canceling out the effects of the mass addition and removal process.

Perng and Dolling [Perng and Dolling 1998] studied the effects of varying cavity dimensions and slotted, slanted and vented geometries on cavity oscillations. They found that vented and slotted walls had little effect.

Franke and Carr [Franke & Carr 1975] screened a variety of baffles and leading and trailing edge modifications in the water tunnel. They tested the most promising configurations in the wind tunnel. They found that the ramps could reduce the pressure oscillations and that frequencies were well predicted by the modified Rossiter's equation.

Smith, Gutmark and Schadow [Smith et. al 1990] utilized multi-steps and pins extending into the supersonic flow to reduce the amplitude of the acoustic oscillations, see Figure 13. A maximum reduction of a factor of 5 was produced by the utilization of the pin profiles shown in Figure 14.

Franke and Sarno [Franke & Sarno 1990] studied static and pulsating fences and steady and pulsating flow injection. Static fences at the leading edge were the most effective suppressor.

Loewen [Loewen 2008] investigated the effects of a rod in a crossflow and found the suppression of cavity tones was primarily due to blockage and lofting effects from the rod.

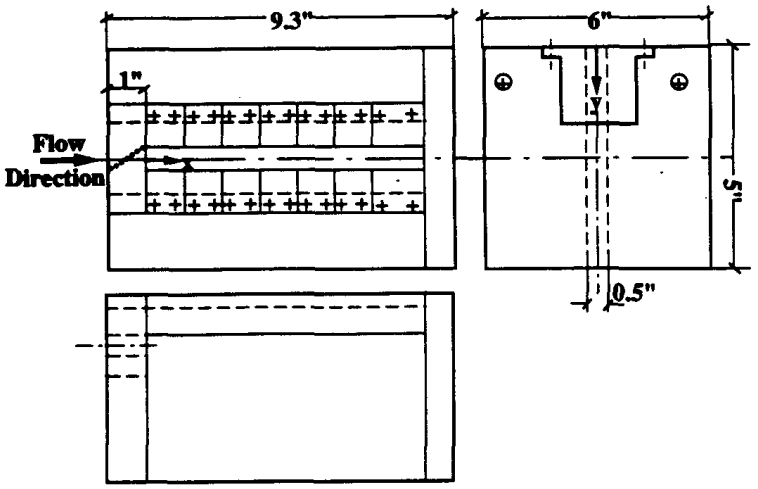

Figure 13. Modular Structure of the Slot in the Flat Plate. [Smith et. al 1990].

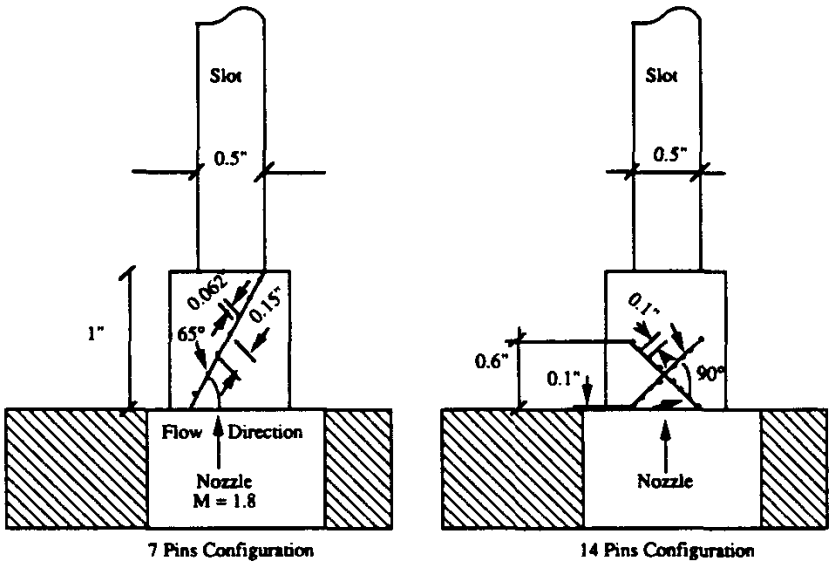

Figure 14. Two Configurations of Pins Which Were Used Most Effectively to Suppress Acoustic Resonance in the Slot. [Smith et. al 1990].

Givogue, Fowler, and Vakili [Givogue et. al 2011] investigated the use of two dimensional cylinders to alter the resonant tones and shear layer. The experiment was designed to assess whether the unsteadiness attenuation accomplished was a shear layer lofting effect or due to high frequency vortex shedding in the wake. Their results clearly indicate that the changes in shear layer were due to wake lofting effects and not high frequency vortex shedding. The wake size and location of the wake have a direct effect on the initial reflected wave generation and feedback mechanisms that drive the high amplitude pressure pulses in the cavity.

Milne [Milne 2012] and Thiemann [Thiemann 2013] studied the use of vertical rods that were placed upstream of the cavity projecting into the flow, Figure 15. There were sixteen rod size and layout configurations tested. Configurations with staggered patterns distorted the vorticity in the shear layer more effectively, and these were more effective at suppression of the resonant acoustic tones in the cavity.

Peltier et.al [Peltier et.al 2013] investigated cavity response to oblique shocks generated upstream to simulate shock induced flow distortion like that caused by a forebody upstream of the inlet. They found that the cavity flow was unsteady and the shear layer displacement was increased when the shock generator was located is in the furthest upstream position.

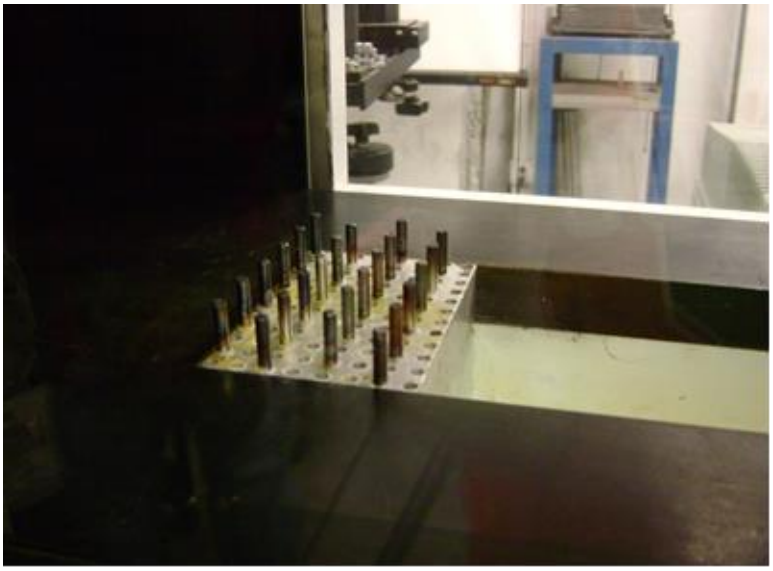

Figure 15. Configuration 12, Pin Plate in Test Section [Thiemann 2013].

Active Cavity Flow Control

There have been a number of instigations of active flow control methods [Sarno and Franke 1994, Vakili & Gauthier 1994, Wolfe 1995, Lamp and Chokani 1997, and Arunajatesan et. al 2008]

Vakili and Gauthier [Vakili & Gauthier 1994] studied the use of upstream mass injection through holes in plates located just upstream of the cavity, Figure 16. They achieved nearly complete suppression of the cavity oscillations with low density injection depicted in Figure 17. They attributed the effectiveness of this method to modifications to the shear layer instability characteristics.

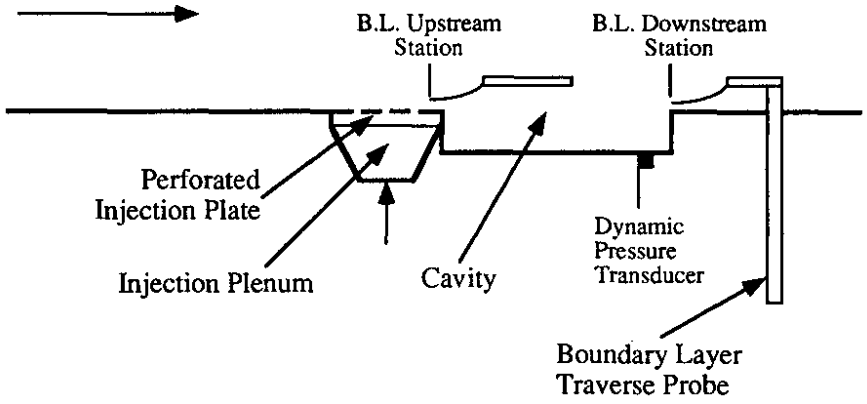

Figure 16. Schematic of the experimental setup. [Vakili & Gauthier 1994].

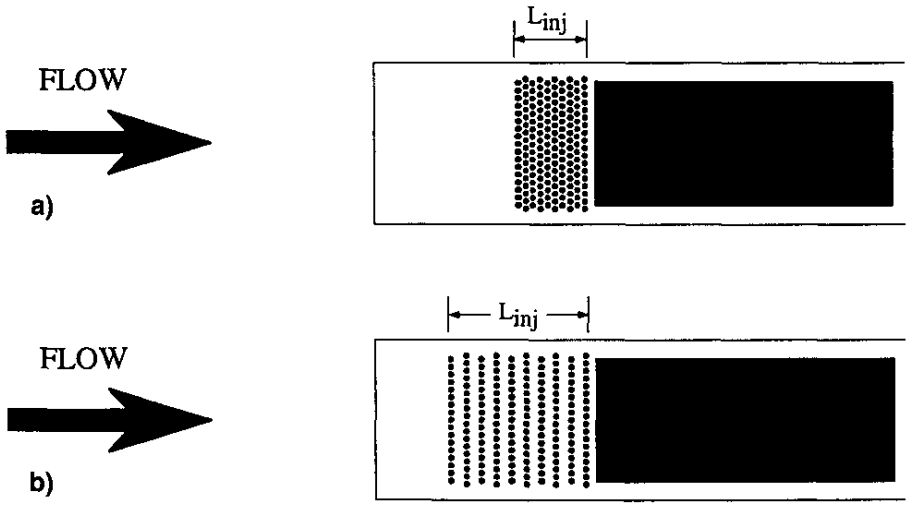

Figure 17. Schematic of the distribution of holes for two mass-injection systems: a) High-density injection and b) low-density injection, [Vakili & Gauthier 1994].

Wolfe [Wolfe 1995] found a correlation between the amount of mass injection and the effectiveness of the injection on suppression of acoustic tones in the cavity.

Arunajatesan et. al [Arunajatesan et. al 2008] compared the reduction in cavity acoustic resonance between blowing through slots or microjets at the leading edge of a cavity and the use of a fence the thickness of the boundary layer at the same location.

This study concluded that bowling concepts, using a small amount of mass injection, could be as effective as a leading-edge fence.

George, Ukeiley, Cattafesta and Taira [George et. al 2015] found that leading edge blowing through slots could reduce the acoustic resonance by as much as 40%.

Houpt et. al [Houpt et. al 2018] recently performed a study of Cavity-Based Flow Control in a Supersonic Duct Utilizing Q-DC Plasma Shock Wave Generator, in a Mach 2 flow with transverse fuel injection upstream of the cavity. They employed plasma generated oblique shocks from the opposite wall, so that the shocks impinged on the cavity shear layer at different positions, resulting in lifting the shear layer into the main stream, Figures 18 and 19. The lifting of the shear layer is expected to increase the mixing between the core flow and the cavity.

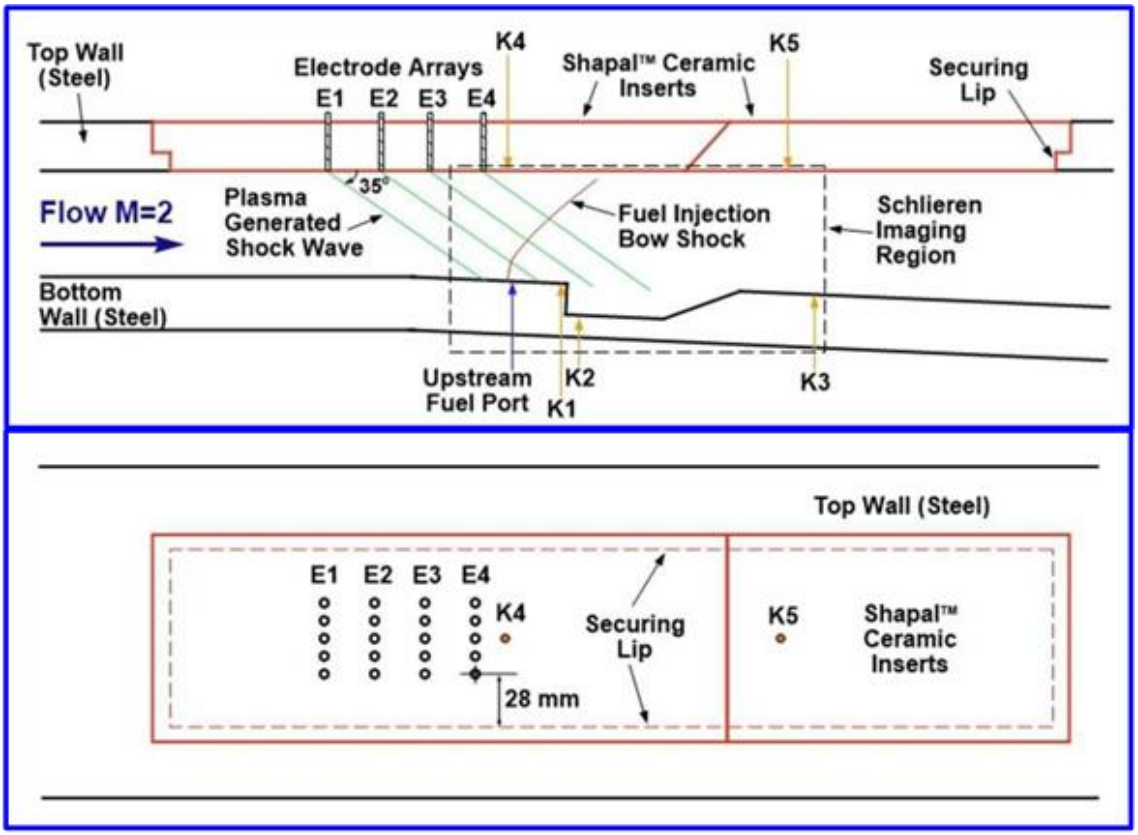

Figure 18. Cavity configuration [Houpt et. al 2018].

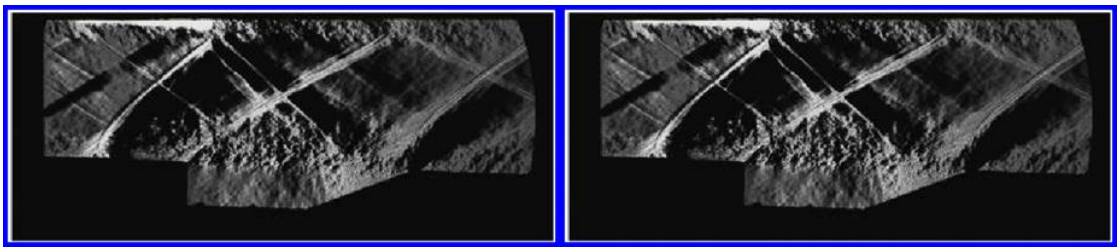

Figure 19. Schlieren images for different injection rates [Houpt et. al 2018].

Cavity Enhanced Mixing and Flame Holding

In turbine engine augmentors and ramjet propulsion systems flame holding is normally accomplished by the use of bluff bodies in the flow field. These bluff bodies create recirculation zones in their wake. Fuel penetration and mixing is accomplished by the use of strut injectors across the flow field to distribute fuel across the airstream. In scramjet combustors these techniques create blockage and strong shock structures leading to high drag losses.

Fuel Injection and flame holding techniques for efficient combustion in scramjets has been the focus of ongoing research. Ben-Yakar and Hansen [Ben-Yakar and Hanson 2001] and Pandy and Sivasakthivel [Pandy and Sivasakthivel 2011] have conducted detailed reviews of recent advances.

A variety of fuel injection and flame holding schemes have been proposed and studied [Billig 1993, Abbitt et.al 1993, Hartfield 1994, Riggins 1995, Riggins and Vitt 1995, Curran et. al 1996, Tishkoff et. al 1997, Fuller et. al 1998, In et. al 1998, Sung et. al, 1999, Huber et. al 1979, Ben-Yakar and Hansen 1998, Hartfield et .al 1994, Curran 2001, Nenmeni & Yu 2002, Fry 2004, Gruber et. al 2004, Gruber et. al 2006, Tuttle et. al 2012, Grady et. al 2012, Tam 2012, Boles et.al 2012, Kirik et. al 2013, Barnes et. al 2014, and Arial et. al 2015].

As shown in Figure 20, early scramjet fuel injection was accomplished by injecting fuel transversely into the flow [Billig 1993, Gruber et. al 1995, and VanLerberghe 2000].

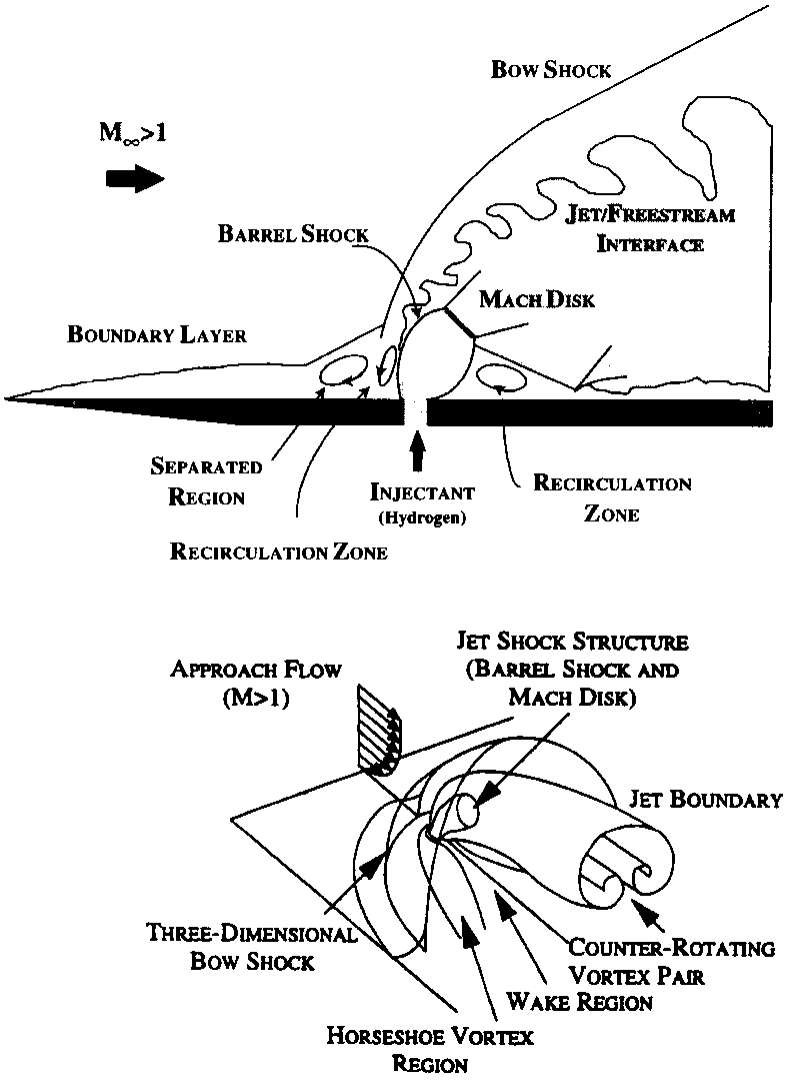

Figure 20. Schematic of underexpanded transverse injection into supersonic flowfield [Gruber et. al 1995].

In Figure 20 the upstream boundary layer separates and a normal shock is created causing this type of injection scheme to have high drag.

Abbitt et.al studied transverse injection behind a rearward facing step [Abbitt et.al 1993]. Here the expansion wave and shear layer interact with a bow shock created by the hydrogen fuel jets as shown in Figure 21.

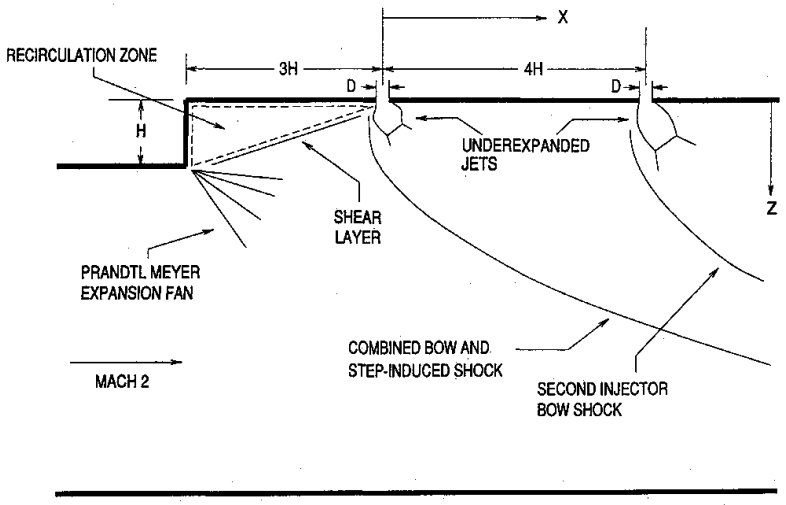

Figure 21. Fuel injection behind a rearward facing ramp [Abbitt et.al 1993].

Hartfield, Hollo, and McDaniel [Hartfield et .al 1994] investigated vortex enhanced mixing behind a swept ramp injector Figure 22. The fuel injection was accomplished nearly parallel to the freestream flow. They found that the flow is turned away from the wall downstream by the ramp generated vortices, but the effect of the ramp generated vortices dissipates after 10 ramp height distances downstream, and that mixing rate decreases with increasing Mach number.

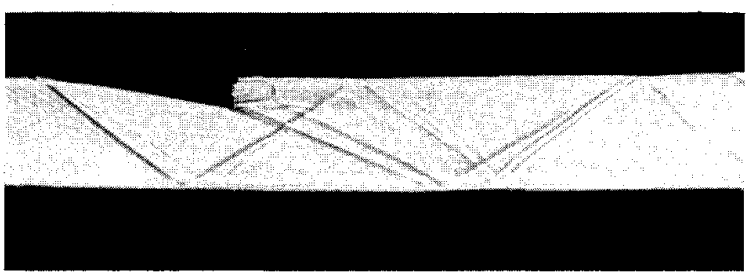

Figure 22. Swept Ramp injector [Hartfield et .al 1994].

Fuller et.al [Fuller et. al 1998] compared the effectiveness of ramp injectors to aerodynamic injectors, Figure 23. They found that the physical ramp injector reached fully mixed conditions in approximately half the length of the aerodynamic ramp but that the aerodynamic ramp had lower pressure losses.

Nenmeni and Yu [Nenmeni and Yu 2002] from the University of Maryland investigated cavity induced mixing in confined supersonic flows, Figure 24. Nenmeni and Yu [Nenmeni and Yu 2002] found that flow induced cavity resonance may be utilized to improve mixing over a broad array of cavity dimensions and Mach numbers, Figure 25.

Yu and Shadow, Sato et. al, and Arial et.al [Yu and Shadow1994, Sato et. al 1999, and Arial et.al 2015] investigated the interactions between cavities and fuel injection.

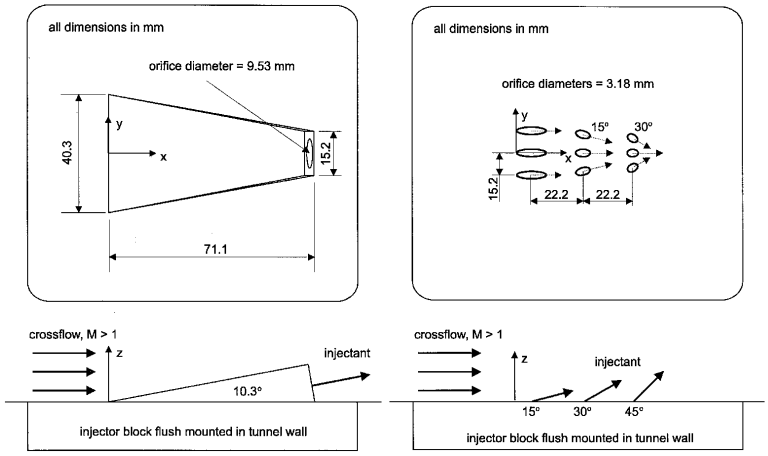

Figure 23. Physical and aerodynamic ramp schematics [Fuller et. al 1998]

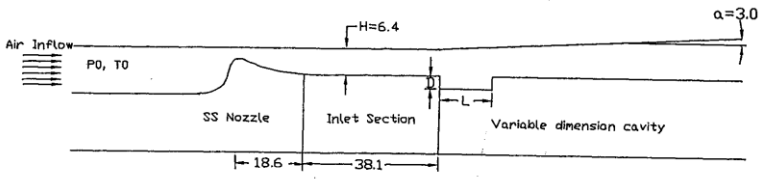

Figure 24. Experimental Schematic (dimensions are in mm) [Nenmeni & Yu 2002].

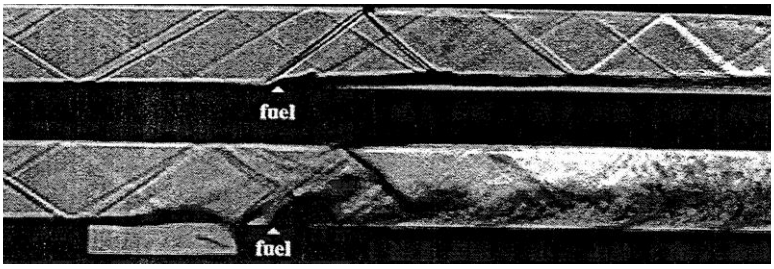

Figure 25. Schlieren images of mixing between Mach 2 air stream and transverse fuel injection without (above) and with (below) the cavity for mixing enhancement [Nenmeni & Yu 2002].

Arail, Sugano, Tsukazaki, and Sukaue [Arial et. al 2015] conducted research on the interactions between cavity flow and a ramp injector. In their study the cavity was placed on the opposite wall and upstream of the ramp injector. They found that the acoustic tones improved mixing of the fuel with the freestream flow. Figure 26 shows the improved fuel mixing in the presence of the cavity, and Figure 27 highlights the acoustic waves due to the cavity interacting with the fuel injection region.

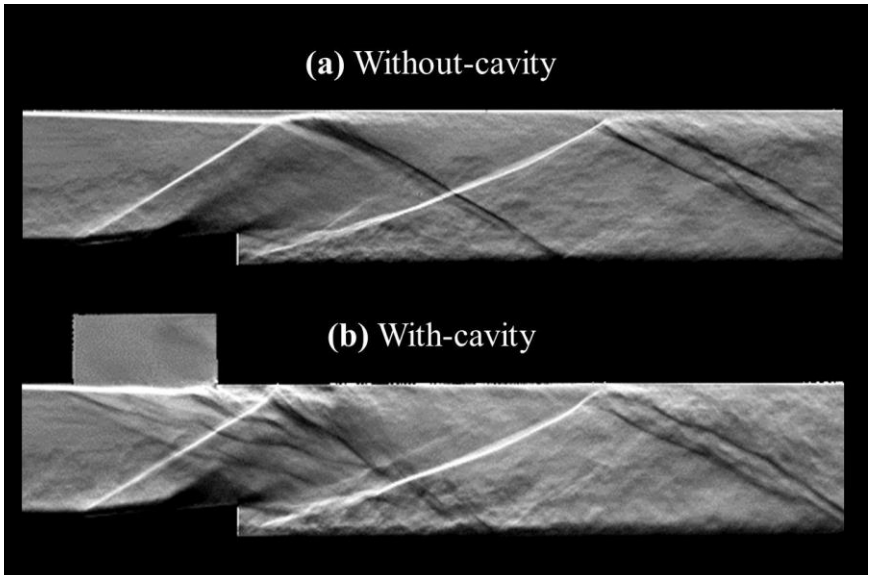

Figure 26. Schlieren flow image with and without cavity [Arial et. al 2015].

Barnes, Tu, and Segal [Barnes et. al 2014] conducted research on the effect of mass injection in the cavity on flame holding capability and the mass exchange into the freestream. They injected flow into the cavity through the leading edge and compared that to injecting fuel at a rearward angle into the floor of the cavity. Both injection

locations created fuel rich regions interacting with vortices trapped in the cavity. The forward injection location resulted in a larger fuel rich zone in the cavity. They also found that the shear layer was entirely within flammability limits and would be a likely location for flame anchoring.

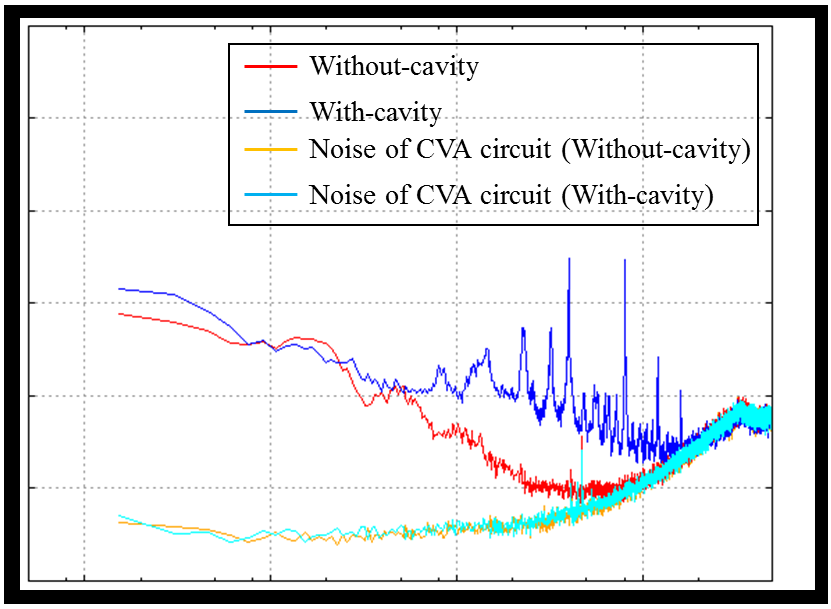

Figure 27. Power Spectrum distribution, Power Spectrum (dB) vs Frequency (Hz) [Arial et. al 2015].

State of the Art in Supersonic fuel injection and mixing

From the open literature, as shown in the above review, there are continuing efforts to facilitate efficient supersonic combustion through efficient fuel injection and mixing in short distances. Increased penetration into the cross flow has remained as the strongest challenge. Various sizes of struts with or without built in cavities are used to

increase fuel penetration and mixing into the main flow, but result in strong shocks and losses. Pulsed fuel injection if appropriately implemented, has been shown to help penetration and mixing away from the boundaries [Vakili et. al 1990, Vakili et. al 1994, Chang et. al 1995, and Williams 2016]. However, generating very high frequency pulsed fuel injections, needed for supersonic flows, is a challenge of its own.

This research is a first and introductory study of a new approach for increased fuel penetration for more efficient mixing in supersonic flow. Such a passive flow path design with distributed fuel injection for flow mixing control is new and represents a major step forwards in this developing field. Here we utilize passive geometry in coordination with strategically positioned fuel injection within a cavity to generate resonant cavity oscillations for increased local mixing coupled with passively generated streamwise vortices which help increase fuel rich flow mixing and penetration into the cross flow. This innovative approach, developed and improved based on flow physics, help to overcome the various challenges associated with supersonic fuel injection and mixing. The author believes and hopes that this work will establish a fundamental milestone in the direction of and state of the art for supersonic mixing enhancements.

Chapter 3: Experimental Apparatus

This experimental study was completed the 8 inch by 8 inch cross section supersonic blowdown wind tunnel in the Gas Dynamics Laboratory at the University of Tennessee Space Institute. Testing was completed on two different configurations designed to have low shock losses and to generate vorticial flows that enhance mixing. Instrumentation included Schlieren video, Particle Image Velocimetry (PIV), and high frequency pressure measurements.

Wind Tunnel

The University of Tennessee Space Institute wind tunnel is a blowdown wind tunnel. A schematic of the wind tunnel is provided as Figure 28. Air is compressed and stored in 18 High pressure cylinders at 3000 pounds per square inch. The tunnel operation is controlled with LABView software. The air is routed to the wind tunnel plenum via a pneumatically driven flow control valve. In the plenum the flow is straightened by four stages of honeycomb and grid flow straighteners. The flow then travels through a convergent divergent nozzle designed for Mach 1.85. The nozzle has an axisymmetric entrance and an 8-inch by 8-inch square exit. The test section is 4 feet long with observation windows on the top and sides. The bottom has a removable floorplate where the test articles are mounted. The flow exits the test section and is expanded to atmospheric pressure through a diffuser.

The top window of the test section provides access for the Particle Image Velocimetry (PIV) laser sheet. The PIV system is used to provide velocity vectors and Z-

vorticity of the flow. The side windows of the test section provide a view of the test section for Schlieren imaging.

The stagnation temperature (T_0) and stagnation pressure (P_0) are measured in the stilling chamber and the static pressure (P) is taken via static ports in the test section.

The Mach number (M), static temperature (T), speed of sound (a), and freestream velocity (U_∞) can be calculated using the following equations [National Advisory Committee for Aeronautics (NACA) Report 1135]:

$$(3) \qquad M = \sqrt{\left(\frac{2}{\gamma - 1}\right)\left[\left(\frac{p_o}{p}\right)^{\frac{\gamma-1}{\gamma}} - 1\right]}$$

$$(4) \qquad T = \frac{T_o}{1 + \frac{\gamma - 1}{2} M^2}$$

$$(5) \qquad a = \sqrt{\gamma R T}$$

$$(6) \qquad U_\infty = Ma$$

Where: T_0=470.39 °R, P_0=27.94 psi, P=4.58 psi, $\gamma = 1.4$, and $R = 1716.49 \left[\frac{\text{lbf-ft}}{\text{slug-R}}\right]$

Calculated Mach Number (M) = 1.84

Calculated Speed of Sound (a) = 821 ft./s

Calculated Velocity in Test Section (U) = 1511 ft/s

Schlieren

The University of Tennessee Space Institute Schlieren system was installed in the test cabin so that the shock structure changes could be recorded via video camera. Schlieren is a flow visualization technique that relies on density changes in the flow field to be visualized due to the density changes in the flow leading to changes in refraction index. A sketch of the system is provided in Figure 28. A high intensity light sources is focused upon a concave mirror. The light is then reflected through the test section and onto another concave mirror. The image is then reflected off of a plane mirror and across a sharp edge and onto a screen. The image is then captured by a video camera and recorded and displayed in the wind tunnel control room.

Acoustic Instrumentation

High speed acoustic measurements were taken with Kulite® XCS-133-093-15D pressure sensors. These sensors were flush mounted to static pressure ports, located in the bottom floor of the test article cavity. Data was acquired at 40 kHz rates for several seconds for spectral analysis. Figure 29 provides a typical example of an acoustic spectrum, along with the Rossiter Modes predicted by the modified Rossiter Equation, for the 11-inch cavity utilized by Milne [Milne 2012] in previous experimental studies at UTSI.

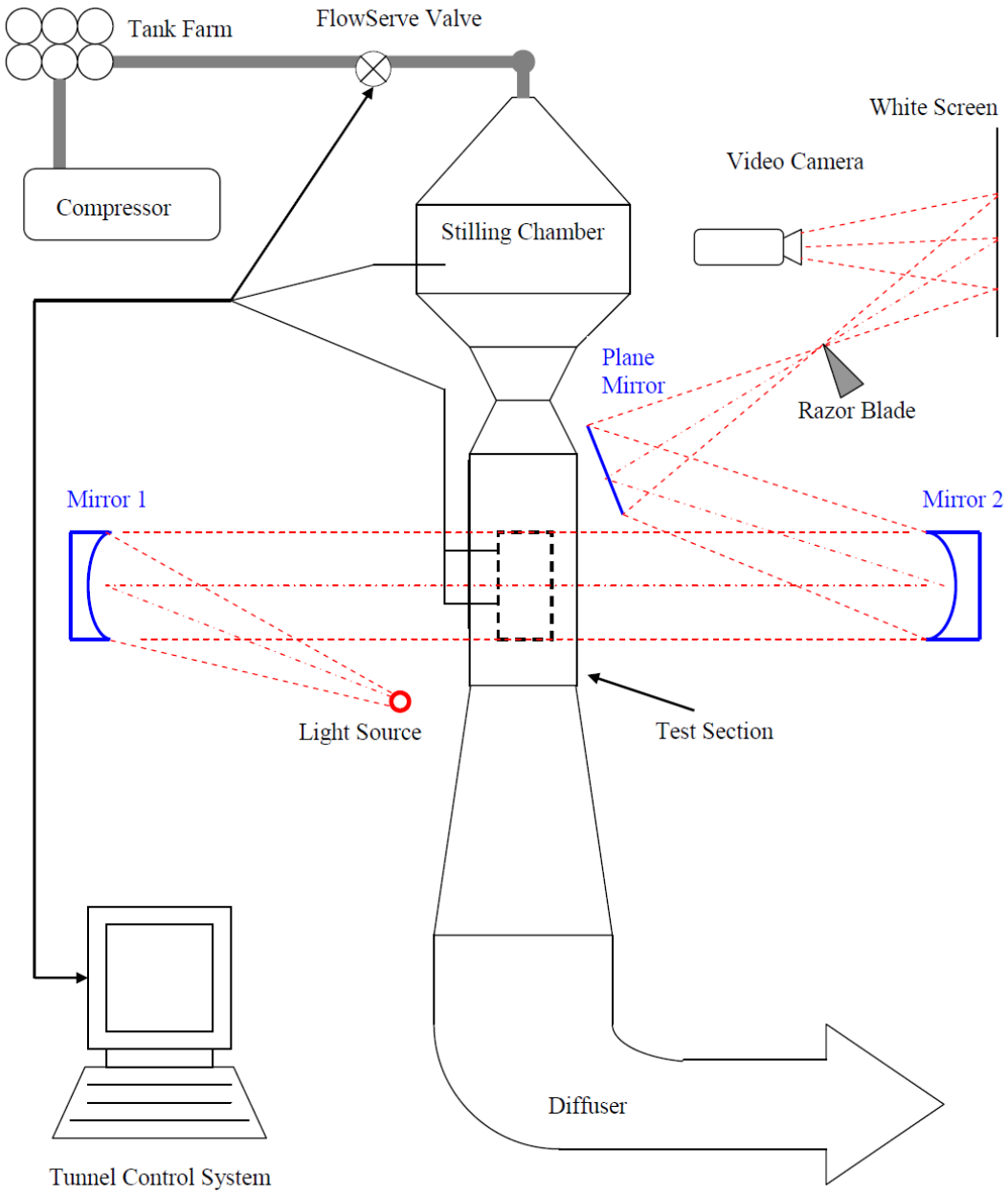

Figure 28. Sketch of HSWT with Schlieren Setup [Fowler 2012]

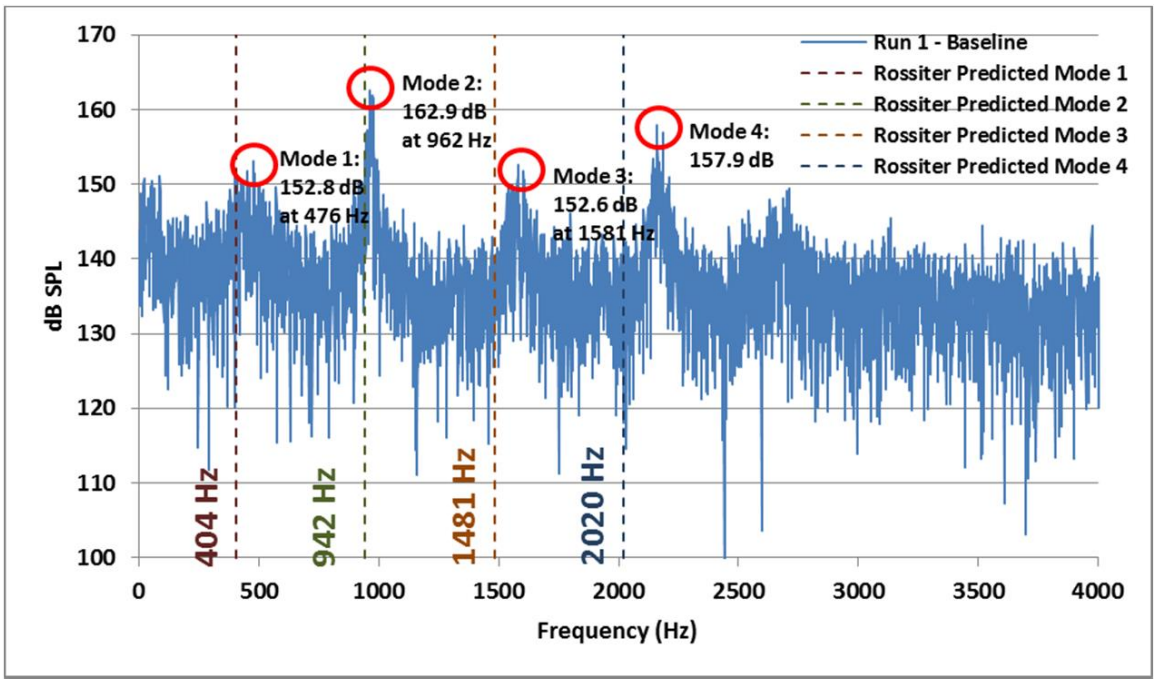

Figure 29. Baseline cavity spectra [Milne 2012].

Particle Image Velocimetry (PIV)

Particle Image Velocimetry (PIV) was used to provide an understanding of the flow vectors and vorticity in the region around the test article and above the tunnel floor. PIV uses a laser sheet to excite molecules that have been seeded into the flow upstream of the test section. This seed moves with the airflow and is assumed to have the same velocity vector as the airflow. When excited by the laser the molecule of seed fluoresces. The laser is pulsed, like a photographer's flash, with very precise timing so that the images can be compared. Since the time between the images is known, the change in the particles position allows the velocity vector to be calculated.

The seeding is comprised of 70% isopropyl alcohol, 30% water, with a small amount of fluorescein dye powder, nominal diameter of 2 micrometers. The fluid borne seed is injected into the tunnel flow using pressurized air via a coaxial tube in the convergent section of the nozzle.

The TSI LASERPULSE PIV system contains two neodymium-doped yttrium aluminum garnet (Nd:YAG) lasers. The beam is directed to the top of the test section through an articulated laser arm. This arm included a series of prisms and mirrors and finally the beams pass through spherical and cylindrical lenses creating a 0.04 inch by 4-inch laser sheet. This sheet is used to illuminate the leading-edge device and the forward portion of the cavity, Figure 30.

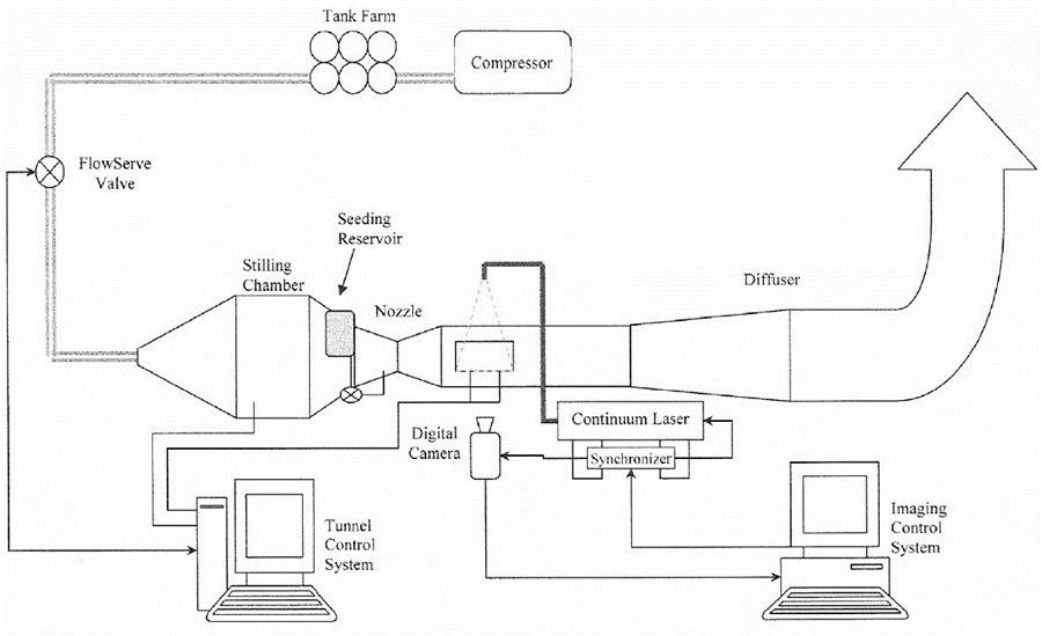

Figure 30. HSWT with PIV Apparatus [Loewen 2008].

The TSI LASERPULSE PIV system utilizes INSIGHT™ PIV Software to operate the system components. INSIGHT utilizes a "frame straddling" procedure to create the two images that will be compared to generate the velocity vectors. This procedure compensates for the camera's relatively low frame rates. The 1st laser pulse occurs near the end of the 1st camera exposure and the 2nd laser pulse occurs at the beginning of the second camera exposure, Figure 31. The time between the laser pulses (dT) is precisely controlled to 2 microseconds.

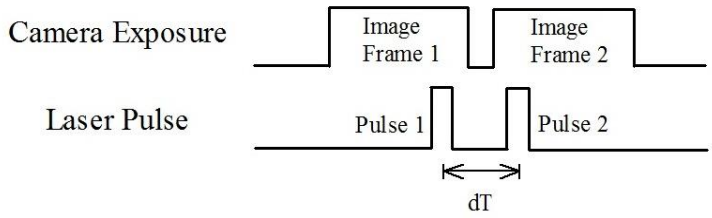

Figure 31. Frame Straddling Exposure Technique [Thiemann 2013]

The camera has a charge coupled device (CCD) with a sensor that has 1016 pixels high (y - from the tunnel floor toward the top of the test section), by 1000 pixels wide (x - in the flow direction). The INSIGHT PIV calibration procedures were followed [] resulting in a conversion factor of 115.60672 micrometers per pixel. Additional details concerning the TSI LASERPULSE PIV system and INSIGHT™ PIV Software operation, calibration and error analysis are included in references [Fowler 2010, Thiemann 2013, Loewen 2008, and Givogue et. al 2011].

After post processing of the data with Insight, the velocity vector data was imported into Tecplot. Tecplot enabled the vector fields to be plotted and the vorticity in the z direction (ω_z) to be plotted. The z direction is directed out of the side window of the wind tunnel test section.

Test Articles and Cavity Configurations

Mixing in supersonic flows is limited by slow shear layer growth. Passive flow control techniques are typically the most robust in harsh environments like supersonic combustors. They are typically the best choice for enhancing fuel mixing in this type of environment.

Two test articles were developed. The test articles consisted of a vortex generating shape on the leading edge of a cavity. Each had ports for air injection as well as for pressure measurements. The test articles configurations were developed to provide reduced acoustic signature and increased vorticity to provide mixing downstream of the cavity.

Two cavity and flow device configurations were chosen from a wider selection of configurations researched based on their potential mixing enhancement with lowest drag and shockwave losses. Additionally, these cavities were fitted with (simulated fuel) flow injection jets to accommodate this additional aspect of flow control. There were two jets located in the sidewall of the cavity, and three jets located in the front wall of the cavity.

The flow device and cavity geometries were innovatively designed to generate a relatively weak shock structure and thus have relatively low shock losses when compared with other flame holding and mixing schemes.

Independent CFD predictions were conducted by Dr. A.J. Meganathan in support of conceptual design and to predict the resulting flow fields. The CFD initially helped in minimizing the number of physical models which were fabricated and tested in the tunnel.

The two configurations and the experiments that resulted were specifically designed to provide a broad base information to assess the effectiveness of this novel concept. The two flow devices were selected to provide counter rotating vortices that would be lofted into the flow downstream. One was designed to concentrate the vorticity in the center of the cavity and the second was to concentrate the vorticity near the sidewalls. One cavity was designed to maximize the pressure oscillations within the cavity and the second was designed to minimize them. The locations of the fuel injection ports were chosen to maximize interaction with the vortex flow structures.

Test Article #1, Figure 32, had a pyramid like structure to generate vorticity just upstream of the cavity. This structure was designed to concentrate the vorticity in the center of the cavity. The cavity was slightly wider in the upstream than in the downstream and the bottom of the forward edge of the cavity had a radius of 0.5 inches and the bottom of the cavity tapered to the trailing edge. The bottom of the cavity had three ports for high frequency pressure measurements. At the base of the pyramid were

three ports for blowing downstream with the direction of flow. These ports were designed to change the shear layer location with respect to the cavity. There was also one port on each wall just down-stream of the cavity leading edge. These ports simulated injection ports that should enhance fuel mixing with the vortex structures coming into the cavity. This should enhance flame holding in the cavity and increase fuel penetration into the mean-flow downstream of the cavity. In this test article, the cavity was designed, with a tapered floor and rear cavity wall, to passively reduce the acoustic response.

Test Article #2, Figure 33, has a trapezoid ramp vortex generation device upstream of the cavity. The trapezoid is wider upstream and is the same width as the cavity at the trailing edge. This shape was chosen to concentrate vorticity near the cavity side walls. The cavity was nearly a square planform and is constant in depth. The cavity had an L/D of 4. There were 3 static pressure ports in the bottom of the cavity.

Like test article #1, at the base of the trapezoid ramp were three ports for blowing downstream with the direction of flow. These ports were designed to change the shear layer location with respect to the cavity. There was also one port on each wall just down-stream of the cavity leading edge. These ports simulated injection ports that should dampen the acoustics and enhance fuel mixing with the vortex structures coming into the cavity. This should enhance flame holding in the cavity and increase fuel penetration into the mean-flow downstream of the cavity.

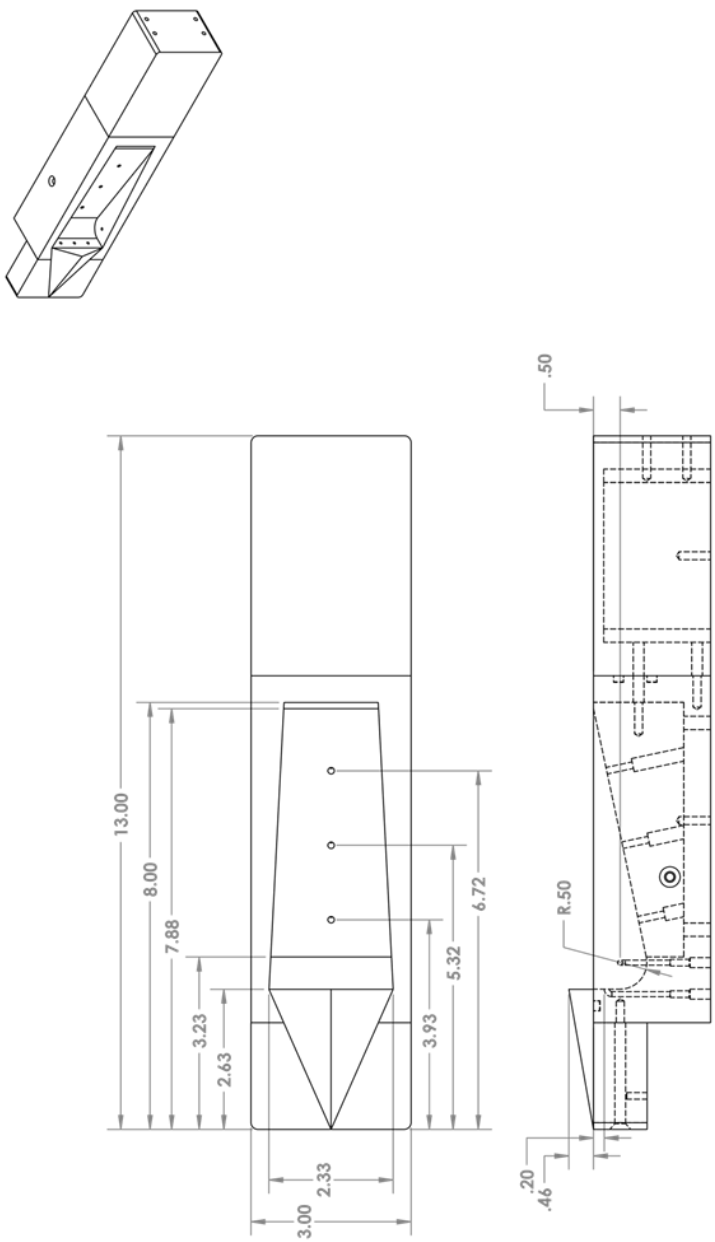

Figure 32. Test article number 1, dimensions in inches.

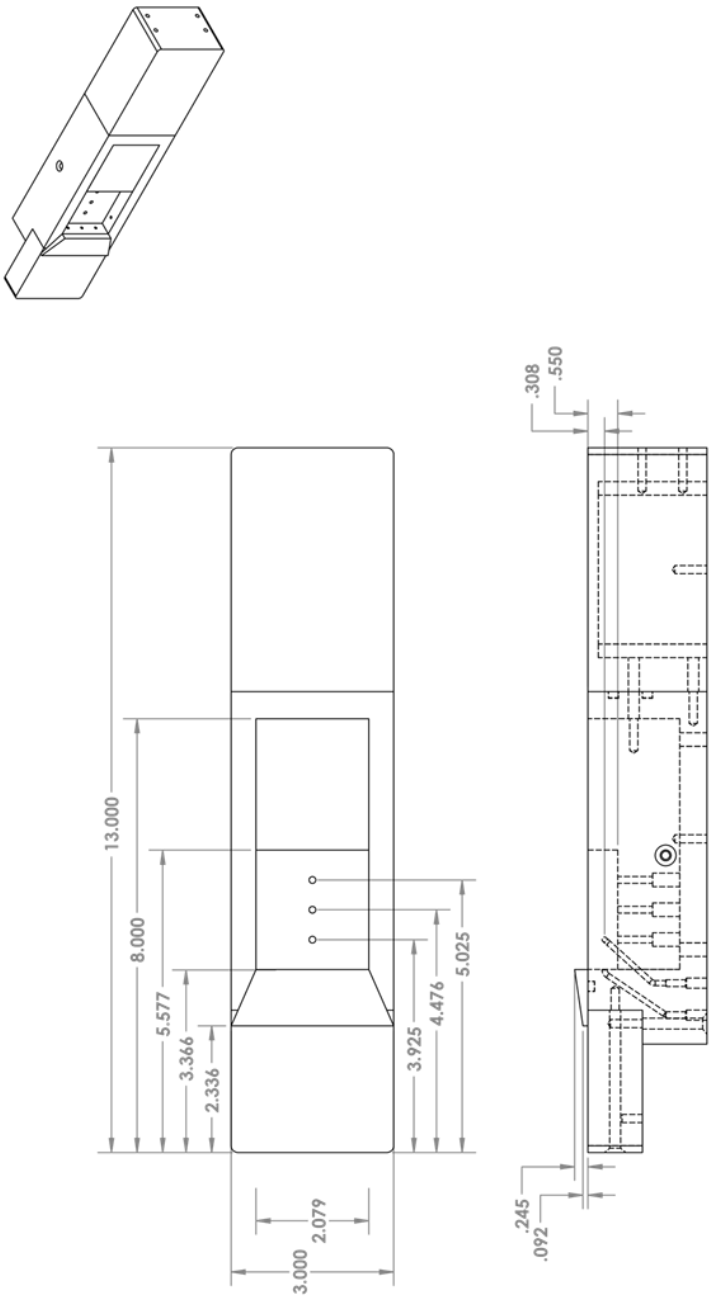

Figure 33. Test article number 2, dimensions in inches.

The two test articles were constructed by a 3d printing process at the UTSI Gas Dynamics Laboratory. The parts were printed in sections and bolted together as can be seen in Figure 34. The parts were then shaped with filler and sanded to provide the proper surface finish. They were then painted and installed into the removable floorplate of the supersonic tunnel test section, Figure 35. Tubing was attached to the blowing and transducer ports in the cavity. The air supply for blowing was plumbed to the five tubes on the left side in Figure 36. The transducers were connected to the three tubing ports that are along the base of the cavity, shown on the right side in Figure 36. The test articles were then installed into the tunnel along with the floorplate, Figures 37 and 38

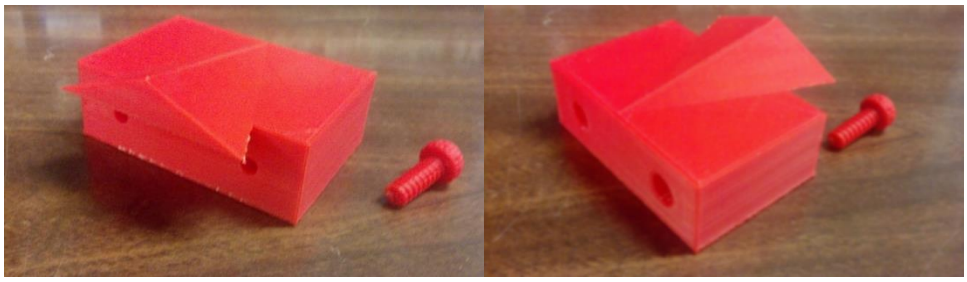

Figure 34. 3d Printed leading edge Section for test article #1

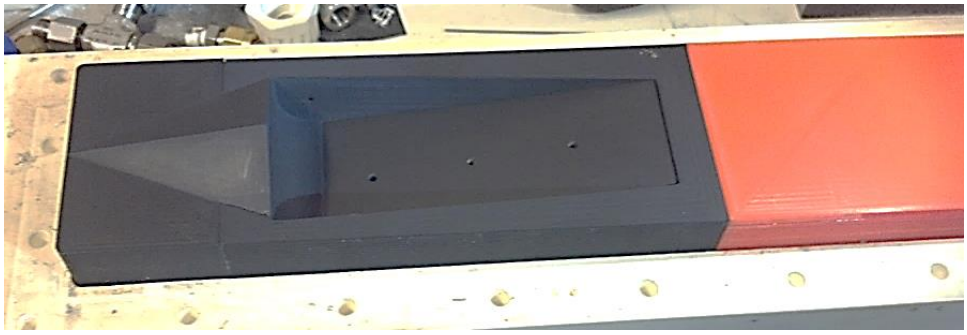

Figure 35. Test article assembled into the tunnel floorplate.

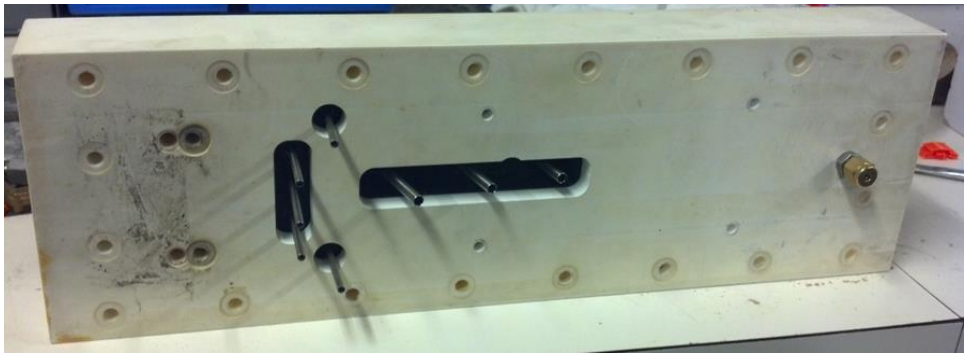

Figure 36. Tubing added to the bottom of the test article for blowing and dynamic pressure measurement.

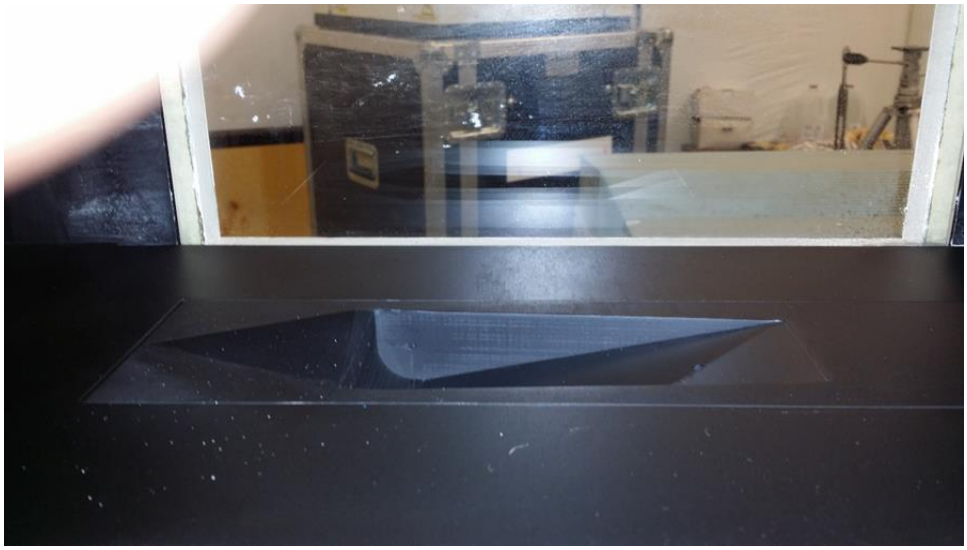

Figure 37. Test article #1 mounted inside the test section.

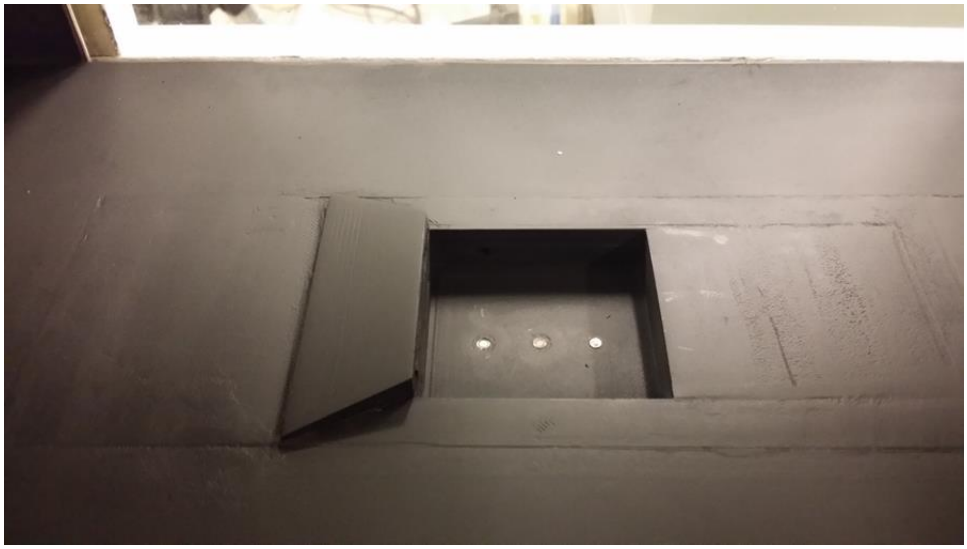

Figure 38. Test article #2 mounted inside the test section.

Chapter 4: Results and Discussion

Introduction

In this chapter, the analysis of the data taken will be presented. The testing was conducted over a period of more than a year. Delays were caused by a number of higher priority tests, forcing interruptions in the availability of the wind tunnel. These interruptions caused additional delays in the test program by requiring reinstallation and recalibration of test articles and data systems.

While there were compromises in the data systems and optics, the results are clear enough to generate conclusions concerning the flow control techniques in question. The Schlieren data was quantitatively analyzed to make quick assessments of blowing effectiveness. The PIV data was reduced and velocity, vorticity, turbulence, and Reynolds Stress were calculated. Pressure data were analyzed to obtain spectra to help better understand the effects of the injected flow into the cavity on the flow field. The results will be discussed in the following sections.

Testing was completed with simulated fuel injection by blowing pressurized air through orifices in the cavity walls. In the following discussion the label “No Jets” indicates that none of the flow orifices in the cavity had flow, the label “Axial Jets” refers to blowing flow through the 3 jets at the forward face of the cavity, the label “Side Jets” indicates that blowing is occurring through the orifices in the side of the cavity near the front face, and “all Jets” refers to flow through both the axial and side orifices.

Sources of Error and Uncertainty Analysis

Typical sources of error include the equipment, equipment calibration, sampling, and processing algorithms. The facility and measurement systems were effectively the same as those used in previous experiments in the same UTSI supersonic wind tunnel. A full description of the statistical error analysis is provided in references [Fowler 2010, Thiemann 2013, Loewen 2008, and Wolfe 1995]. In the following paragraphs, some additional factors contributing to the uncertainty of the results are described.

Initial testing was completed with a Schlieren system. The Schlieren system was compromised in two ways. The first was the lack of adequate spacing for optimum mirror and screen spacing. The second compromise was inadequate light source intensity. The low intensity of the light source provided, resulted in low contrast and weak gradients, making the Schlieren images difficult to read and analyze. Another contributing factor was the presence of Mach waves in the test section of the tunnel test section.

PIV measurements were taken along the test unit centerline and along the side edge of the cavity. One difficulty in taking PIV measurements off of the test cell centerline is the ability to get adequate seeding of the flow off centerline. The seeding device is located in the plenum chamber on the cell centerline. This device consists of two concentric rods with an orifice on one side. The inner tube supplies the seed and the outer tube supplies blast air to atomize the seeding fluid. But since this rod is inserted at the tunnel centerline in the plenum, most of the seed is along the test section centerline.

To compensate for this fact the rod that supplied the seed was turned at an angle to the flow in an attempt to get additional seeding at the cavity edge. This technique had limited effect on the quality of seeding along cavity edge.

The camera used to acquire the PIV images was compromised due to the presence of a bad pixel. The inoperative pixel resulted in a line across the screen from the top to the bottom behind the cavity. This created a discontinuity in the data which can be seen in all of the PIV images and the results. Care must be taken to not mistake an artifact of this bad pixel for an actual flow phenomenon.

A number of different factors can contribute to increasing uncertainties and errors in pressures, Schlieren, and PIV measured data for calculating and generating flow field information. They can be broadly classified into errors associated with hardware and setup. These types of errors are related to the sensors, equipment component setup, acquisition and data analysis for the measured variables.

The Schlieren images obtained in this study were utilized as qualitative information and are used to detect relative changes in the flow field due to changes in model geometry and jets flow.

Pressure measurements are affected by details of pressure transducer's specifications such as accuracy and linearity; error band determined via calibration can be taken into account to estimate the overall order of accuracy for the measurement.

For the PIV data, the measurement system is composed of the laser beams with Gaussian profile in Transverse Electro Magnetic mode 00, which translate into laser light

sheets uniformity and alignment, CCD camera resolution, synchronizer for timing between different frames, optical magnification is calibrated. Aberrations inherent in the optics govern the overall uncertainty in the PIV data. Even though most of these are carefully set up and selected for about one percent accuracy, the combined effects of the various factors increase the uncertainty to about 5%-10%, with the higher accuracy applicable to the higher speed ranges. In the PIV setup used for our measurements, there was a damaged pixel in the CCD chip. This resulted in a vertical line loss of data corresponding to the bad pixel, in each image matrix, and resulted in contamination of the calculated data in the proximity of the line. Due to the averaging and interrogation sub window size of 32x32 pixels, this effect is evident in most processed data and images containing velocities, vorticity and stresses. Since the affected area is in the downstream of the cavity its effect is not detrimental to the understanding of the flow field. For this reason, the local patterns are generally not affecting the results and conclusions.

Electronics, including timing synchronization circuits are highly accurate. Therefore, the error in the timing is normally ignored for the flow speeds in this study. For a given flow field, using a camera with highest density CCD with a nominal dT, (or Del t), improves the accuracy of calculated particle displacements. Normally, a larger separation time is recommended, within the maximum feasible dT for a particular flow measurement equipment setup and a chosen interrogation window size.

Estimating errors in PIV measurements are affected by components resolutions, optical set up and data analysis methodology. The interrogation sub window size in this

study was 32 x 32 pixels including a 70 % overlap to increase the number of calculated vectors. Usually a 50% overlap related to the Nyquist criterion is used. Using a higher overlap only increases the number of vectors and not the scales that could be truly resolved. Finer resolution of velocity vectors help to improve calculations of vorticity and turbulence properties. The dynamic spatial range is basically fixed by the image size and interrogation spot size. The interrogation process is repeated to cover the entire image for each pairs of images. Detailed studies have shown that cross-correlation methods, Figure 39, perform much better than any other method in terms of signal-to-noise ratio and flexibility of choosing parameters for PIV imaging [Meganathan 2005].

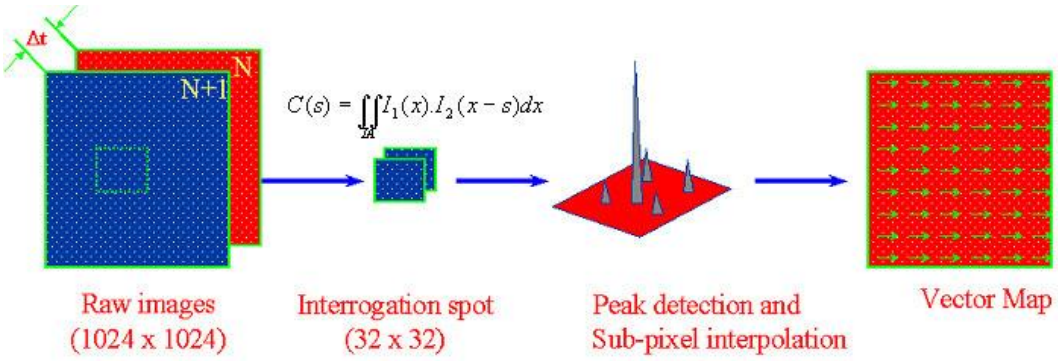

Figure 39. A schematic of the cross-correlation process is shown [Meganathan 2005].

PIV is typically set up to provide a required spatial resolution, which is balanced between the size of the flow structures to be resolved with the interrogation spot size and image magnification. The setup used in this study was to resolve the shear layer and the flow near the boundary including its effects into the main flow.

The recorded size of particles on the image is usually larger than the particle size due to magnification. This increase in size comes from different parameters including diffraction limit of the recording optics and the experiment specific intensity of image [Adrian 1997]. This is only the optical effect and the actual image size is substantially larger than what is calculated (possibly up to an order of magnitude larger). For good spatial resolution displacement of particles due to the maximum gradient should be less than 5% of the interrogation spot size. Selecting the best dT between images and the best spot size (interrogation) is ideal for the expected upper flow velocities. Best practices established by various investigators limit the displacement due to the highest velocity be less than or equal to 25% of interrogation spot size.

Post processing of the raw vector field involves removal of the outliers using range, local median, standard deviation and mean filters, built into the PIV software. The eliminated vectors were filled through interpolation using Gaussian smoothing with exponent 1.3 [Meganathan 2005].

With the above considerations, all images were processed with an interrogation spot size of 32 x 32 pixels. The distance between any two adjacent vectors was 10 pixels. The calibration of the images was about 50 μm/pixel. The resolution of the vector map is 0.5 mm. In order to determine what minimum size vortex structures can be visualized, we have to decide how many data points are needed to determine a structure. When measuring flow turbulence, to characterize mixing effects, the dynamic spatial range and the dynamic velocity range are more important than the spatial resolution [Adrian 1997].

These set the smallest size of the structures and the velocity fluctuations that would be resolved in a setup. The dynamic spatial range (DSR) is defined as the field-of view in the object space divided by the smallest resolvable spatial variation. [Adrian 1997]. The smallest resolvable scale is the smallest resolved particle displacement, which is due to with the maximum velocity.

The dynamic velocity range (DVR) is defined as the ratio of maximum velocity to the minimum resolvable velocity. Westerwheel [Westerwheel 1994, Westerwheel et.al 1997] estimates that usually the error in resolving the location of a correlation peak is in the order of 0.1 pixels. The capability of a PIV system to have both a large dynamic velocity range and a large spatial range is determined by the product of DSR and DVR, which is a constant for a given experimental setup. PIV systems having a large constant are best suited for turbulence research, and measurements in higher Reynolds number flows. [Abraham 2005, Adrian 1997] calculated the constant for a nearly similar set up as used in this study obtained approximate values of DSR = 200 and DVR = 40, resulting in a constant of about 8000, which would resolve velocities between 10 m/s - 300 m/s. This was for an assumed upper limit of image diameter of 10%, which will be improved to 1 m/s – 300 m/s, if 1% is used. This is important to be aware of for flows with a wide range of velocities [Meganathan 2005].

Experimental setup errors include calibration errors, non-optimal choice of tracer particles and laser sheet alignment [Meganathan 2005]. The need to choose ideal seeding materials and seeding dispersion system has already been discussed.

"Computational errors include truncation errors, detection errors, and precision errors. Truncation errors are very similar to truncation error in numerical analysis caused by approximations using numerical discretization. Most PIV algorithms use a simple forward differencing interrogation scheme in which the velocity at time t is calculated using particle images recorded at time t and t+del t. This approximation is accurate to the order of del t, and second order in space increments" [Meganathan 2005]. These errors are systemic and cannot be completely eliminated due to the inherent nature of image correlations. There also exist certain small errors due to correlations between random particles that are not the same pair which influence the peak-searching algorithm. Various data processing smoothing operations, including sub pixel interpolations introduce certain amount of errors. Particularly of importance is the higher % errors introduced into the lower speeds regions are in the flow field in the cavity or near the boundaries, from the high-speed regions of the flow.

Vorticity and stresses components are obtained by evaluating the velocity derivatives with a suitable finite difference, second order central difference scheme in this case. Here the typical numerical truncation errors and original errors in calculating the velocity itself are key contributions to the overall uncertainty in these variables. As noted before, the complete PIV set up affects the uncertainty of these variables [Meganathan 2005].

Table 1. Effect of sub pixel interpolation resolution on velocity uncertainty [Meganathan 2005].

Velocity (m/s)	Pixel Size (micro-meter)	Sub pixel interpolation precision (±pixels)	±% Uncertainty
300	9	0.1	0.38
250	9	0.1	0.45
200	9	0.1	0.56
150	9	0.1	0.75
100	9	0.1	1.12
50	9	0.1	2.25
25	9	0.1	4.5
20	9	0.1	5.63
15	9	0.1	7.5
10	9	0.1	11.25

Clean Tunnel

To be able to ascertain the effect of the flow control devices, it is first necessary to capture clean tunnel flow data. The "clean tunnel' can be described as an empty test section. The cavity section of the floor plate was filled with a blank, and the area where the flow device is installed is left clean. Therefore, the test section has no flow devices or cavities present. Due to test facility conflicts, it was decided to utilize clean tunnel data from a previous study. In this case the clean tunnel information is taken from Fowler [Fowler 2010]. Figure 40 is a photograph of the clean test section, showing the locations for the ramps and cavities in the smooth floor plate blocks. Figure 41 is the resulting

calculated pressure spectra associated with the clean tunnel test section, indicating the baseline spectra contains no tunnel acoustic peak.

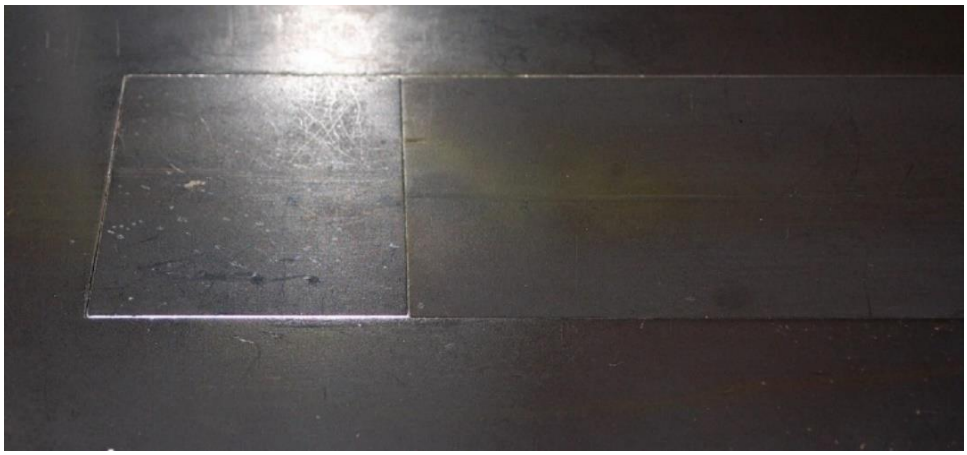

Figure 40. Clean Tunnel Photograph [Fowler 2010].

The clean tunnel broad spectra are relatively flat, at approximately 100dB, and have no large distinct peaks. Because the spectra are so well behaved, i.e. lacked the presence of resonant tones, this spectrum can simply be considered background noise.

Fowler [Fowler 2010] also took Schlieren photographs of the clean tunnel test section. Figure 42 is a summary of the analysis of the clean tunnel Schlieren data from Fowler [Fowler 2010].

There is a thin, 3/8 of an inch, boundary layer along the floor of the tunnel. The Mach waves present in the tunnel are due to slight manufacturing imperfections in the nozzle wall. A trigonometric analysis of the Mach wave angle, 33 degrees, confirms the tunnel operation at a Mach number of 1.84.

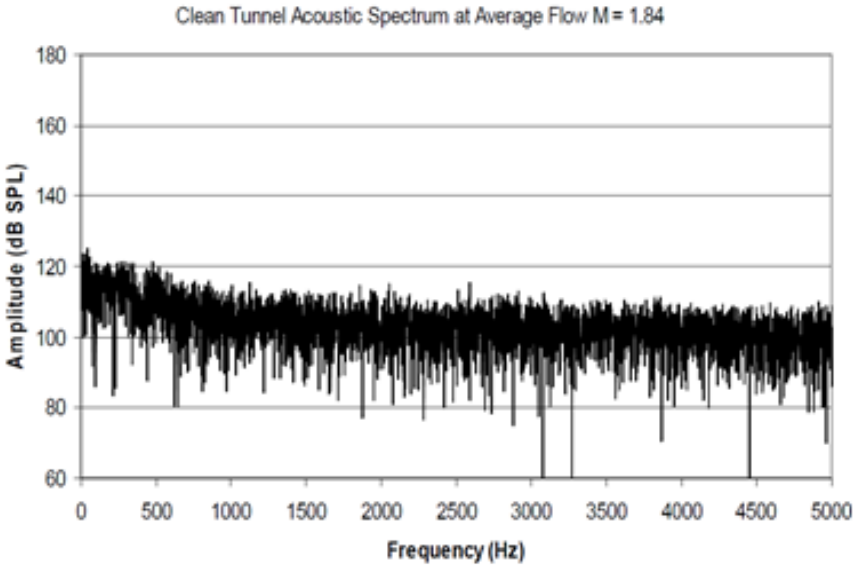

Figure 41. Clean Tunnel Acoustic Spectra [Fowler 2010].

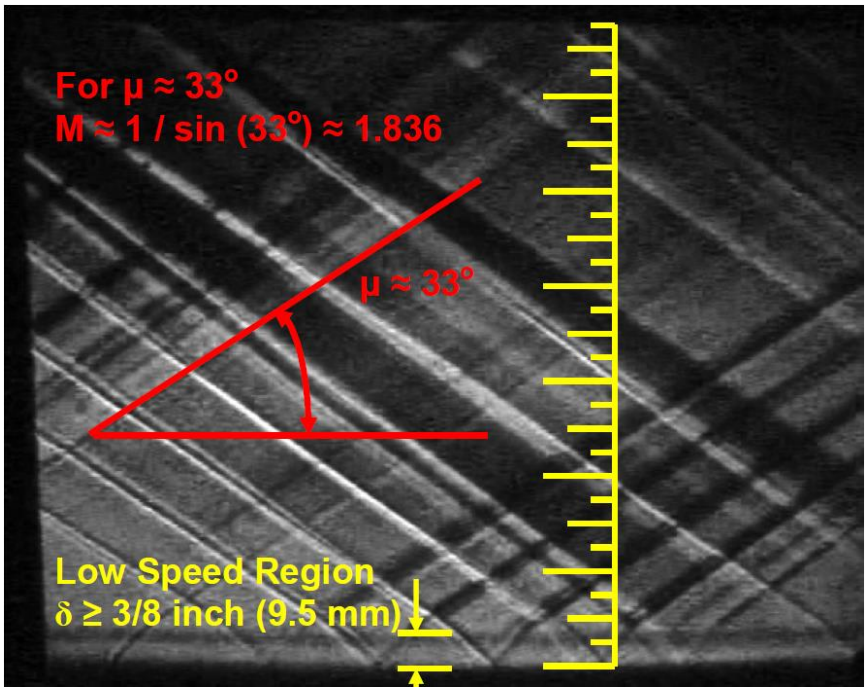

Figure 42. Clean Tunnel – Schlieren Mach waves analysis [Fowler 2010].

Fowler [Fowler 2010] also took PIV data of the clean tunnel, shown below in Figure 43. The flow in the test section is shown to be nearly uniform. The spurious velocity vectors near the surface are due to the boundary layer. The PIV analysis confirms the boundary layer analysis form Schlieren data. Both of Schlieren and PIV analysis are very close to the calculated boundary layer thickness from [Fowler 2010].

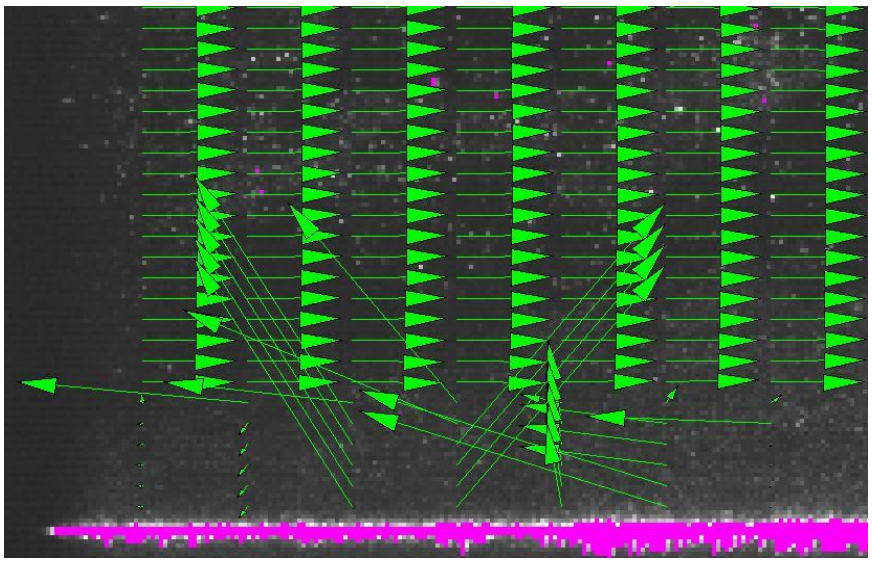

Figure 43. Clean Tunnel – PIV velocity vectors [Fowler 2010].

The clean tunnel data taken by Fowler [Fowler 2010] is an adequate basis for making assessments of the flow control techniques utilized in this study. For details of the clean flow experiment and analysis the reader is referred to Fowler [Fowler 2010].

Schlieren Analysis.

Depicted in Figure 44 are typical Schlieren photographs from the test series. The test noted in Figure 44 was conducted with test article number 2. It is difficult to see the differences between the blowing and non-blowing cases. However, when the images are examined carefully, there are clear differences. In the case of blowing, the shock structure originating at the leading edge of the wedge is more diffused and appears as a few weaker waves. The same observation applies to the shock structure originating along the top of the wedge. There are also differences in the shock structure along the cavity, as the shock structure is more diffuse along the cavity with no blowing, indicating the shear layer effect due to blowing is affecting the main flow shocks.

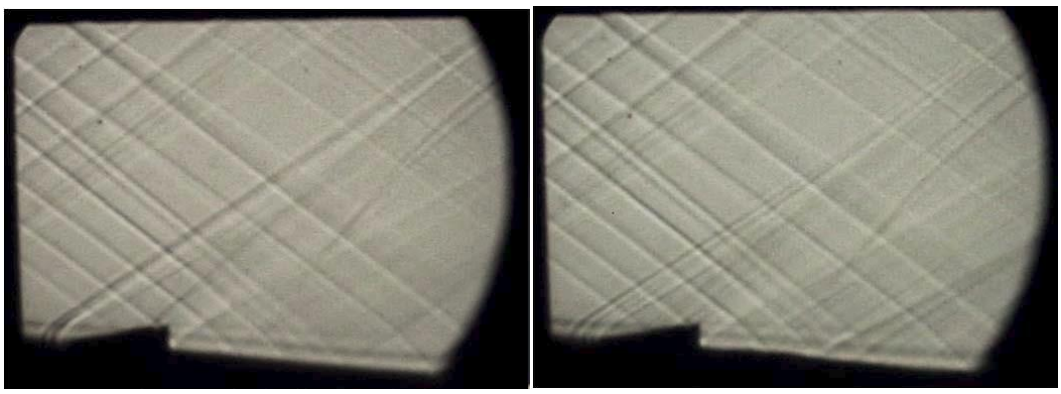

No Jets **All Jets**

Figure 44. Schlieren photographs with and without blowing (note a slight tilt in the image, tunnel floor is horizontal).

Computational Predictions

Simulations (for a number of configurations) were performed, by Dr. A.J. Meganathan, using ACE+ and FASTRAN, finite volume based CFD flow solvers [Boudaghi, et..al 2018]. Figure 45 shows (only results for final configurations close to the ones which were tested are shown here) a computational prediction depicting the Mach contours and the streamlines, with and without blowing. The prediction with blowing shows a thicker and more lofted shear layer. In addition, the mixing is more intense from the vortices that are shedding from the corners of the flow device, upstream of the cavity, down into the cavity.

Figure 46 is a CFD prediction of test article 2 depicting the streamlines with and without blowing. When compared to Figure 45 the test article 2 prediction shows increased vorticity with the streamlines moving more deeply into, and out of, the cavity in Figure 46. These simulations were in support of understanding, clarifying details and comparative validation.

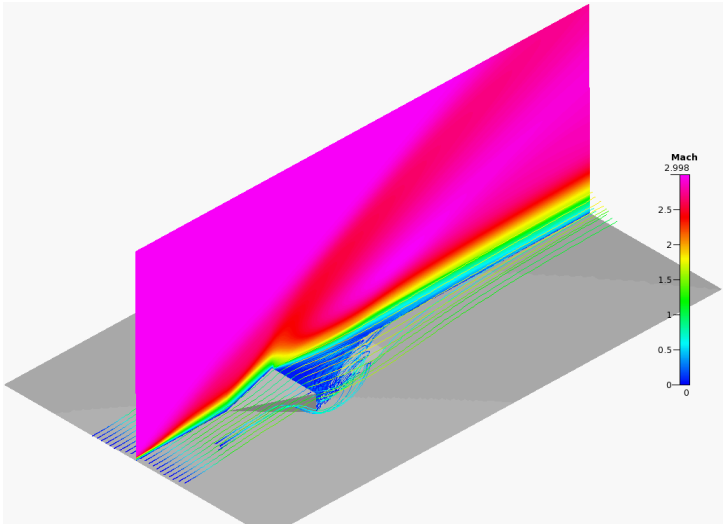

No Jets

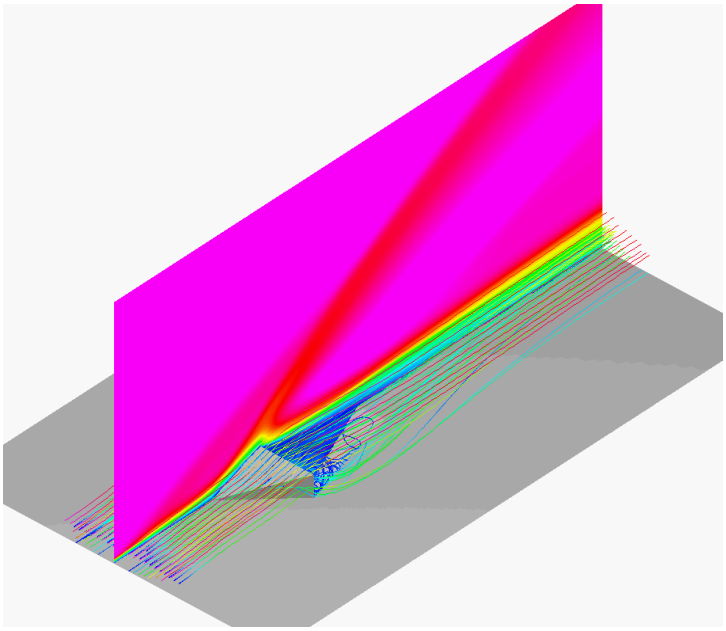

All Jets

Figure 45. CFD Predictions, Mach number contours and streamlines, with and without blowing.

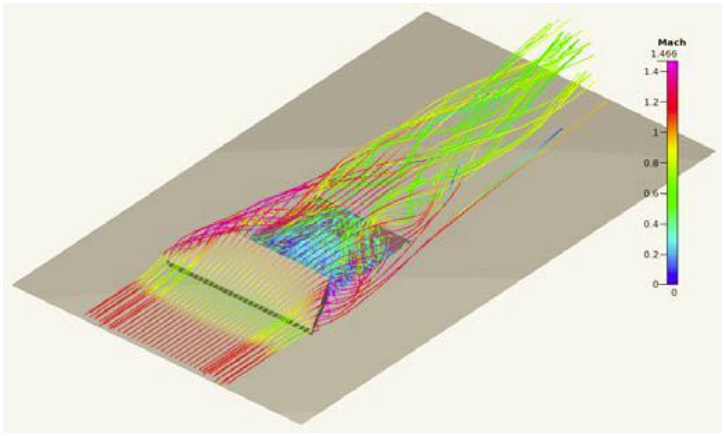

No Jets

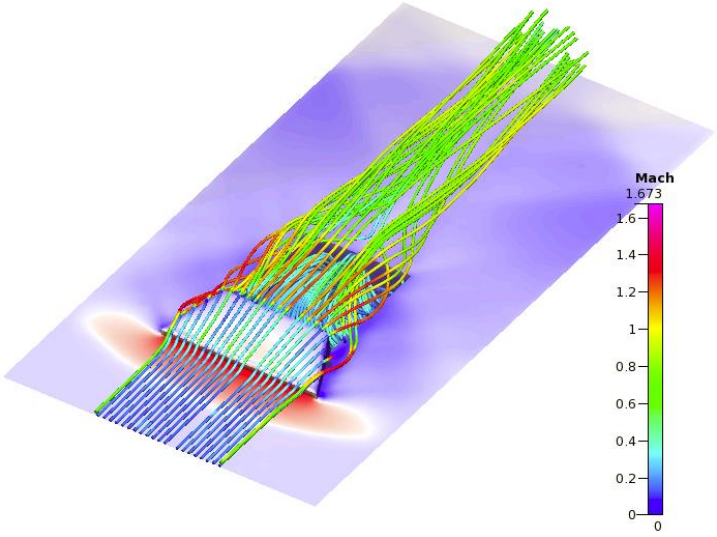

All Jets

Figure 46. Test Article Number 2 CFD Prediction with and without blowing.

PIV Measurements

Initially the PIV laser sheet was located along the centerline of the cavity. One shortfall of choosing this location is that it does not allow the PIV system to capture the corner vortices at the edges of the cavity. These vortices are significant contributors to the mixing accomplished by the passive flow control device in the upstream of the cavity. In an attempt to capture the flow features and associated information with these important vortices, the test series was repeated with the laser sheet located along the outside edge of the cavity. PIV test data labeled "Off- Centerline" refers to data taken with this second laser sheet location near the edge of the cavity.

PIV Images

The PIV system is capable of taking up to 10 image pairs within one second. PIV images were acquired during the test runs. Figure 47 provides a reference schematic, indicating grouping of jets that were active (blowing) in each test configuration. The jets highlighted in red are those that have active blowing in that test run.

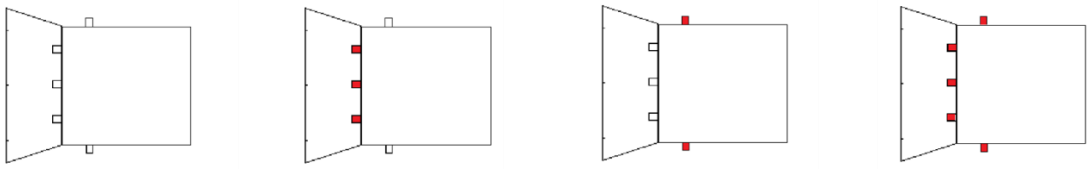

No Jets **Axial Jets** **Side Jets** **All Jets**

Figure 47. Blowing Configurations for PIV analysis.

Figures 48 through 51 include one image from each blowing configuration shown in Figure 47. All of the images in each figure are the same size and scale. All of the figures show adequate seeding of the flow. The vertical line through each image is a bad pixel in the camera CCD. The horizontal line along the bottom of many of the images is the tunnel floor. The bright area along this line on the right side of the image is not the aft wall of the cavity, as the cavity walls cannot be seen in the images. This bright area is caused by seeding impinging on the tunnel floor.

In Figure 48 the "No Jets" image highlights the vorticity being generated by the flow device and as denoted by the concentration of seeding shown trailing behind the top of the flow device. In Figure 48 "Axial Jets" image the three axial jets at the rear face of the flow device are injecting air (or a simulated fuel) into the flow. The shear layer appears to be lower near the surface of the cavity. This is likely due to being entrained into the axial flow of the injectors. In Figure 48 the image labeled "Side Jets" has the injectors on the side walls of the cavity flowing simulated fuel. In Figure 48 image labeled "All Jets" all of the injectors are flowing simulated fuel. The vorticity near the surface of the cavity is more defined in this figure.

Test Article Number 1 Centerline PIV Images

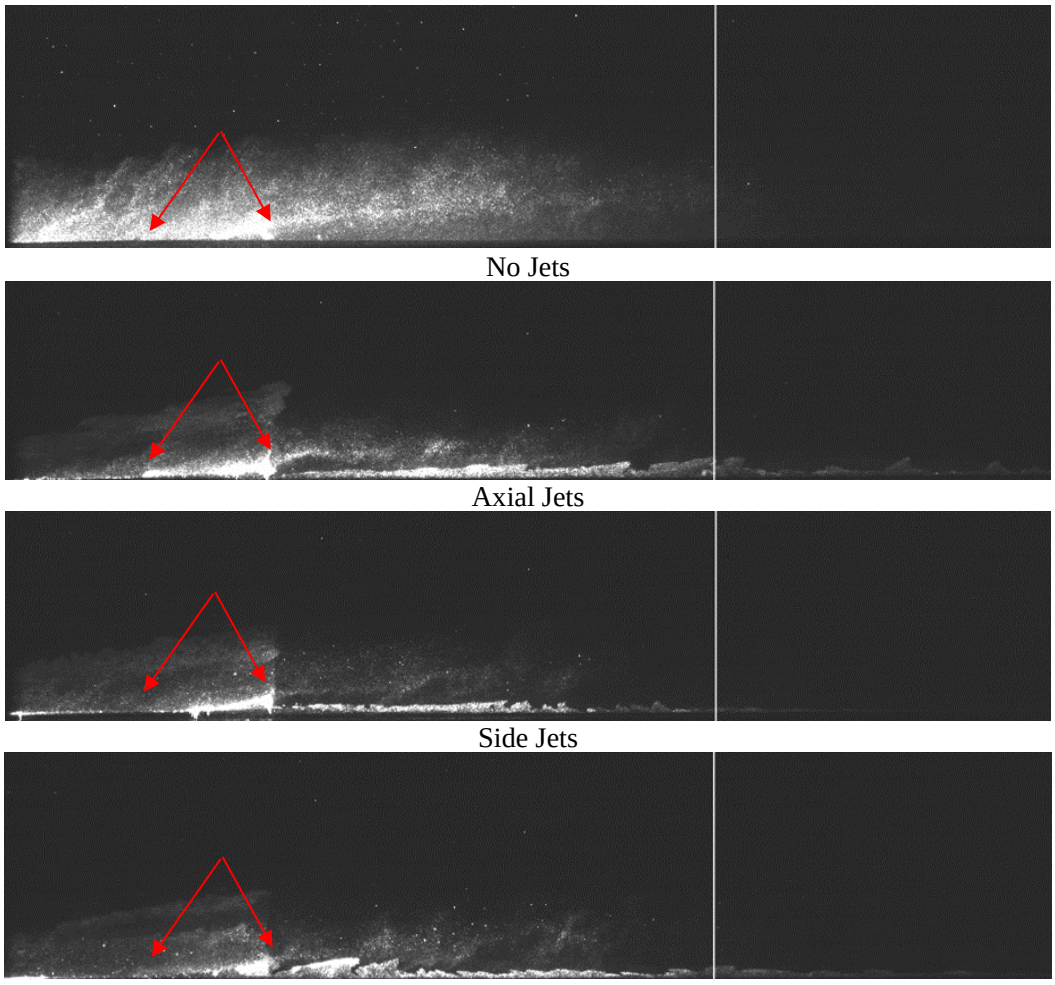

Figure 48. Test Article 1 Centerline PIV Images. The location of the leading and training edges of the flow device are located by the red arrows. The trailing edge of the cavity is not in view

Test Article Number 1 Off-Centerline PIV Images

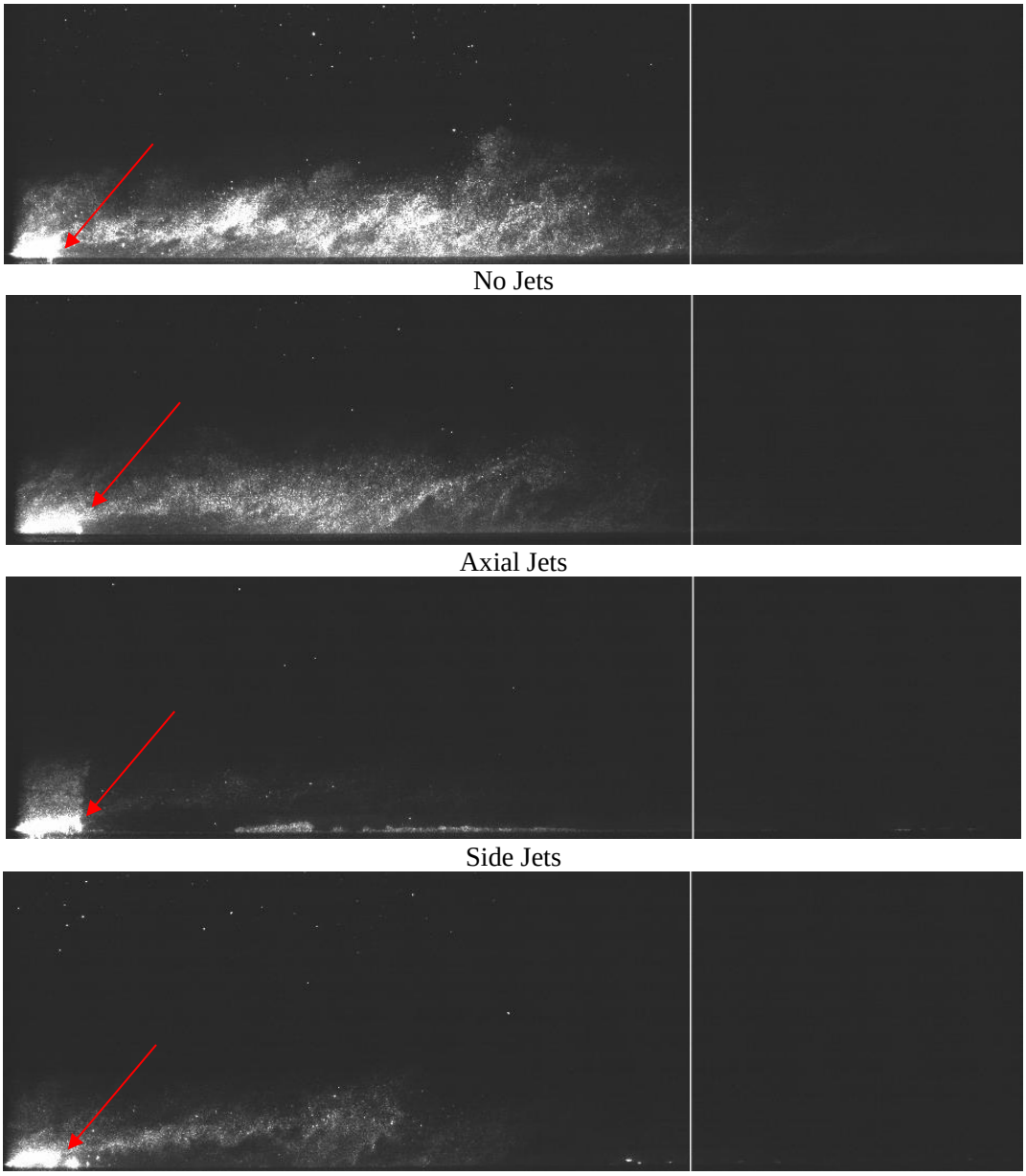

Figure 49. Test Article 1 Off-Center PIV Images. The location of the trailing edge of the flow device is indicated by the red arrows. The leading edge of the flow device and the training edge of the cavity are not in view.

Test Article Number 2 Centerline PIV Images

No Jets

Axial Jets

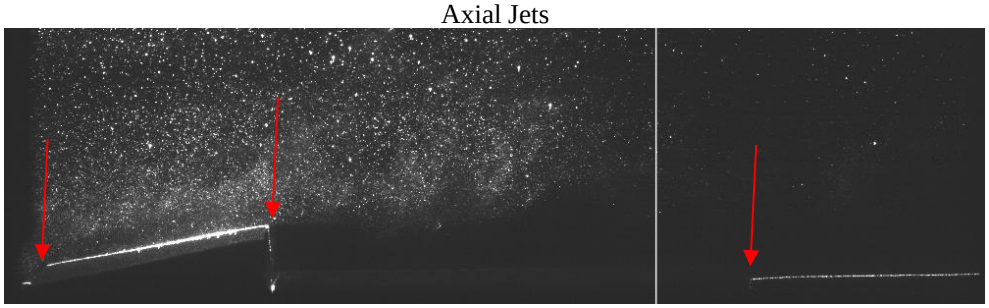

Side Jets

All jets

Figure 50. Test Article 2 Centerline PIV Images. The leading and trailing edges of the flow devise and the training edge of the cavity are indicated by the red arrows.

Test Article Number 2 Off-Centerline PIV Images

No jets

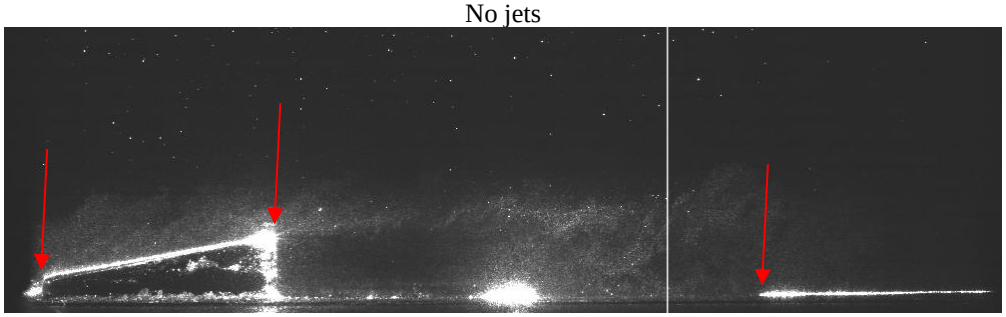

Axial Jets

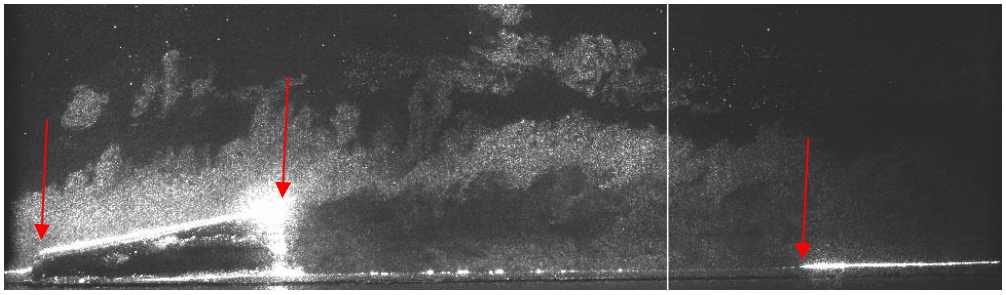

Side Jets

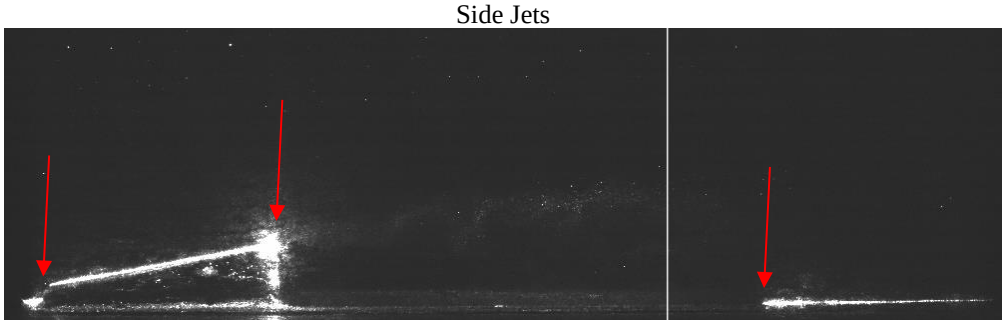

All Jets

Figure 51. Test Article 2 Off-Centerline PIV Images. The leading and trailing edges of the flow devise and the training edge of the cavity are indicated by the red arrows.

Figure 48 is a collage of test article 1 PIV images taken along the edge of the cavity. The images show adequate seeding. The images with the "Side Jets" and "All Jets" blowing, even though the side jets image is lighter due to seeding concentration differences, both show increased lofting of the vortex shedding from the corner of the flow control device. This should improve fuel penetration into the core flow over the cavity.

Test article 2 centerline PIV images are displayed in Figure 50. In the images for test article 2, the rear face of the cavity can be seen. The sheer layers in the "No Jets" and "Side Jets" images appear to be lofted slightly higher than those labeled "Axial Jets" and "All Jets". This is likely due to the axial flow entraining the flow and decreasing the vertical component of velocity.

The off-centerline PIV images for test article 2 are depicted in Figure 51. With the naked eye, no difference can be detected in the shear layer height, likely because of the location of the laser sheet. The clouds of seeding in the image labeled "Side Jets" are likely due to some injection jet flow instabilities, or unsteady operation, of the seeding system. The extra seeding density did not affect the quality of the PIV analysis.

Average Velocity Uave

Figures 52 through 55 are contour plots of average velocity, in meters per second, in the **x** direction, the flow along the tunnel's test section.

Figure 52 is the average velocity along the centerline to the tunnel. The shear layers in the plots with blowing are more defined and closer to the cavity. The overall

average velocity is lower, which is likely due to the affect blowing had on the shock structure at the leading edge of the flow device.

In Figure 53 the off-center average velocity contour image is displayed. The Laser sheet is near the edge of the cavity. The velocity is higher in the non-blowing case. The cases with side blowing have the lowest average velocity.

The centerline average velocity contour plots for test article 2 are depicted in Figure 54. The discontinuity along the vertical line at X=78 is due to the failed pixel in the camera. In this case the average velocity is lowest in the non-blowing case. The shear layer is closest to the cavity in the cases with blowing.

The test article 2 contour plots of average velocity along the cavity side edge are captured in Figure 55. Again, here the lowest average velocities are present in the non-blowing case. The highest average velocity is in the case with the axial jets blowing. This is confirmed by the Schlieren photographs discussed earlier.

Test Article Number 1 Centerline PIV Average Velocity (Uave)

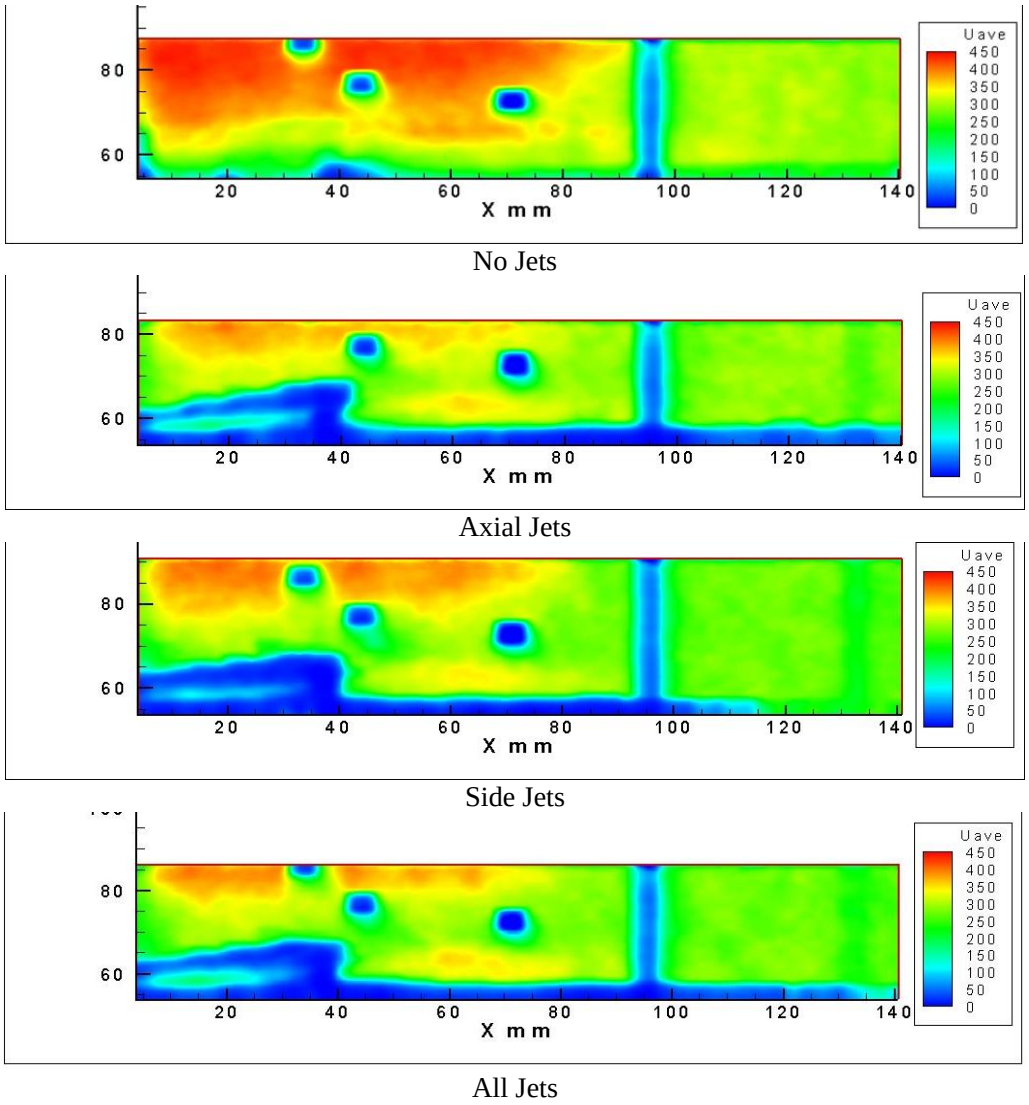

No Jets

Axial Jets

Side Jets

All Jets

Figure 52. Test Article 1 Centerline PIV Uave in meters/second. The trailing edge of the flow control device/leading edge of the cavity is at 40mm. The trailing edge of the cavity is not in view.

Test Article Number 1 Off-Centerline PIV Average Velocity (Uave)

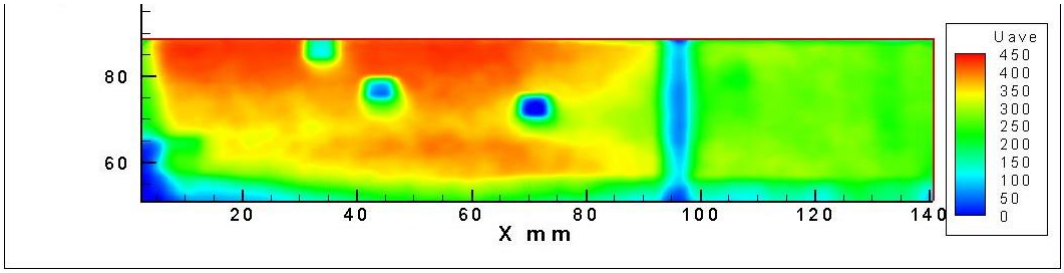

No Jets

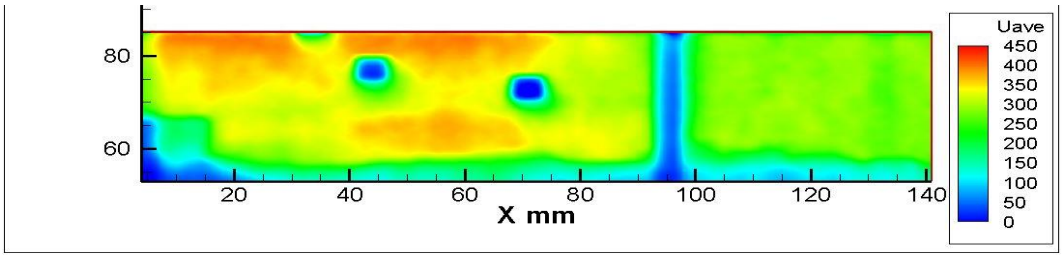

Axial Jets

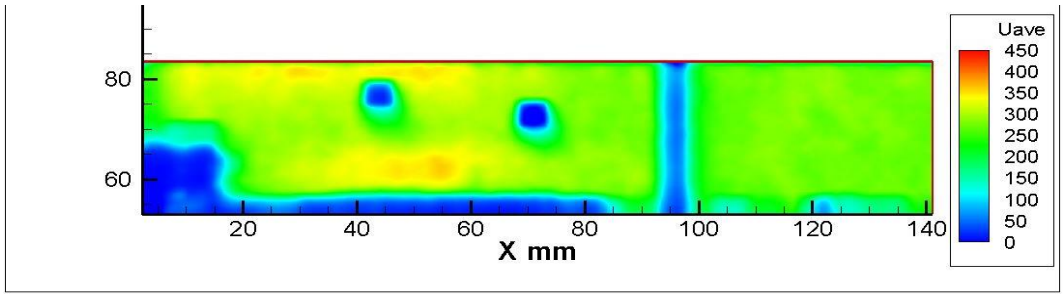

Side Jets

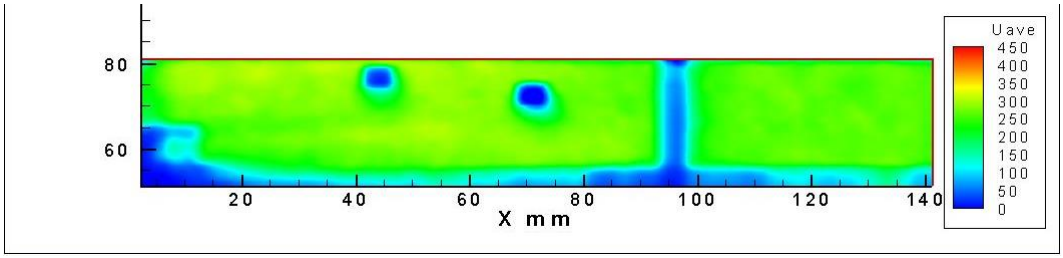

All Jets

Figure 53. Test Article 1 Off-Centerline PIV Uave, m/s. The trailing edge of the flow control device/leading edge of the cavity is at 40mm. The trailing edge of the cavity is not in view.

Test Article Number 2 Centerline PIV Average Velocity (Uave)

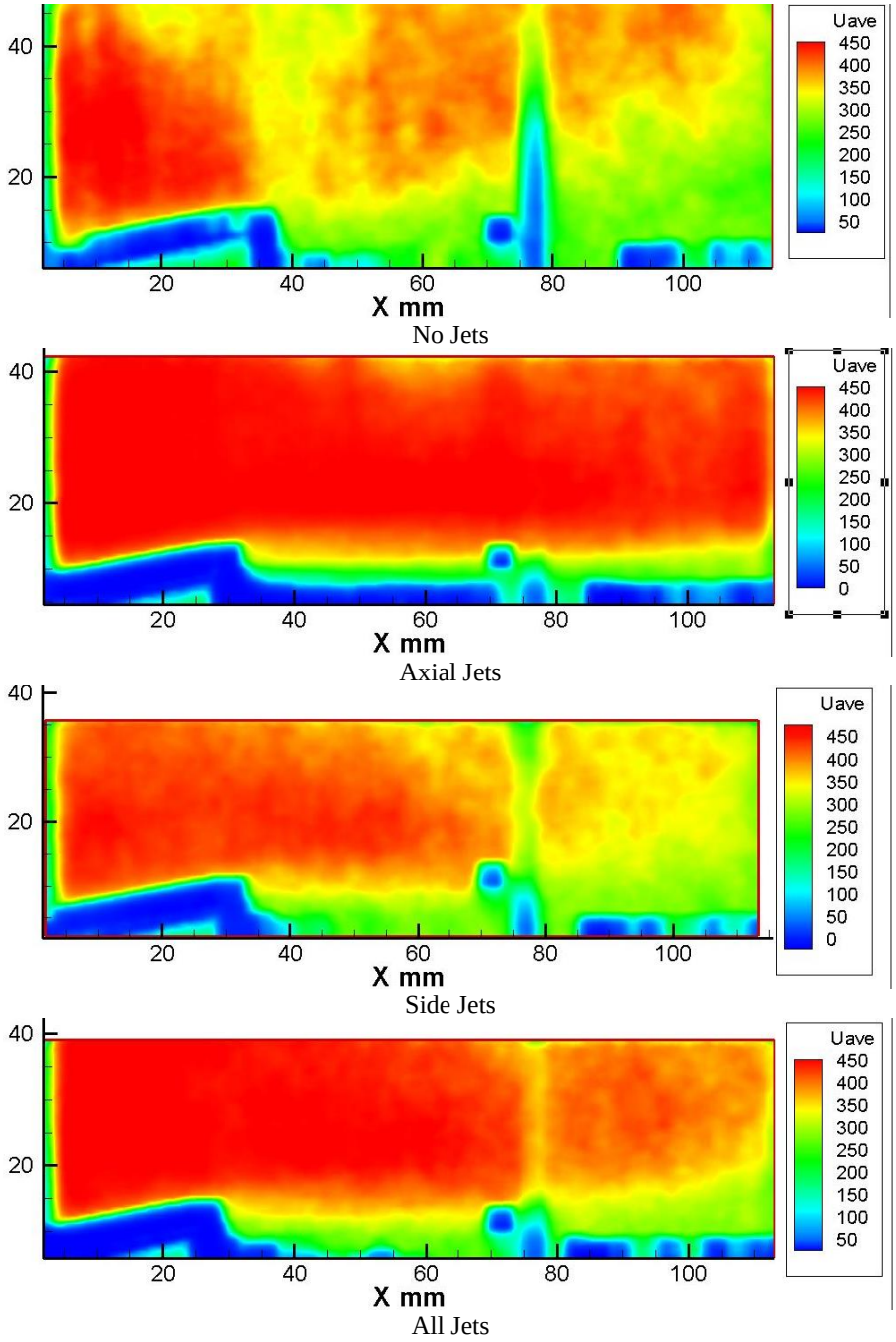

Figure 54. Test Article 2 Centerline PIV Uave, m/s. The trailing edge of the flow control device/leading edge of the cavity is at 40mm. The trailing edge of the cavity is at 95mm.

Test Article Number 2 Off-Centerline PIV Average Velocity (Uave)

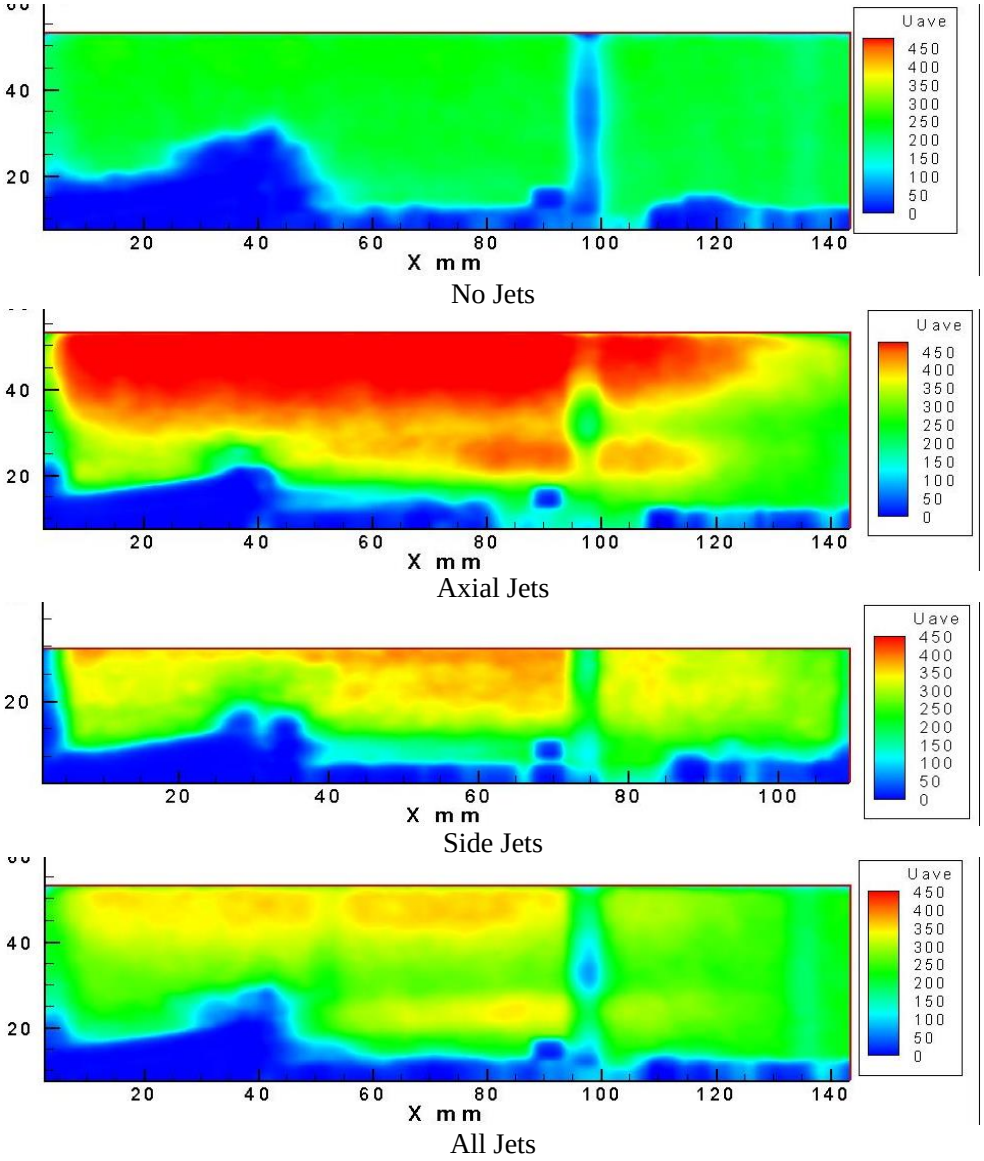

Figure 55. Test Article 2 Off-Centerline PIV Uave, m/s. The trailing edge of the flow control device/leading edge of the cavity is at 40mm. The trailing edge of the cavity is at 95mm.

Average Velocity, Vave

Vave is the average velocity in the **y** direction, or in this case toward the top of tunnel. This vertical component of velocity is important in the transport of fuel from the low velocity recirculation zone in the cavity out into the bulk of the airflow.

Figures 56 through 59 are y velocity average contour plots. In these plots the velocity is in meters/second. In Figure 56 the effect of injection is clear. When the simulated fuel is injected the vertical, or y, component of velocity increases well upstream of the increase in vertical velocity in the non-injection case. This increase in velocity can be clearly seen above the cavity in the fuel injection cases.

In the off-center PIV plots for test article 1, Figure 57, the results are similar to those depicted in Figure 56. In in Figure 57 the side jet plot shows a large average vertical velocity component above the cavity and extending well into the flow. In the side jets case the boundary behind the cavity is much smaller than in the other cases.

The results from PIV, taken on the cavity centerline, in regard to average vertical velocity are somewhat different for test article 2. Here, in Figure 58, the highest y values of Vave occur in the non-injection case. The axial injection reduces the effectiveness of the wedge-shaped flow device in generating velocity upwards into the freestream flow. The side jets, to a lesser extent, also reduce the penetration into the flow. However, when both side jets and axial jets are utilized then they interact together, and the result is somewhere between the axial jets and side jets injections, alone.

Test Article Number 1 Centerline PIV Average Velocity Vave

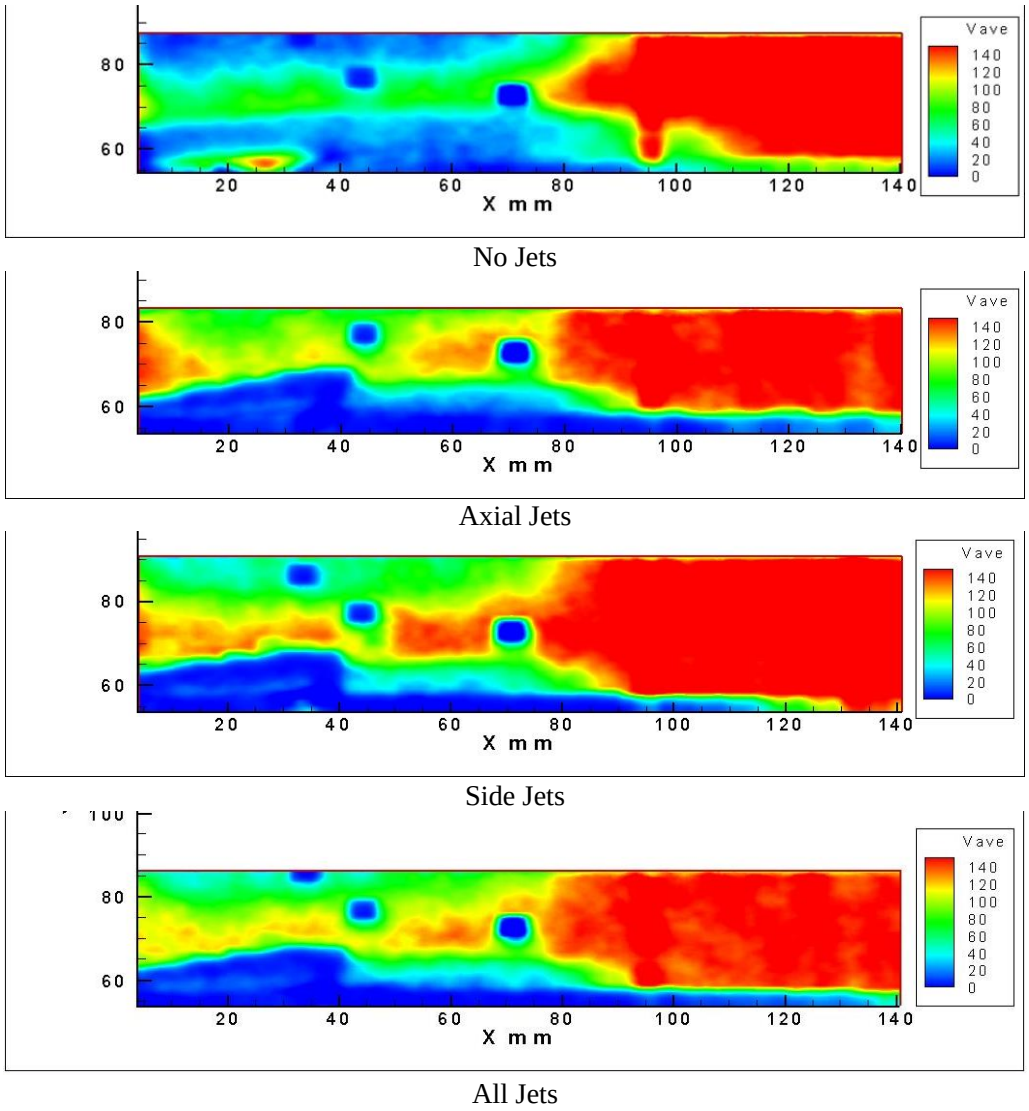

No Jets

Axial Jets

Side Jets

All Jets

Figure 56. Test Article 1 Centerline PIV Vave, m/s. The trailing edge of the flow device/leading edge of the cavity is at 40mm. The trailing edge of the cavity is not in view.

Test Article Number 1 Off-Centerline PIV Average Velocity (Vave)

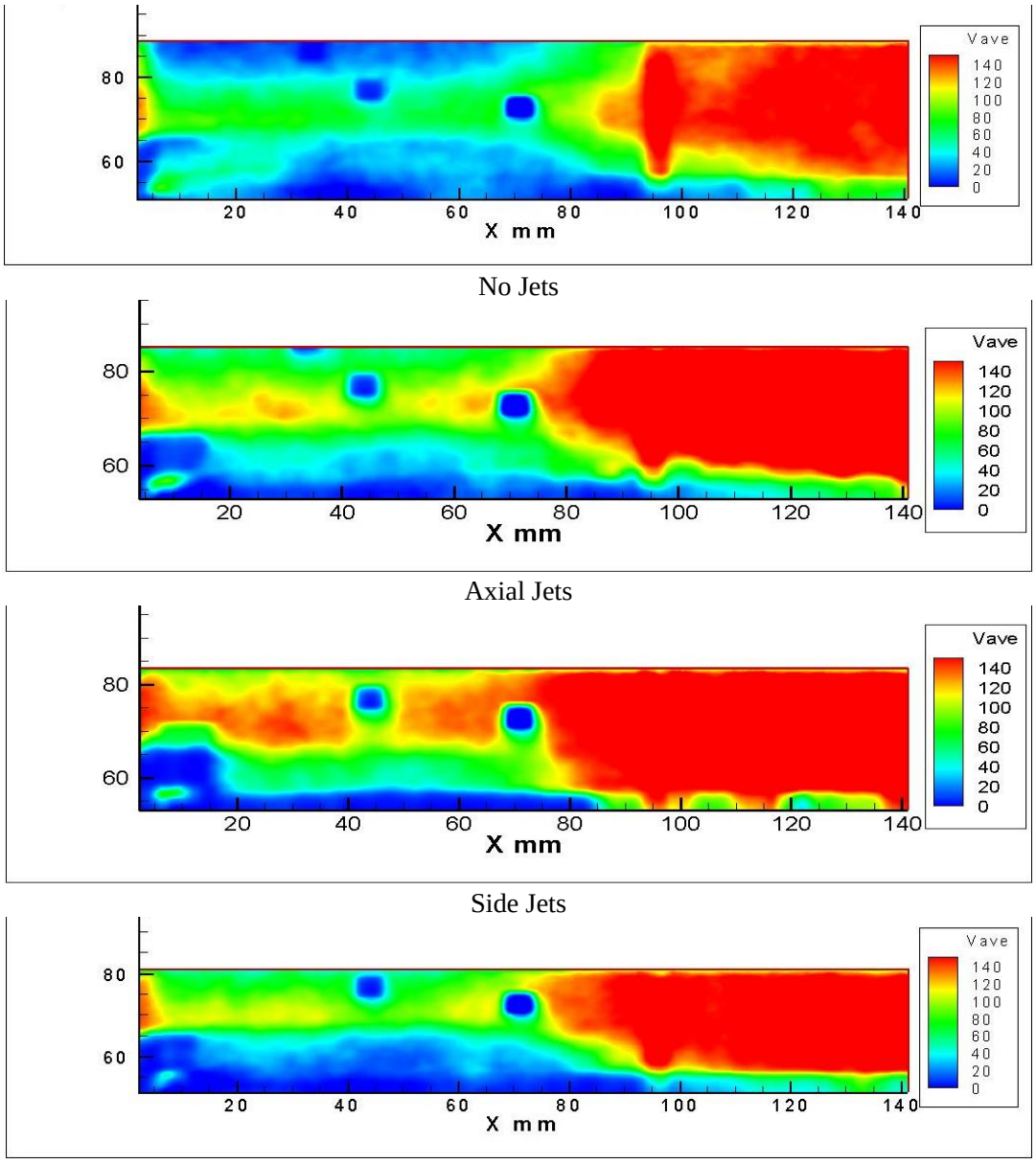

No Jets

Axial Jets

Side Jets

All Jets

Figure 57. Test Article 1 Off-Centerline PIV Vave, m/s. The trailing edge of the flow control device/leading edge of the cavity is at 40mm. The trailing edge of the cavity is not in view.

Test Article Number 2 Centerline PIV Average Velocity (Vave)

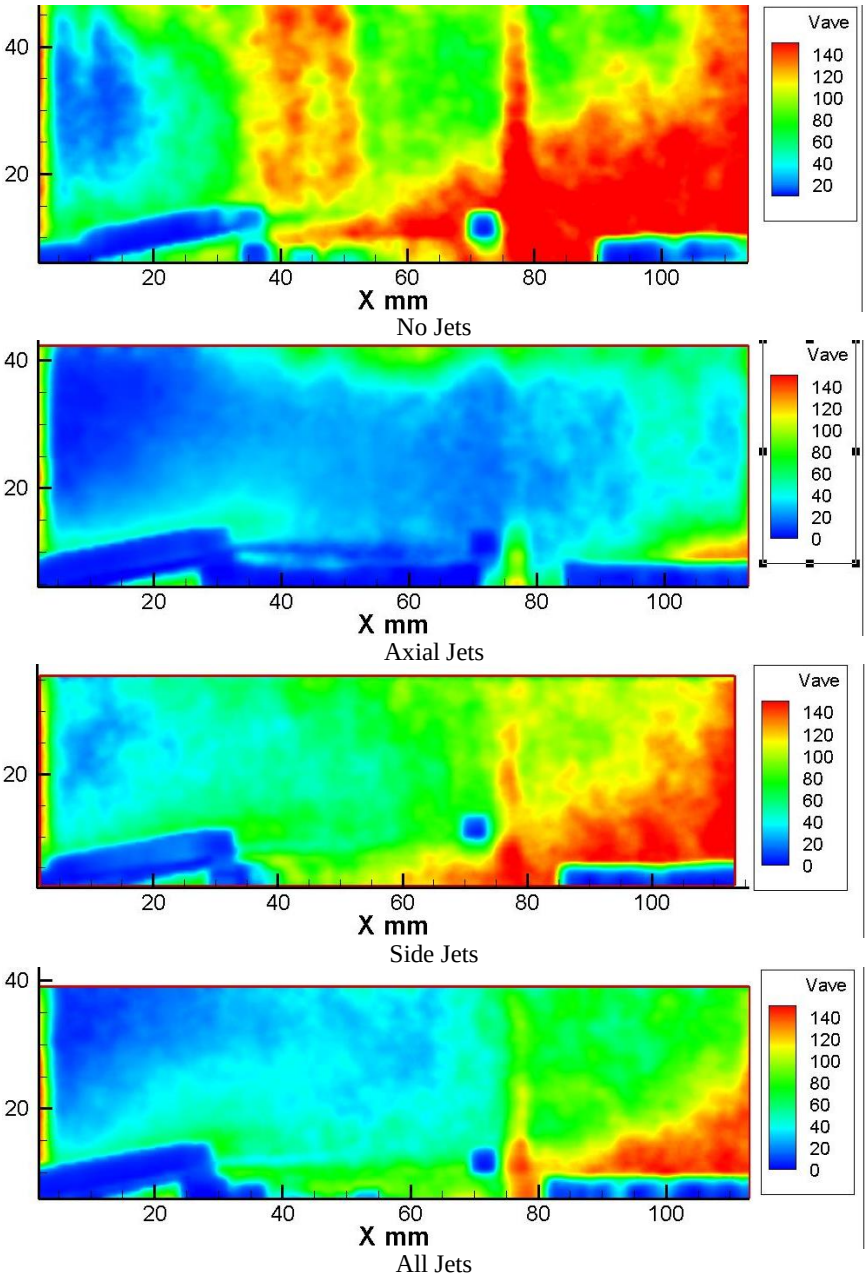

3

Figure 58. Test Article 2 Centerline PIV Vave, m/s. The trailing edge of the flow control device/leading edge of the cavity is at 40mm. The trailing edge of the cavity is at 95mm.

Test Article Number 2 Off-Centerline PIV Average Velocity (Vave)

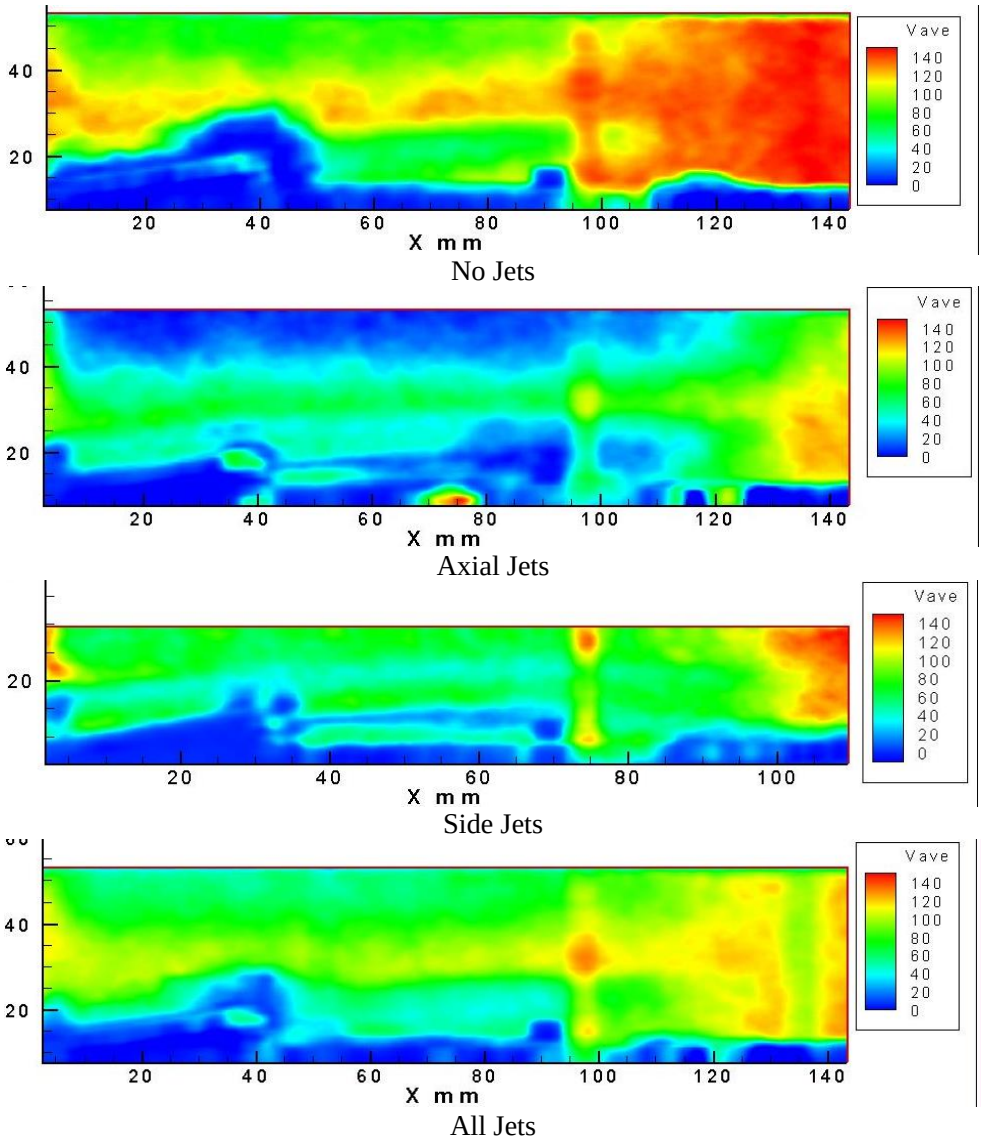

Figure 59. Test Article 2 Off-Centerline PIV Vave, m/s. The trailing edge of the flow control device/leading edge of the cavity is at 40mm. The trailing edge of the cavity is at 95mm.

When the PIV laser sheet is moved off of the cavity centerline, the results are similar, see Figure 59. In the case, where side jet injection is enabled, the y velocity component is larger. The horizontal streaks in the flow are indications of longitudinal vorticity.

Average Z Vorticity

Figures 60 through 63 are vorticity contour plots in the Z direction (out of the side of the test section). `For test article one, PIV measurements along the cavity centerline, Figure 60) show a distinct difference between the injection cases and the non-injection case. Streaks in the flow are clear indications that longitudinal vortexes are forming over the flow device and the cavity.

In the off-centerline case for test article 1, Figure 61, the shear layer at the top of the cavity is visible in the blowing cases. And in the blowing cases vorticity is being generated along the top of the flow device.

For test article 2, Figure 62 on the centerline, there is a shear laver visible above the cavity both with and without injection. There are areas of high vorticity along the top surface of the flow device and along the side edge of the flow device. Off-centerline, Figure 63, there are areas of high vorticity along the top of the flow device and above the cavity. In the injection cases these effects are stronger.

The data depicted in Figures 60 through Figure 63 confirms that we were able to generate vorticity with our flow device-cavity pairs.

Test Article Number 1 Centerline PIV Average Z Vorticity

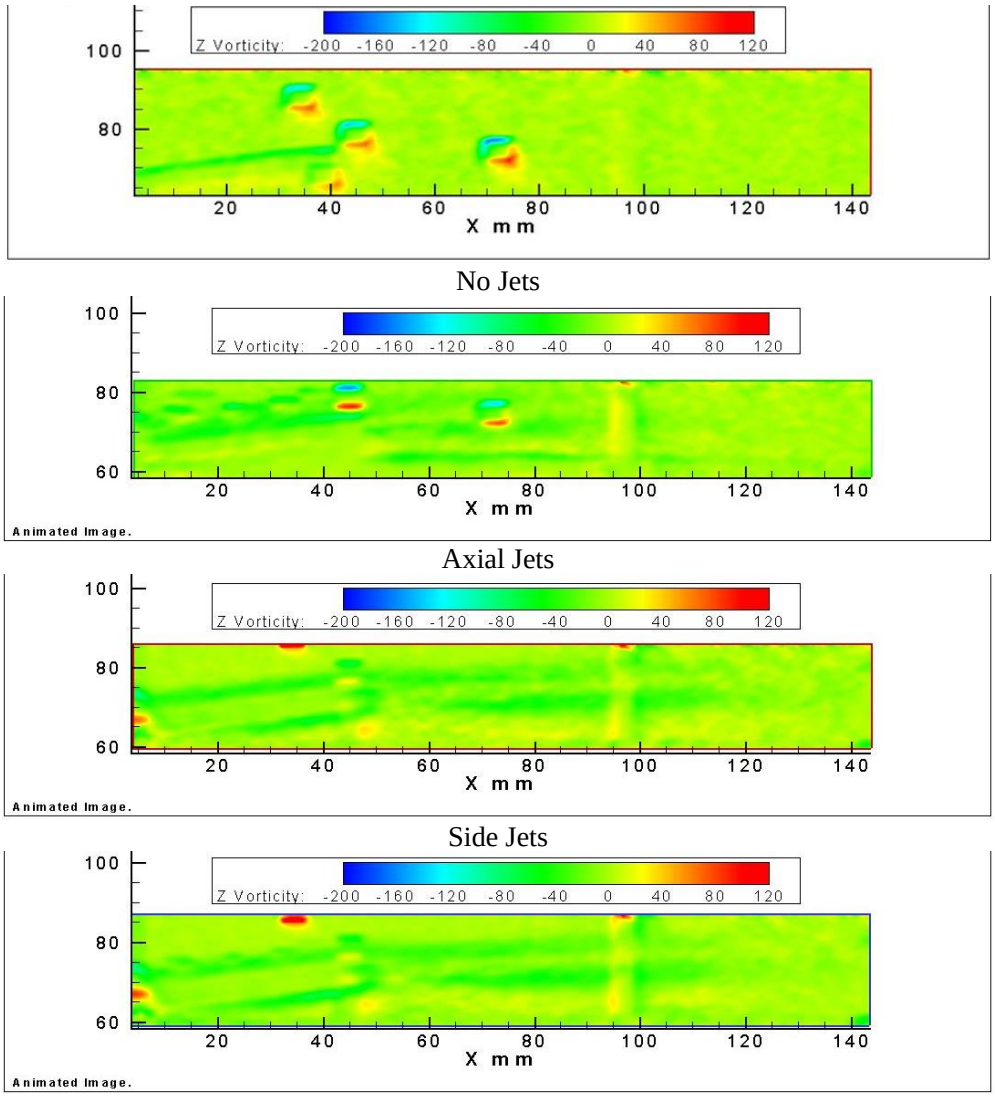

No Jets

Axial Jets

Side Jets

All Jets

Figure 60. Test Article 1 Centerline PIV Zvorticity. The trailing edge of the flow control device/leading edge of the cavity is at 40mm. The trailing edge of the cavity is not in view.

Test Article Number 1 Off-Centerline PIV Average Z Vorticity

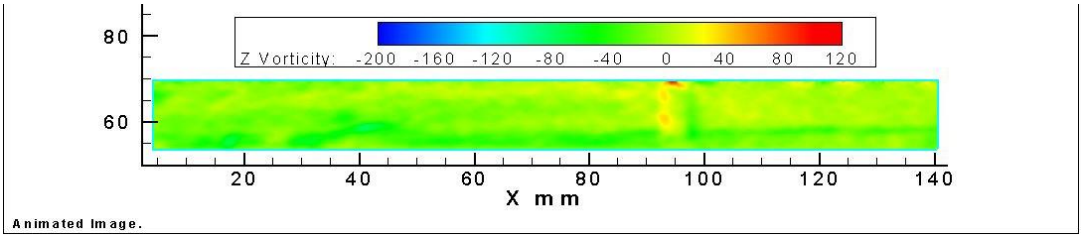

No Jets

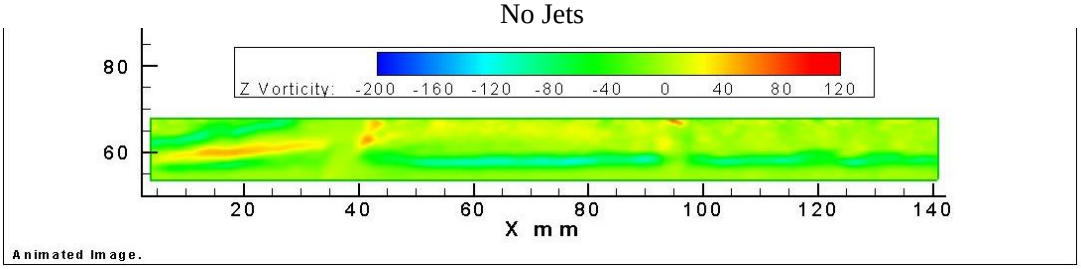

Axial Jets

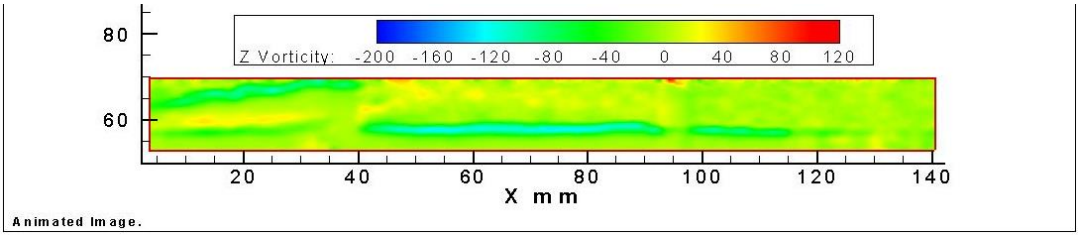

Side Jets

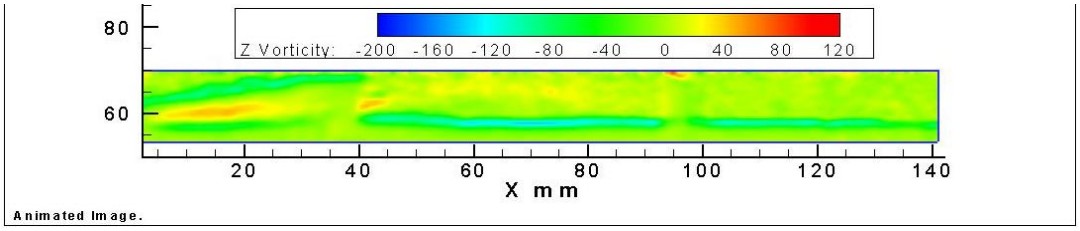

All Jets

Figure 61. Test Article 1 Off-Centerline PIV Zvorticity. The trailing edge of the control device/leading edge of the cavity is at 40mm. The trailing edge of the cavity is not in view.

Test Article Number 2 Centerline PIV Average Zvorticity

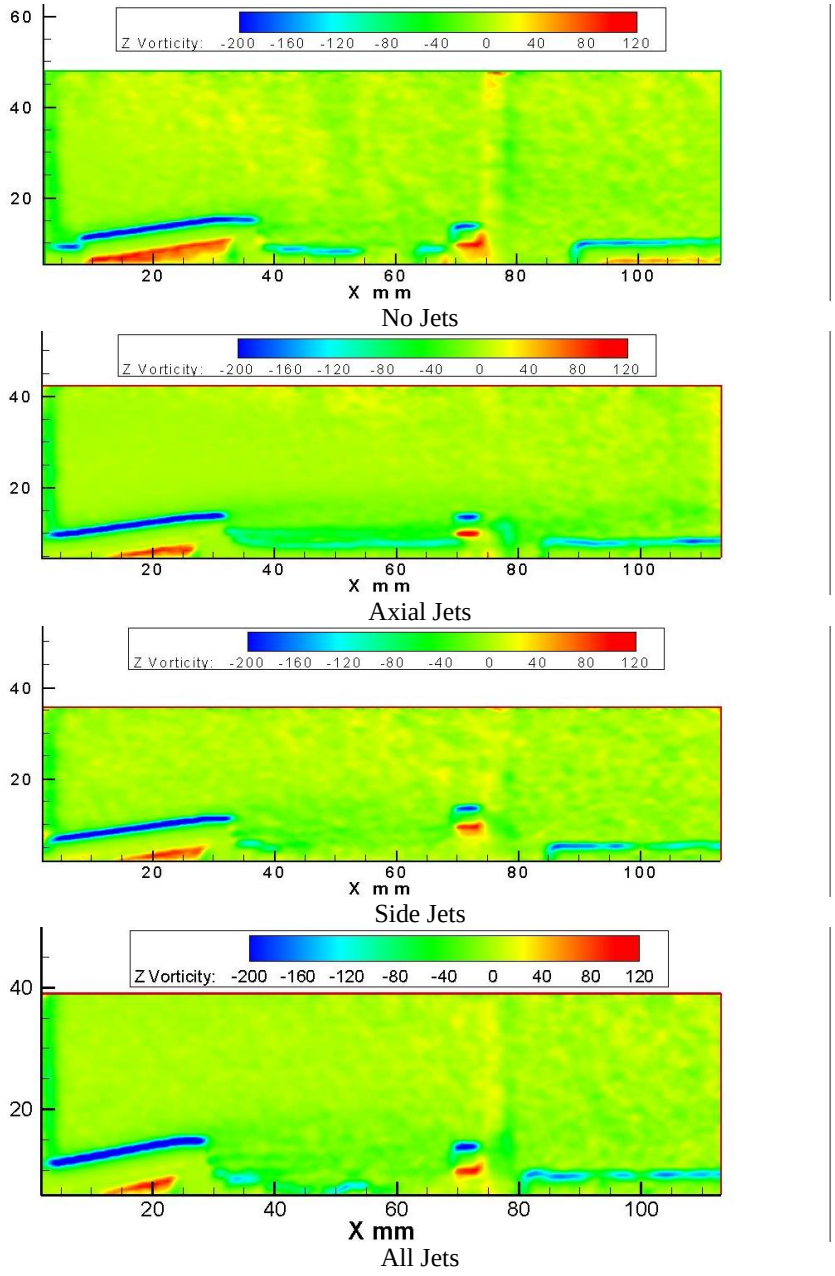

Figure 62. Test Article 2 Centerline PIV Zvorticity. The trailing edge of the flow control device/leading edge of the cavity is at 40mm. The trailing edge of the cavity is at 95mm.

Test Article Number 2 Off-Centerline PIV Average Z Vorticity

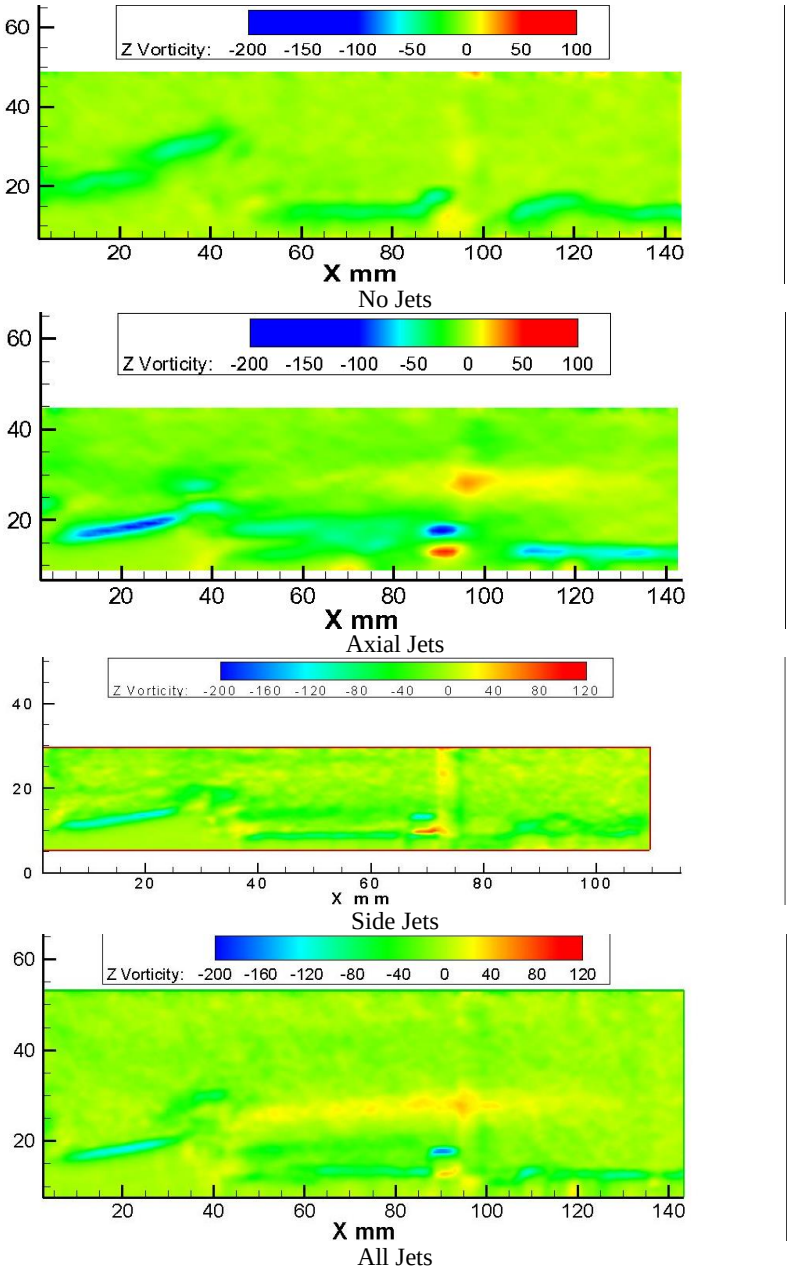

Figure 63. Test Article 2 Off-Centerline PIV Zvorticity. The trailing edge of the flow control device/leading edge of the cavity is at 40mm. The trailing edge of the cavity is at 95mm.

Turbulence intensity

Turbulent intensity is the ratio of the turbulent velocity fluctuations to the free stream velocity. In high flow quality wind tunnels this number is ideally very low. In our case the turbulent intensity provides a measure of how well mixing might occur. Areas with high turbulence intensity will be areas of high mixing.

In the case of test article 1, Figure 64 shows a distinct difference in turbulence intensity between the cases with injection and the case without injection. For the cases with injection, the areas of high turbulence intensity are around the flow control device, above the cavity, and along the boundary layer behind the cavity.

Off center measurements, depicted in Figure 65, indicate that there are areas of low intensity turbulence above the cavity in all cases. The intensity is higher just above the cavity in the injection cases. The boundary layer is an area of increased turbulence intensity for the injection cases, especially in the cases with side jets flowing.

In the case of test article 2, figure 66, on the centerline there are areas of high turbulent intensity along the flow device. The free stream turbulent intensity is lowest in the axial jets case. The axial jets case also has a region of high turbulent intensity along the top of the cavity.

In the off-center case for test article 2, figure 67, the lowest overall turbulence intensity is the case with axial injection. There are regions of high turbulence intensity along the flow device surfaces and along the top of the cavity. These areas are less intense on the axial injection case.

Test Article Number 1 Centerline PIV Turbulence intensity

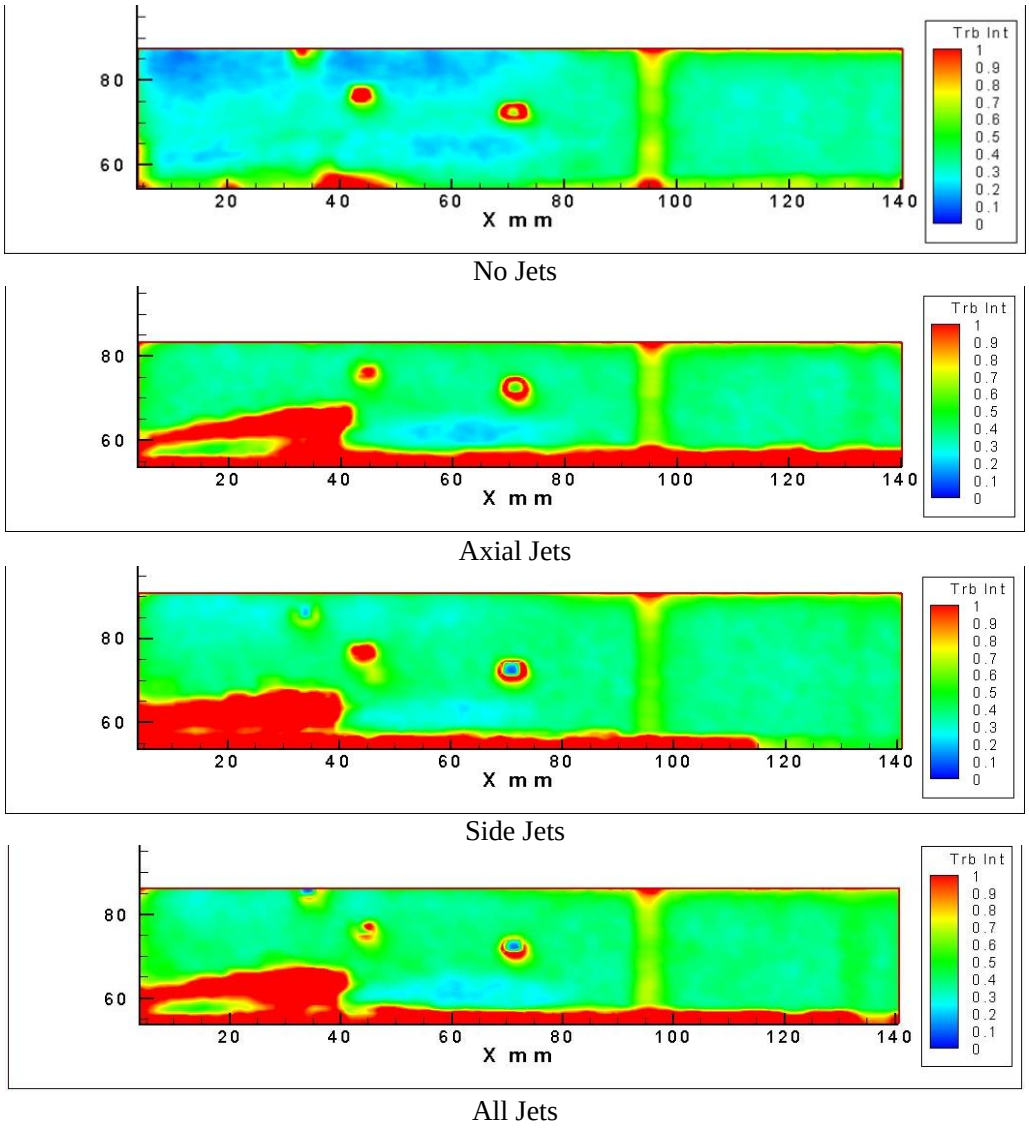

No Jets

Axial Jets

Side Jets

All Jets

Figure 64. Test Article 1 Centerline PIV Turbulence Intensity. The trailing edge of the flow control device/leading edge of the cavity is at 40mm. The trailing edge of the cavity is not in view.

Test Article Number 1 Off-Centerline PIV Turbulence intensity

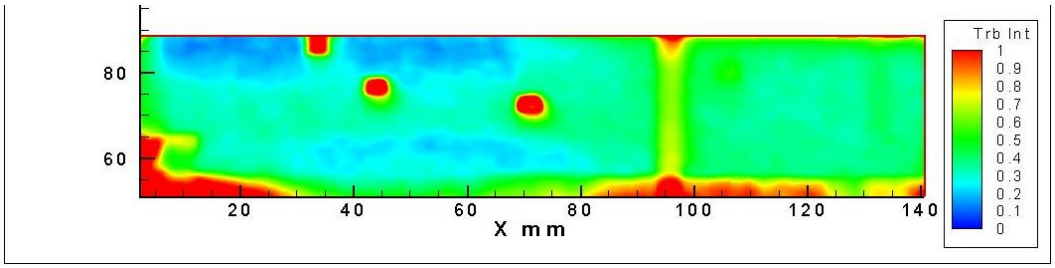

No Jets

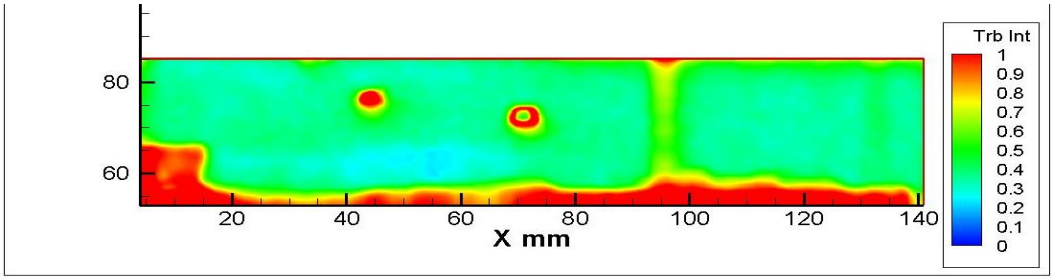

Axial Jets

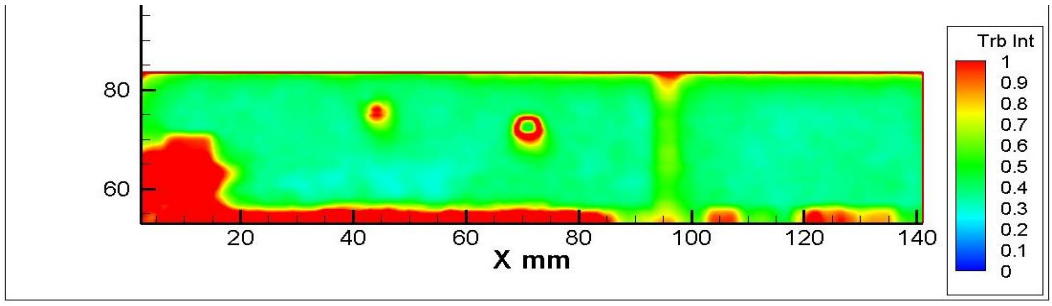

Side Jets

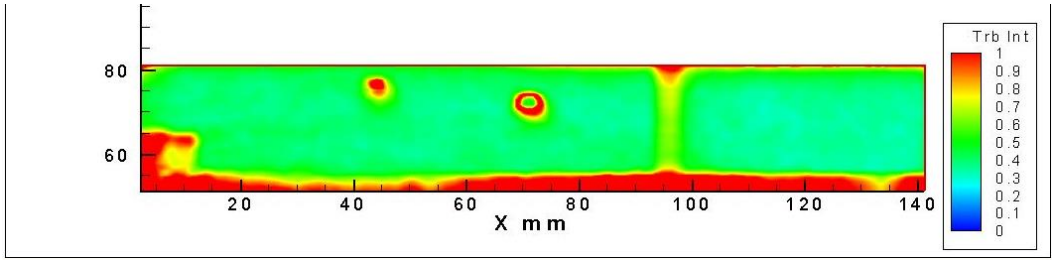

All Jets

Figure 65. Test Article 1 Off-Centerline PIV Turbulence Intensity. The trailing edge of the flow control device/leading edge of the cavity is at 40mm. The trailing edge of the cavity is not in view.

Test Article Number 2 Centerline PIV Turbulence intensity

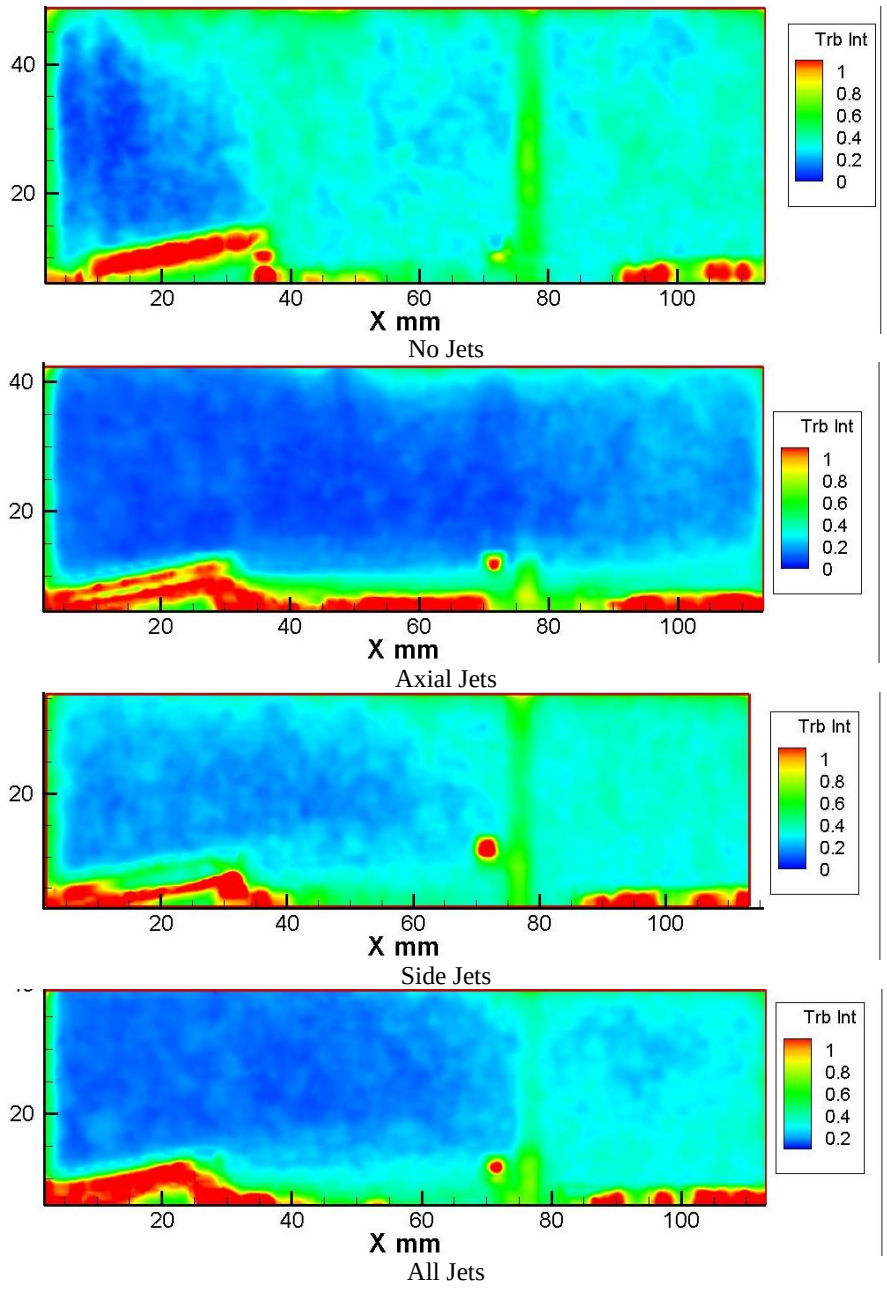

Figure 66. Test Article 2 Centerline PIV Turbulence Intensity. The trailing edge of the flow control device/leading edge of the cavity is at 40mm. The trailing edge of the cavity is at 95mm.

Test Article Number 2 Off-Centerline PIV Turbulence intensity

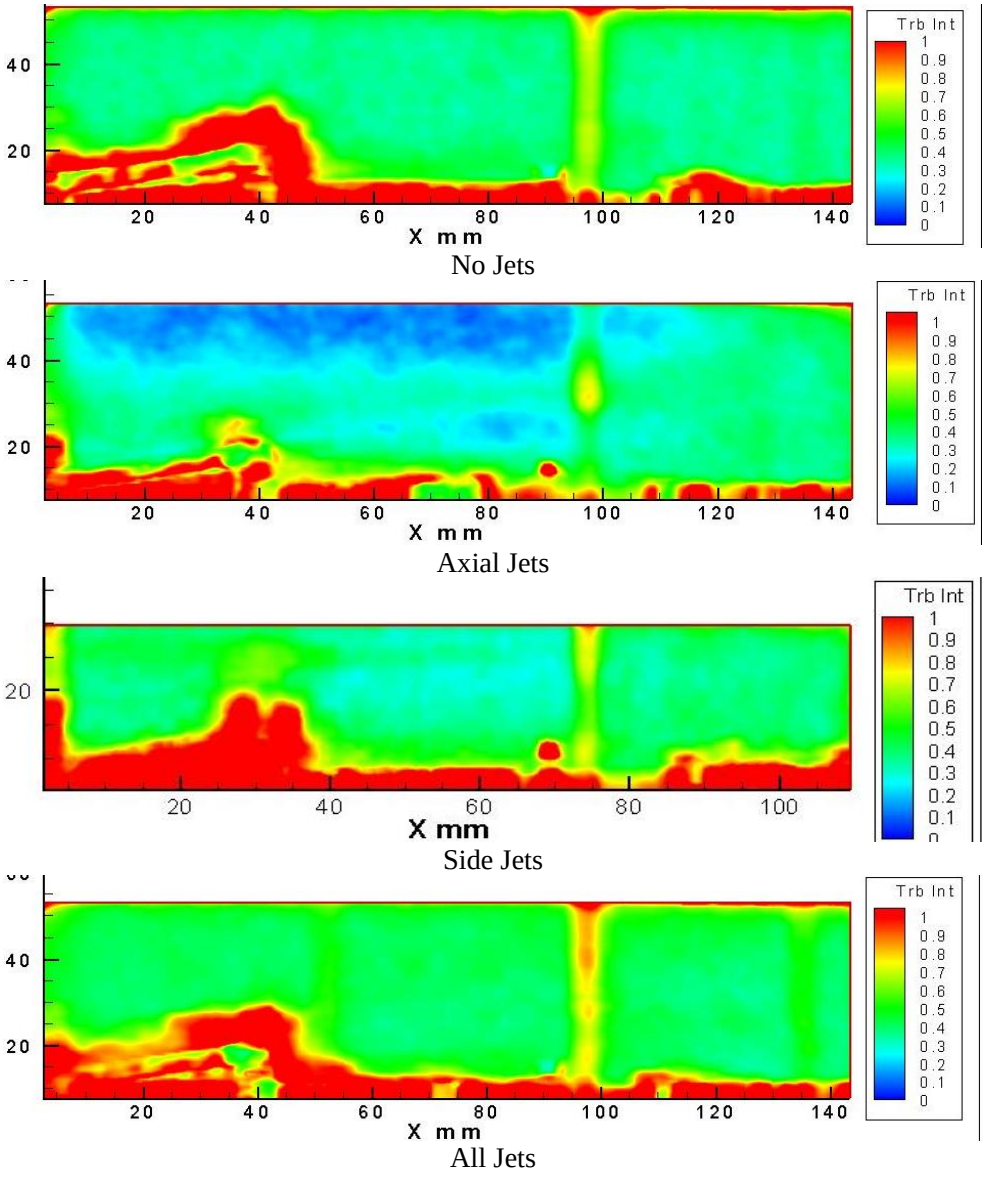

Figure 67. Test Article 2 Off-Centerline PIV Turbulence Intensity. The trailing edge of the flow control device/leading edge of the cavity is at 40mm. The trailing edge of the cavity is at 95mm.

Reynolds Stress

Time averaged Reynolds stresses were computed and displayed in the contour plots. If we had a two-dimensional incompressible flow the xx and yy components would be zero. However, we have a compressible flow that has distinct turbulent fluctuations in all three dimensions.

xy Reynold Stress

The xy component of the Reynolds stress tensor is the Reynolds shear stress. In Figure 68 the Reynolds shear stress is higher for flows with injection in the area around the flow device and along the cavity surface and tunnel wall. This is especially true for the axial jets condition.

In Figure 69 where the PIV laser sheet is off the centerline the results are similar to those in Figure 68. However, the effects of the side jets are now more evident. This is likely due to their close proximity to the measurement location.

For test article 2, on the cavity centerline (Figure 70), the greatest Reynolds shear stress is evidenced near the flow device in the non-blowing case. Things change when you take the measurement off center, Figure 71. Here the lowest Reynolds shear stress occurs with Axial Jets flowing. There are large areas of Reynolds stress around the flow device and in the boundary and shear layers over the cavity.

Test Article Number 1 Centerline PIV xy Reynolds Stress

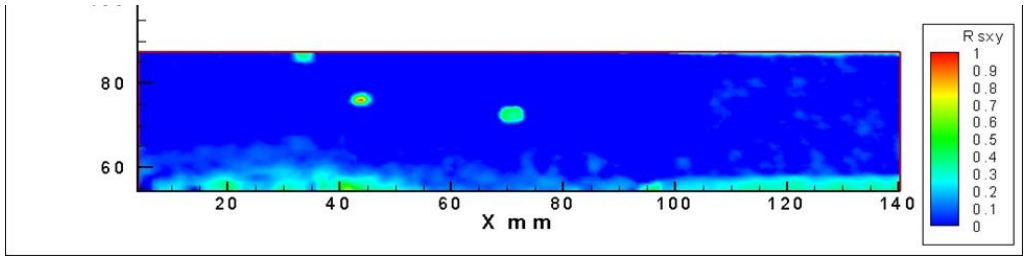

No Jets

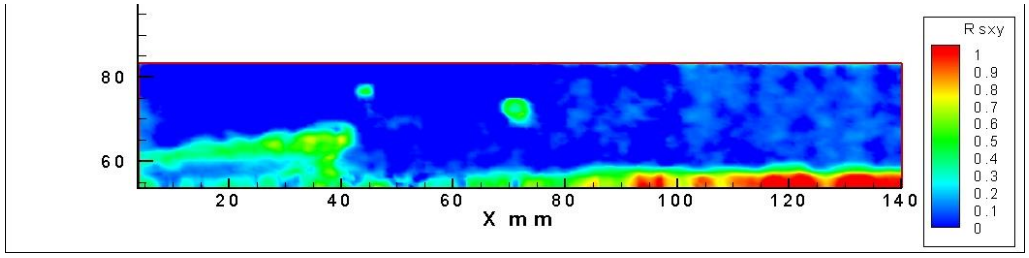

Axial Jets

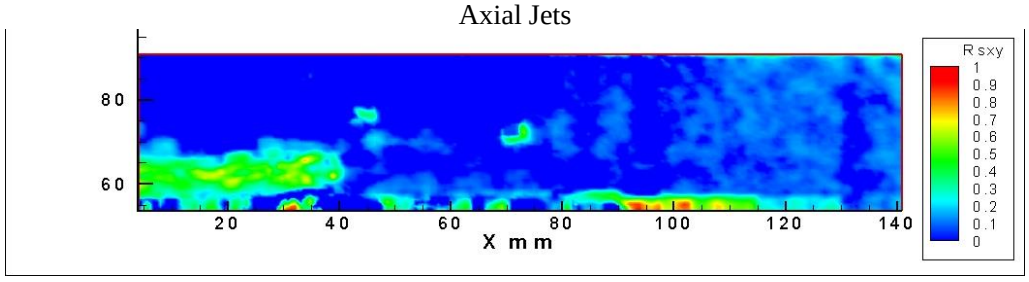

Side Jets

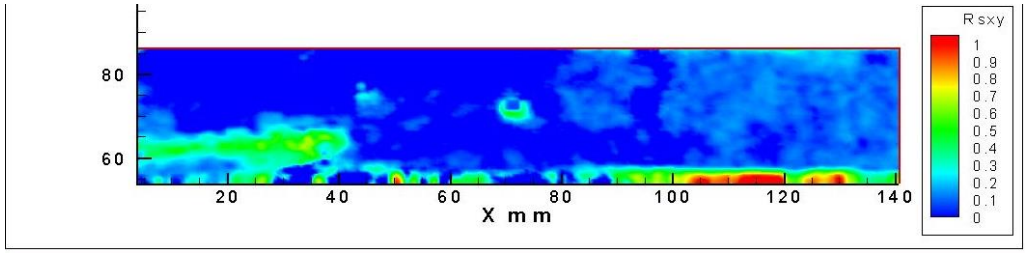

All Jets

Figure 68. Test Article 1 Centerline PIV xy Reynolds Stress. The trailing edge of the flow control device/leading edge of the cavity is at 40mm. The trailing edge of the cavity is not in view.

Test Article Number 1 Off-Centerline PIV xy Reynolds Stress

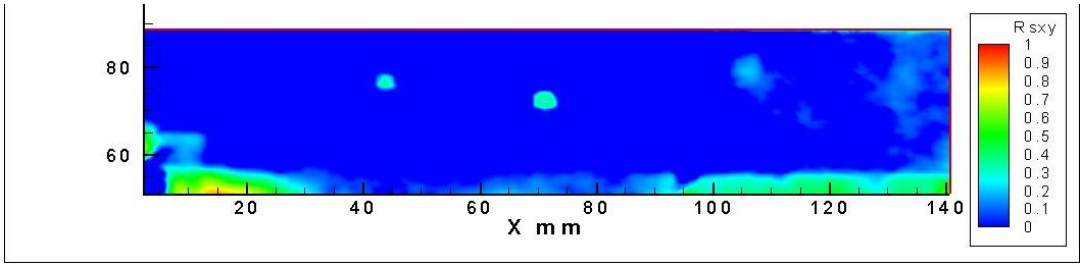

No Jets

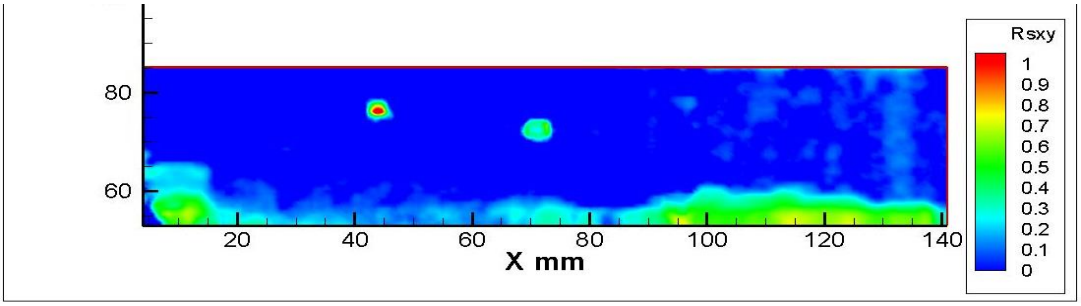

Axial Jets

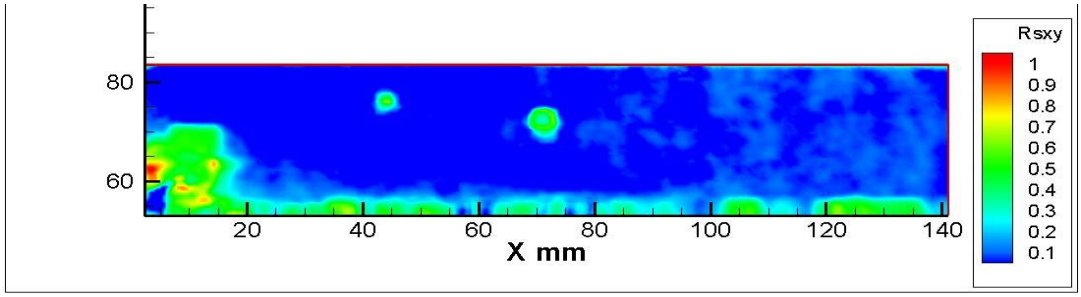

Side Jets

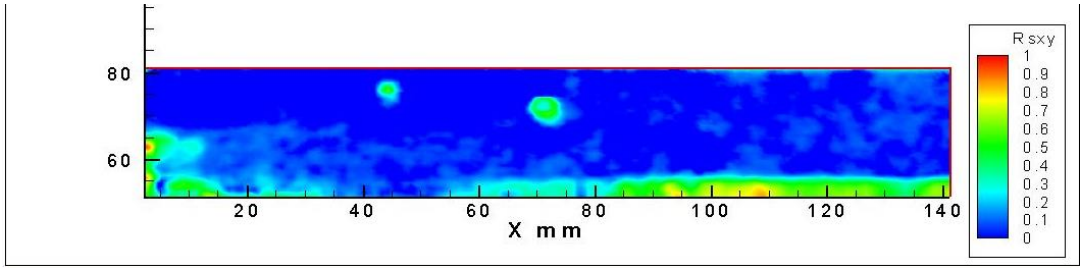

All Jets

Figure 69. Test Article 1 Off-Centerline PIV xy Reynolds Stress. The trailing edge of the flow control device/leading edge of the cavity is at 40mm. The trailing edge of the cavity is not in view.

Test Article Number 2 Centerline PIV xy Reynolds Stress

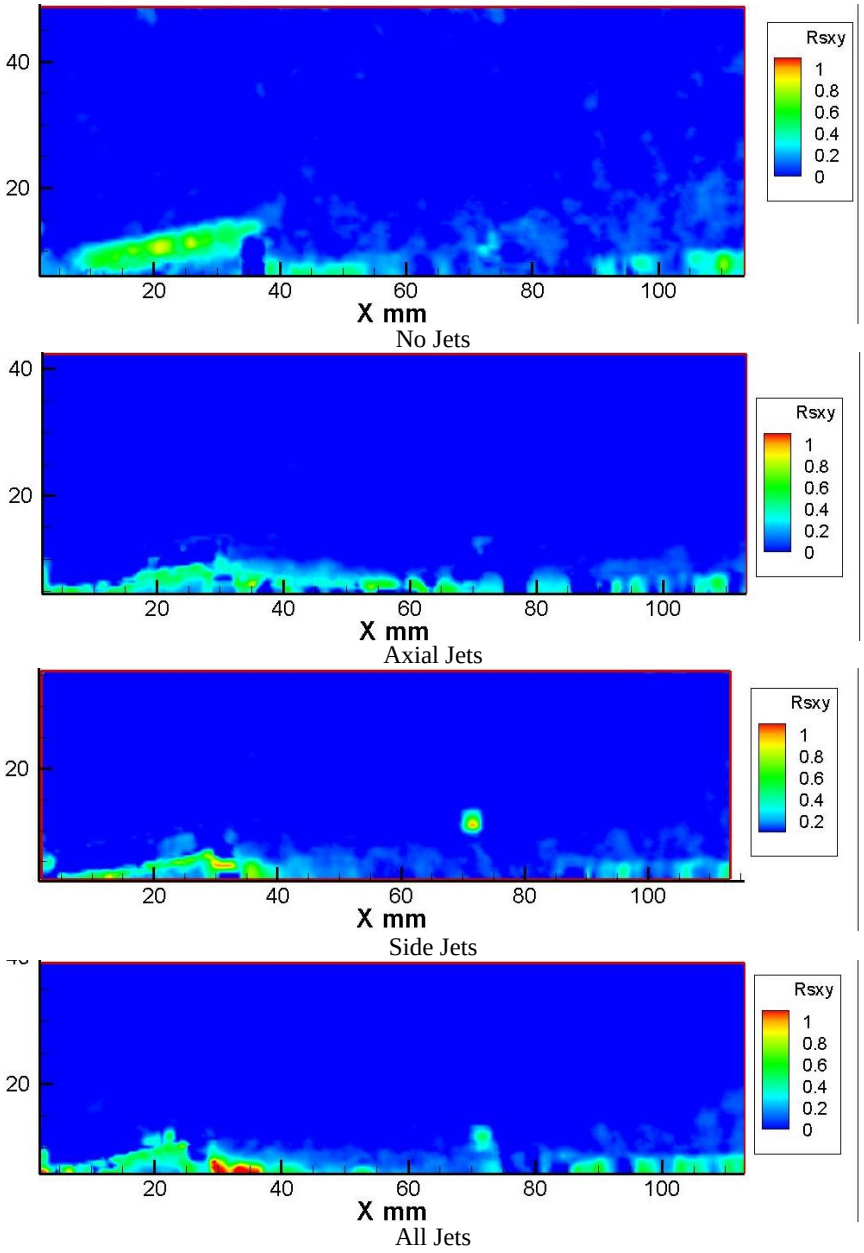

Figure 70. Test Article 2 Centerline PIV xy Reynolds Stress. The trailing edge of the flow control device/leading edge of the cavity is at 40mm. The trailing edge of the cavity is at 95mm.

Test Article Number 2 Off-Centerline PIV xy Reynolds Stress

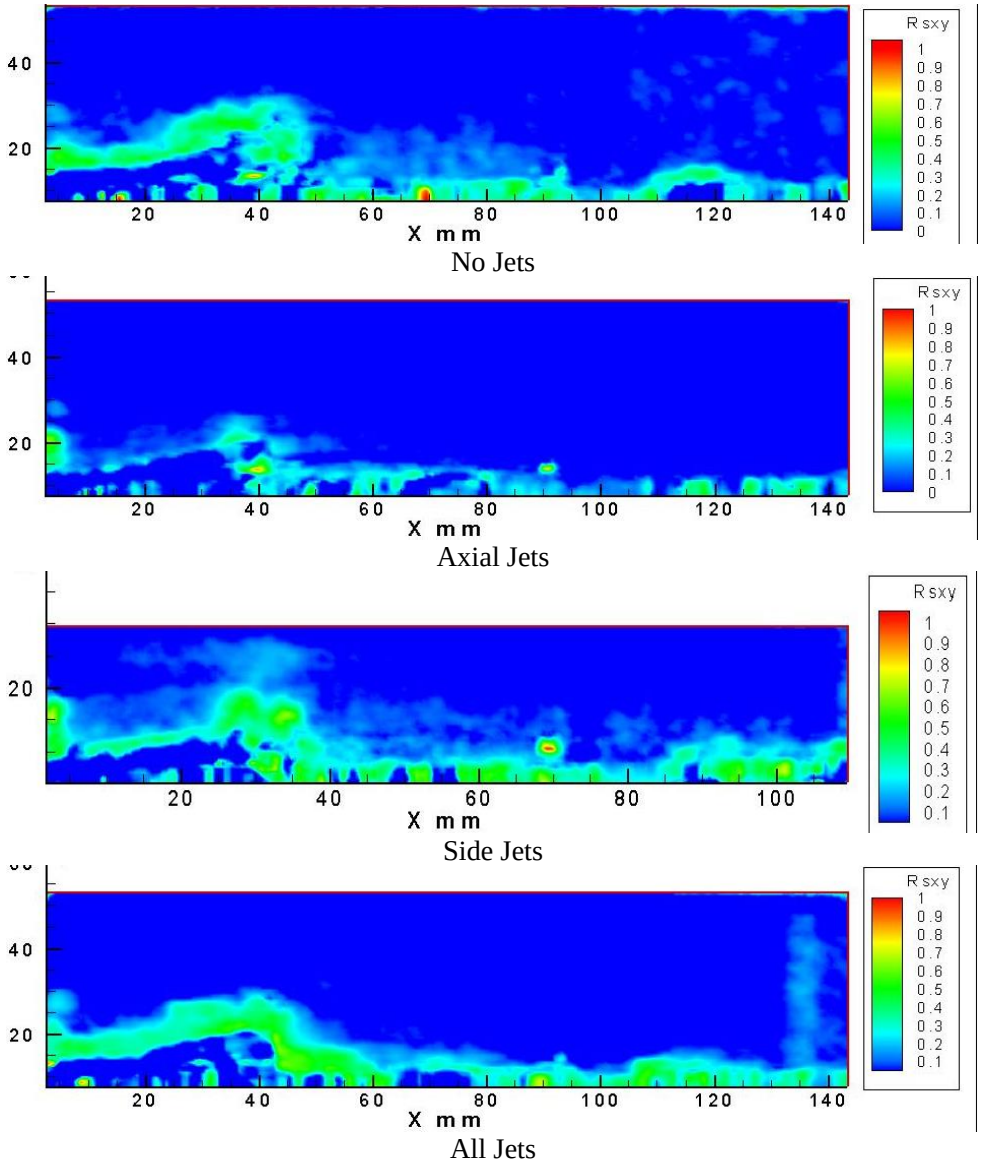

Figure 71. Test Article 2 Off-Centerline PIV xy Reynolds Stress. The trailing edge of the flow control device/leading edge of the cavity is at 40mm. The trailing edge of the cavity is at 95mm.

xx Reynolds Stress

For test article 1, Figure 72 displays the xx Reynolds stress. These plots are very similar to xy Reynolds stress for test article 1, Figure 68. In all cases there is a low stress area above the cavity surface. The cases with injection have a much greater Reynolds stress near the flow device and along the cavity surface and the boundary layer behind the cavity.

Off centerline, Figure 73, the results are very similar to those for xy Reynolds stress Figure 68 and those for the centerline measurements, except for the lower xx Reynolds stress values near the flow device.

For test article 2, Figure 74, the lowest xx Reynolds stresses, in the free stream occurs, with axial blowing. The highest xx Reynolds stresses occurs with no jets flowing. There are high levels of xx Reynolds stress near the flow device surface and the axial jets flowing has a thick layer of high xx Reynolds stress over the cavity.

The off-center measurements in Figure 75 indicate that the lowest xx Reynolds stress is the no injection case. This case also does not have an area of high Reynolds stress at the top of the cavity, however all of the injection cases do.

Test Article Number 1 Centerline PIV xx Reynolds Stress

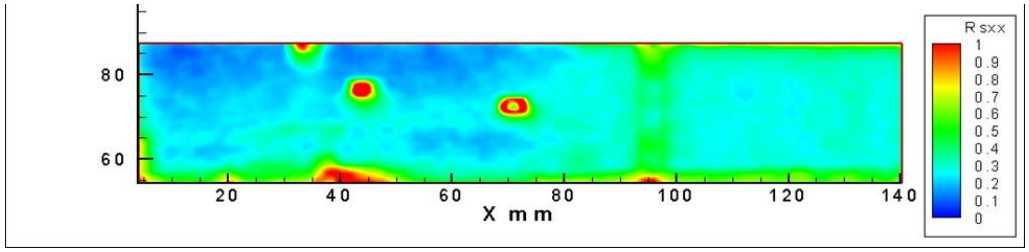

No Jets

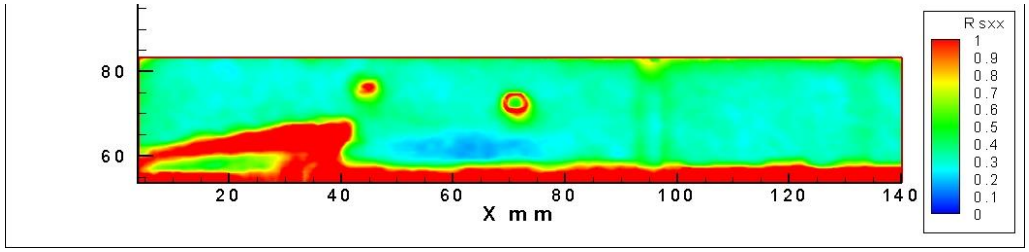

Axial Jets

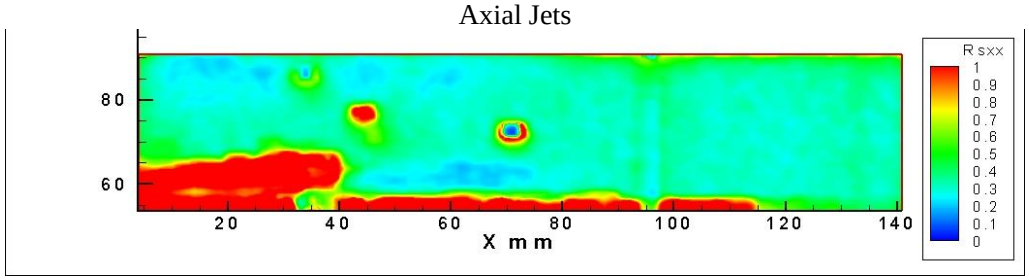

Side Jets

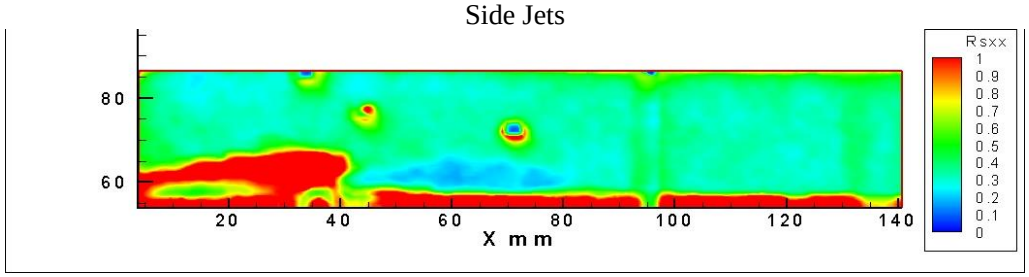

All Jets

Figure 72. Test Article 1 Centerline PIV xx Reynolds Stress. The trailing edge of the flow control device/leading edge of the cavity is at 40mm. The trailing edge of the cavity is not in view.

Test Article Number 1 Off-Centerline PIV xx Reynolds Stress

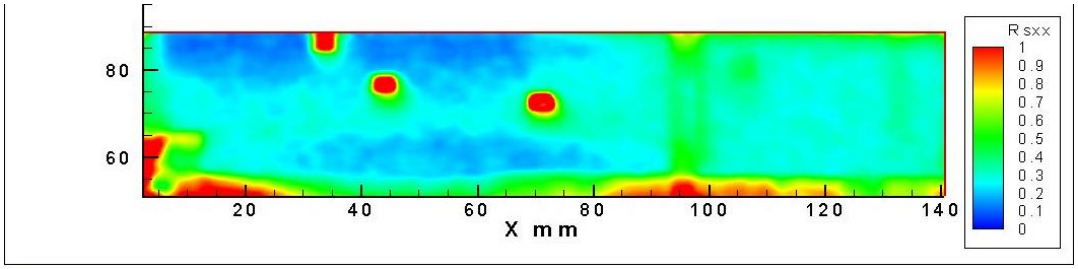

No Jets

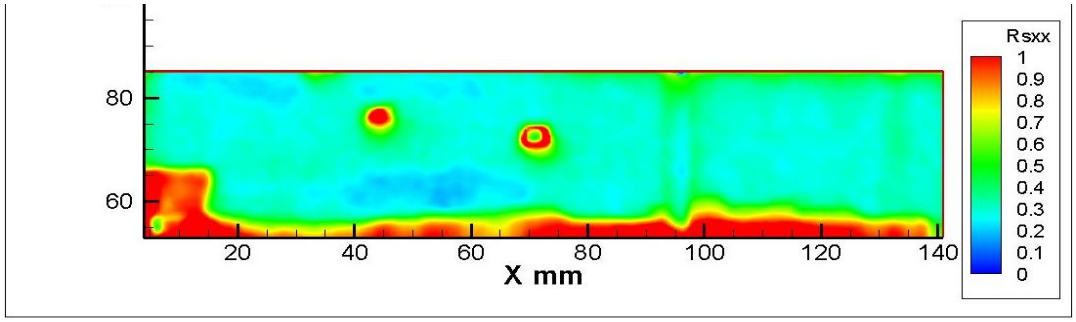

Axial Jets

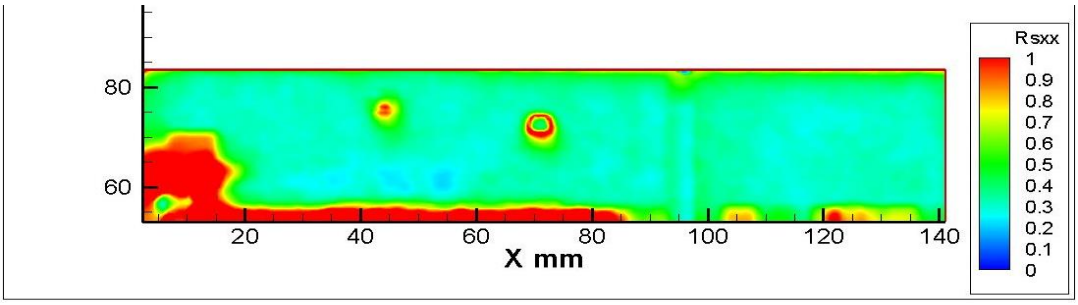

Side Jets

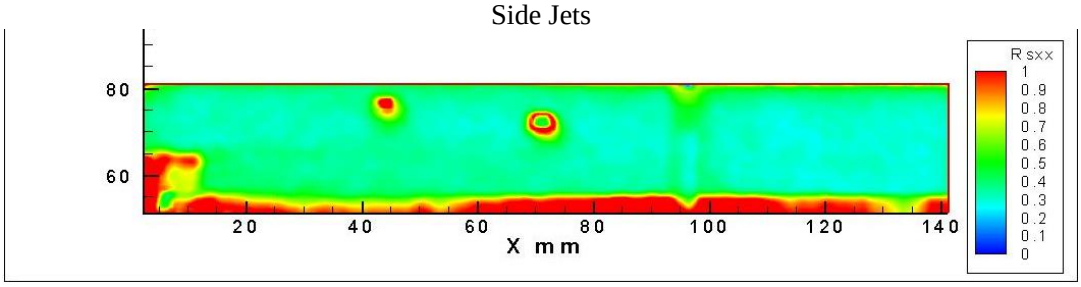

All Jets

Figure 73. Test Article 1 Off-Centerline PIV xx Reynolds Stress. The trailing edge of the flow control device/leading edge of the cavity is at 40mm. The trailing edge of the cavity is not in view.

Test Article Number 2 Centerline PIV xx Reynolds Stress

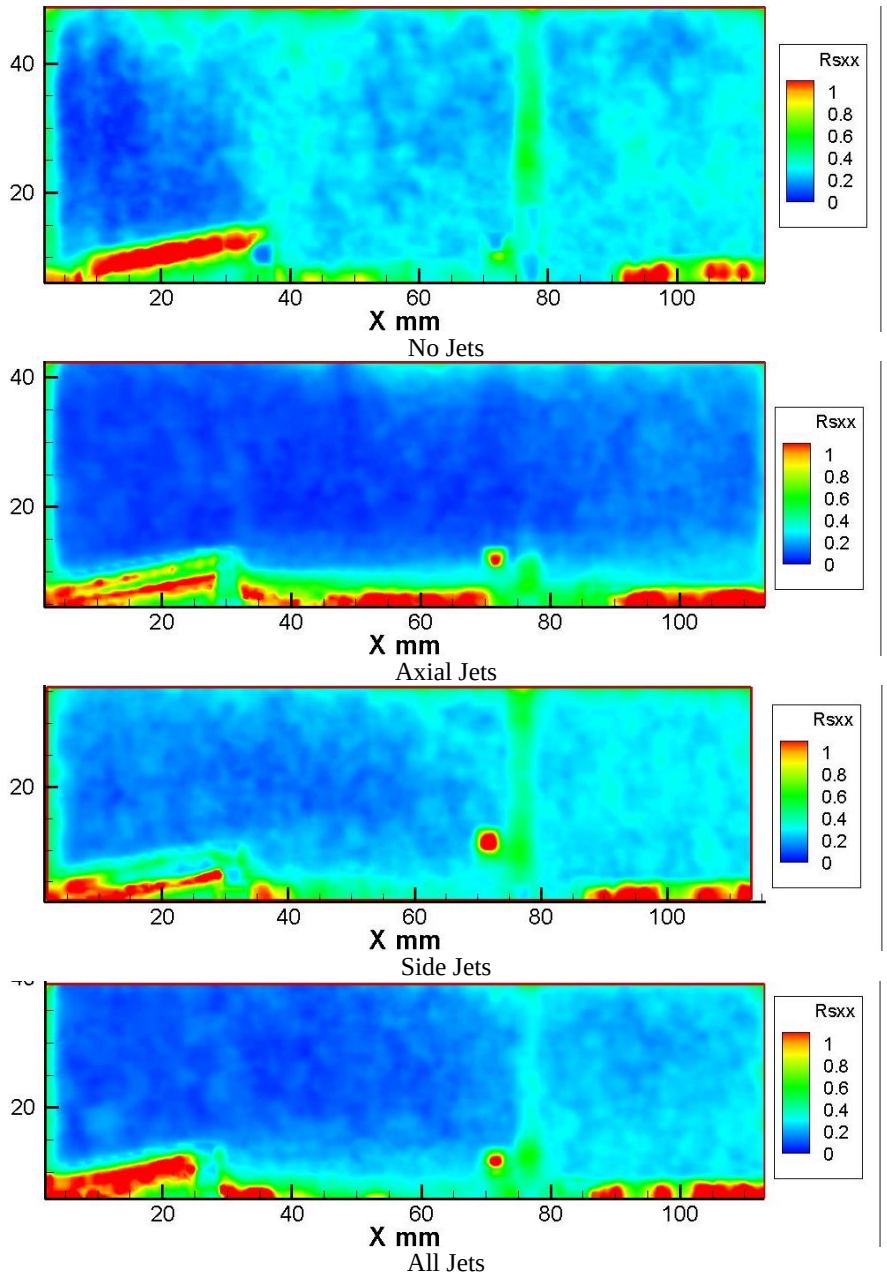

Figure 74. Test Article 2 Centerline PIV xx Reynolds Stress. The trailing edge of the flow control device/leading edge of the cavity is at 40mm. The trailing edge of the cavity is at 95mm.

Test Article Number 2 Off-Centerline PIV xx Reynolds Stress

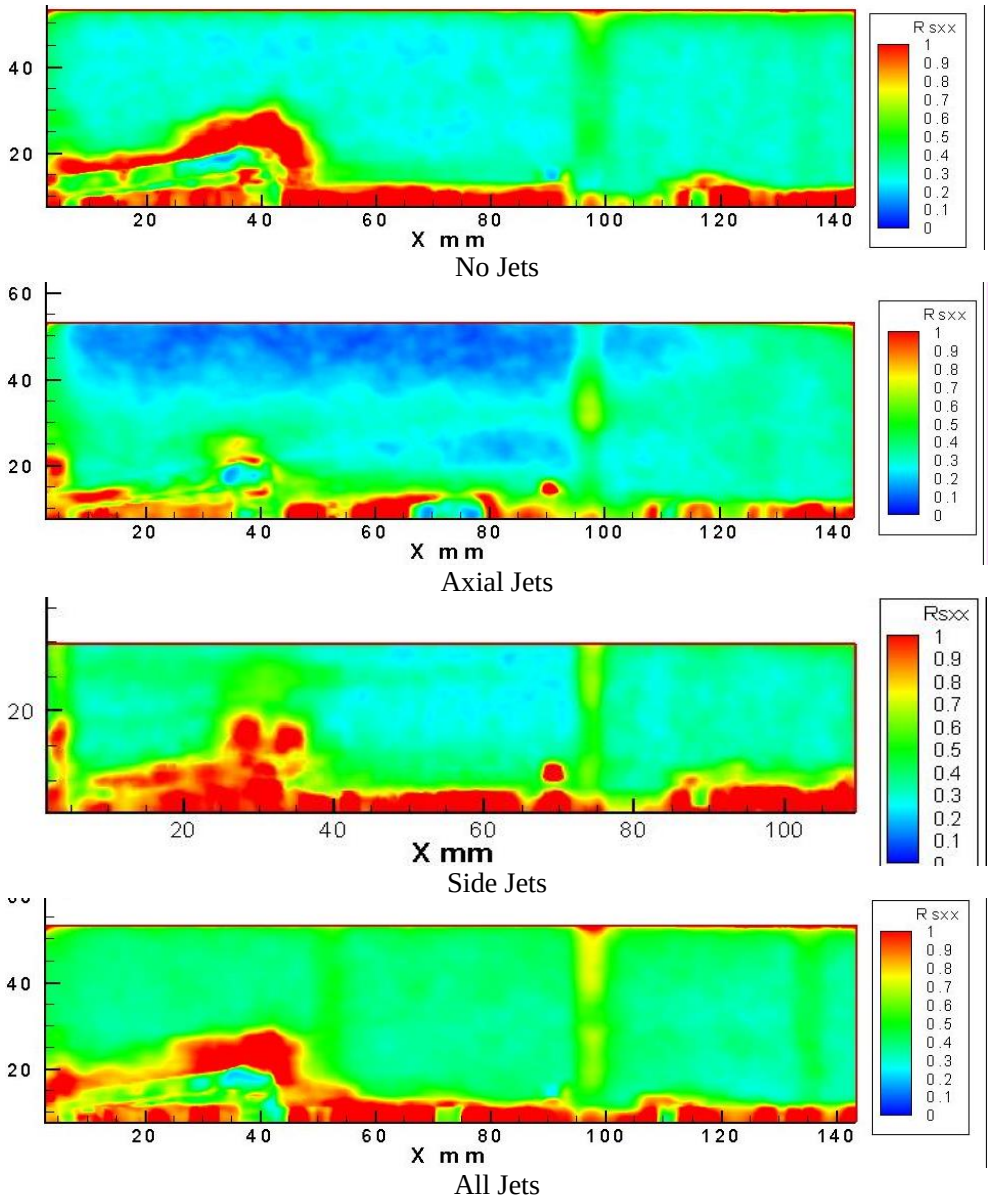

Figure 75. Test Article 2 Off-Centerline PIV xx Reynolds Stress. The trailing edge of the flow control device/leading edge of the cavity is at 40mm. The trailing edge of the cavity is at 95mm.

yy Reynolds Stress

In Figure 76 the centerline yy Reynold stresses for test article 1 are displayed. Like the xy and yy Reynolds stress cases, the lowest stresses occur in the non-injection case. There are some higher stress areas near the flow device in the injection cases and there is a clear low stress area above the cavity in all cases.

Figure 77 shows similar results for the off-center case. This same low stress area is exhibited above the cavity in each case. There is a higher stress level at the top of the cavity in the side jet case, which is likely due to the proximity of the measurement to the side jet.

For test article 2 the yy Reynolds stresses, Figures 78 and 79, look much like the xx Reynolds stresses presented in figure 74 and figure 75. The lowest stresses occur with the axial jets flowing. There are high Reynolds stress areas at the rear of the flow device in the cases where the measurements were taken on the centerline, Figure 78. The shear layer is visable just above the cavity in the side jet and all jets cases.

In the off-center Reynold stress plots for test article 2 (Figure 79), there are high yy Reynold stress areas near the flow device. The All Jets and Axial jets cases have a low stress area above the cavity just above a high stress area at the cavity surface.

Test Article Number 1 Centerline PIV yy Reynolds Stress

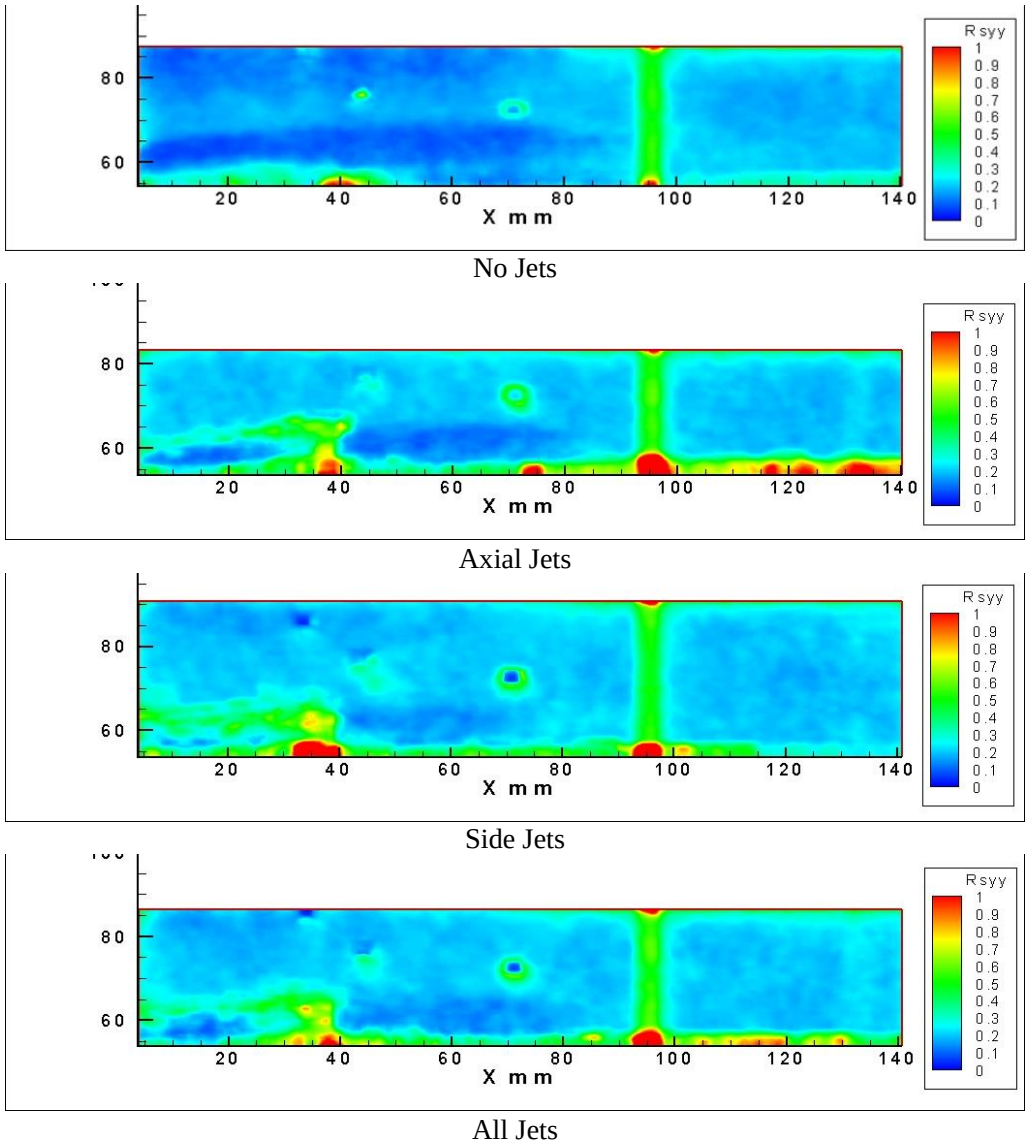

No Jets

Axial Jets

Side Jets

All Jets

Figure 76. Test Article 1 Centerline PIV yy Reynolds Stress. The trailing edge of the flow control device/leading edge of the cavity is at 40mm. The trailing edge of the cavity is not in view.

Test Article Number 1 Off-Centerline PIV yy Reynolds Stress

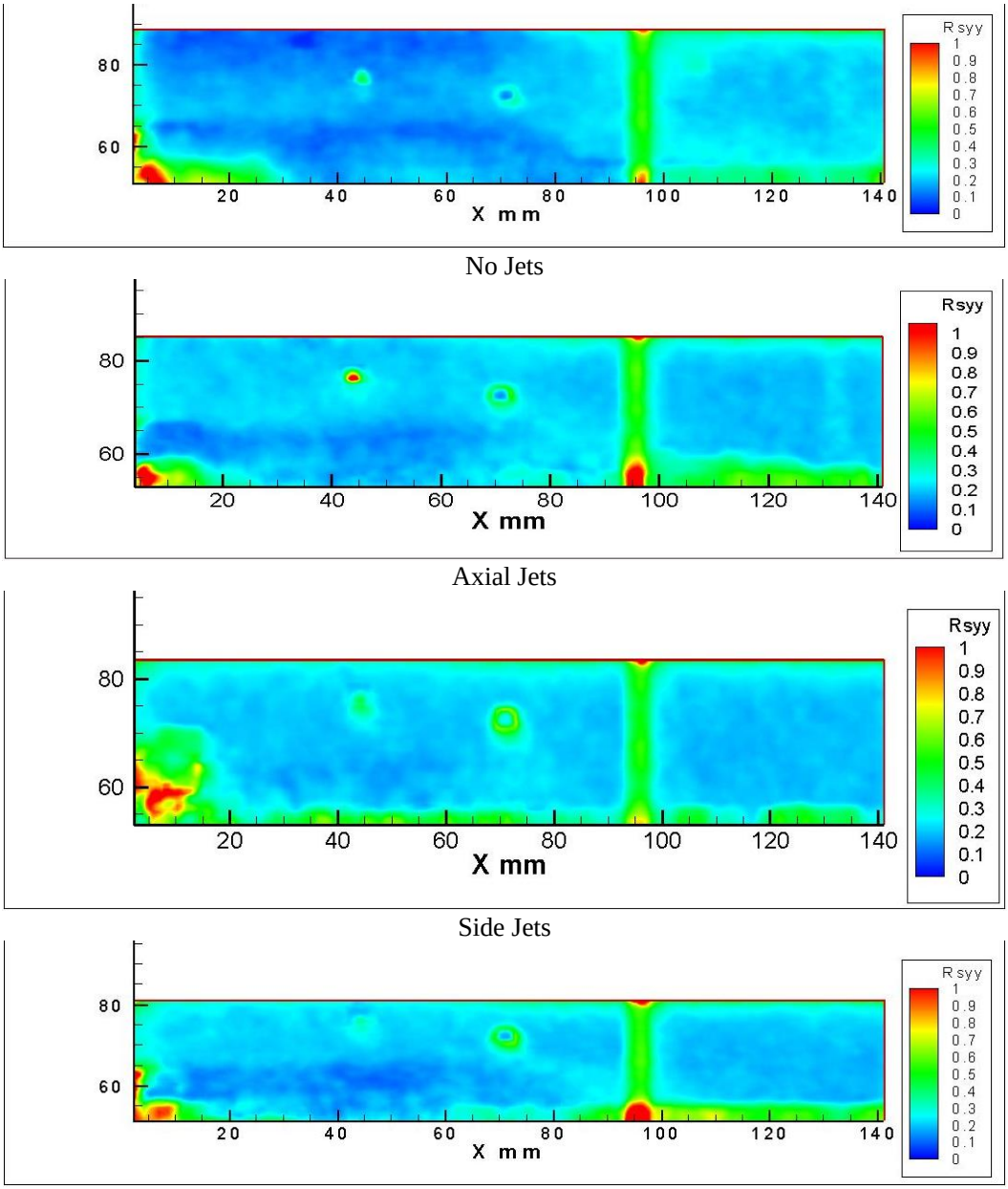

No Jets

Axial Jets

Side Jets

All Jets

Figure 77. Test Article 1 Off-Centerline PIV yy Reynolds Stress. The trailing edge of the flow control device/leading edge of the cavity is at 40mm. The trailing edge of the cavity is not in view.

Test Article Number 2 Centerline PIV yy Reynolds Stress

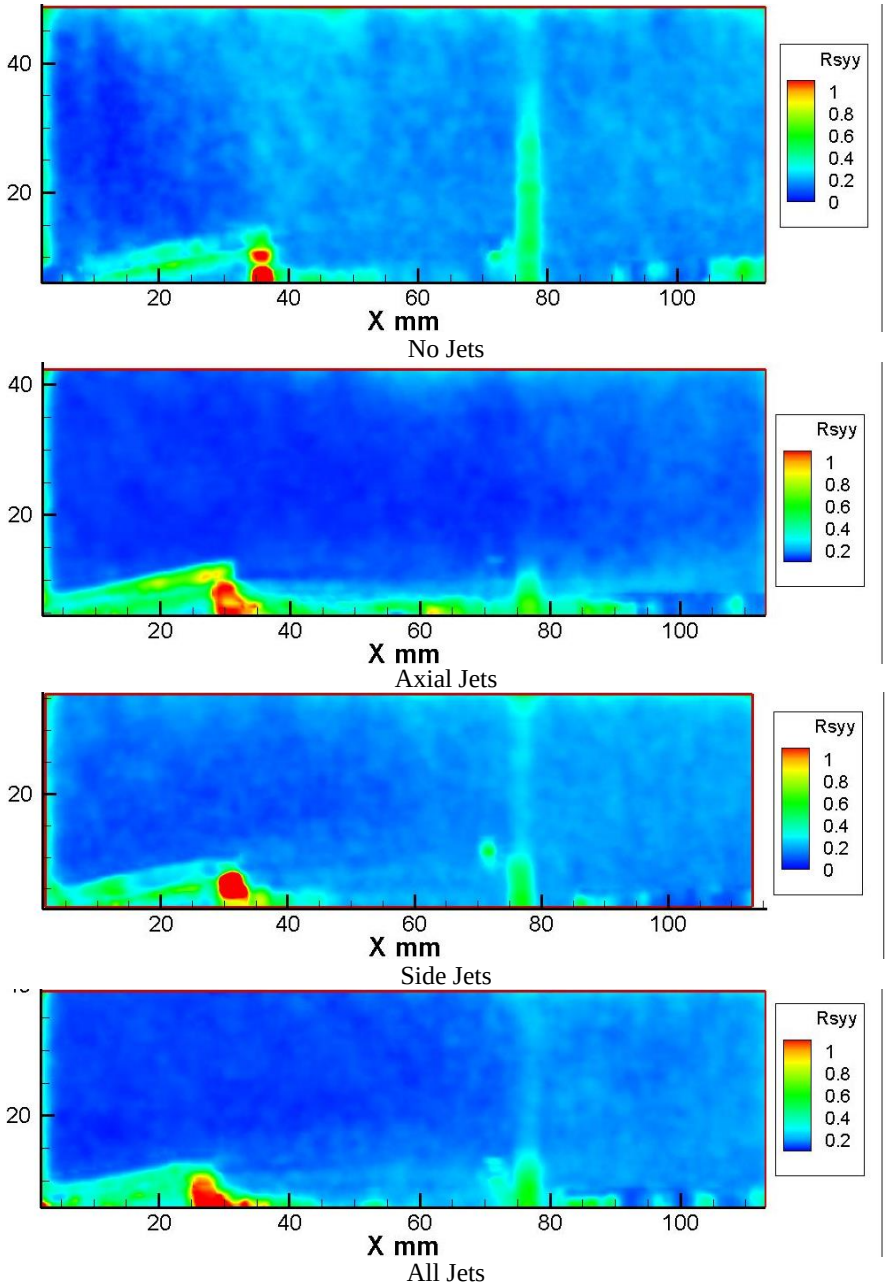

Figure 78. Test Article 2 Centerline PIV yy Reynolds Stress. The trailing edge of the flow control device/leading edge of the cavity is at 40mm. The trailing edge of the cavity is at 95mm.

Test Article Number 2 Off-Centerline PIV yy Reynolds Stress

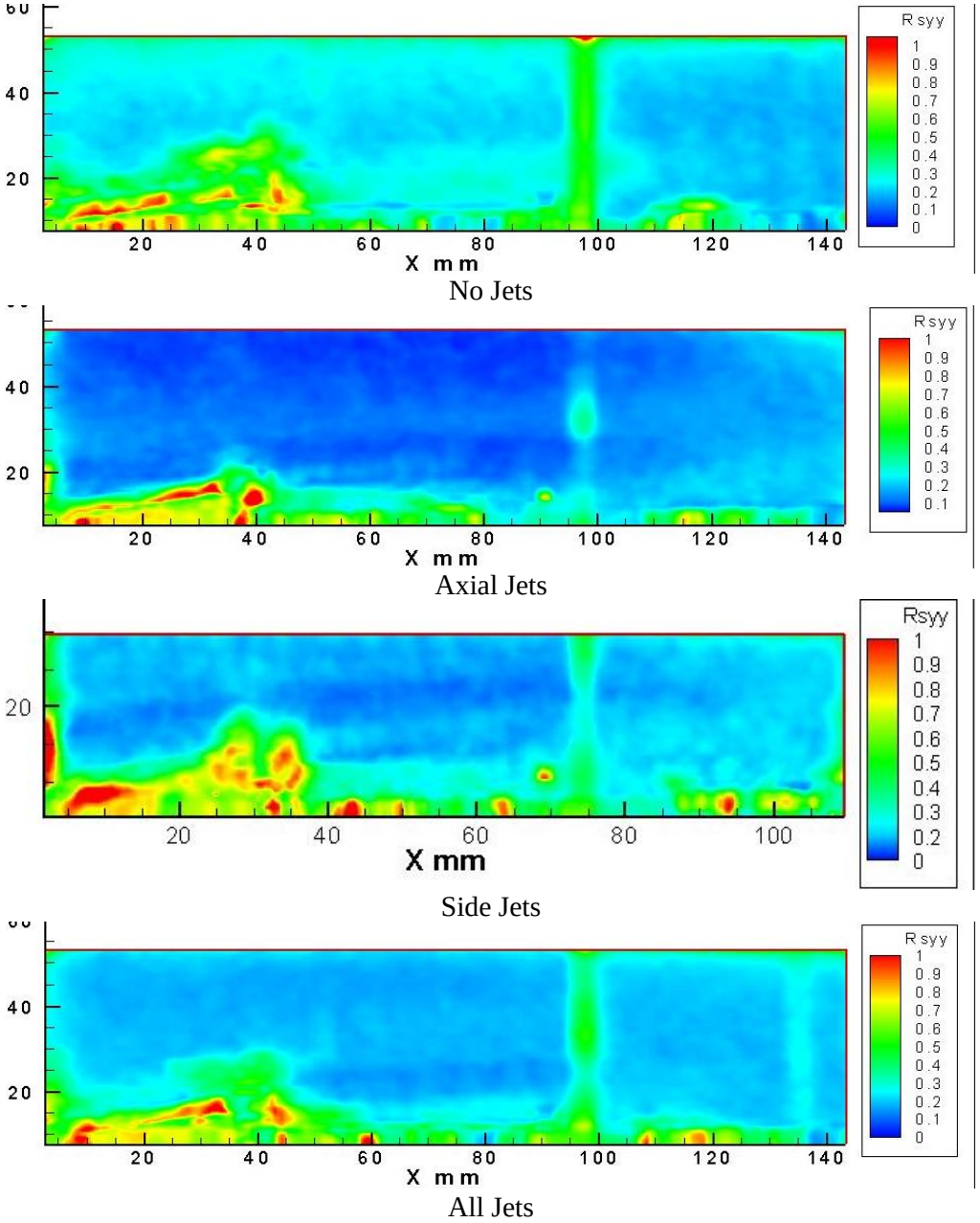

Figure 79. Test Article 2 Off-Centerline PIV yy Reynolds Stress. The trailing edge of the flow control device/leading edge of the cavity is at 40mm. The trailing edge of the cavity is at 95mm.

Acoustic Spectra

An analysis of the acoustic spectra taken from the pressure taps in the floor of the cavities was completed. Figures 80 and 81 illustrate the frequency behavior inside the cavity and dominant acoustic modes. In Figures 80 and 81 Power Spectral Density (PSD) is plotted verses frequency.

An experiment was conducted without tunnel mean flow to determine if the injection scheme would have an effect of the cavity resonant tones. The results of this experiment conducted on test article 2 are depicted in Figure 82. This experiment proved that each jet configuration had a distinct effect on cavity acoustics.

In Figures 80 and 81, the transducer located in the bottom of the cavity near the aft wall of the cavity provides the best representation of the pressure oscillations created by the flow over the cavity. In all cases, injection into the cavity increases the amplitude of the pressure oscillations. Side jet injection is more effective than axial jet injection and all jets flowing is more effective than either single injection mode at increasing high frequency pressure fluctuations in the cavity.

Table 2 compares the calculated Rossiter modes to those measured experimentally. The differences are likely due to the fact that modified Rossiter's equation is best suited for flows up to Mach 1.5, and this testing was conducted at Mach 1.84.

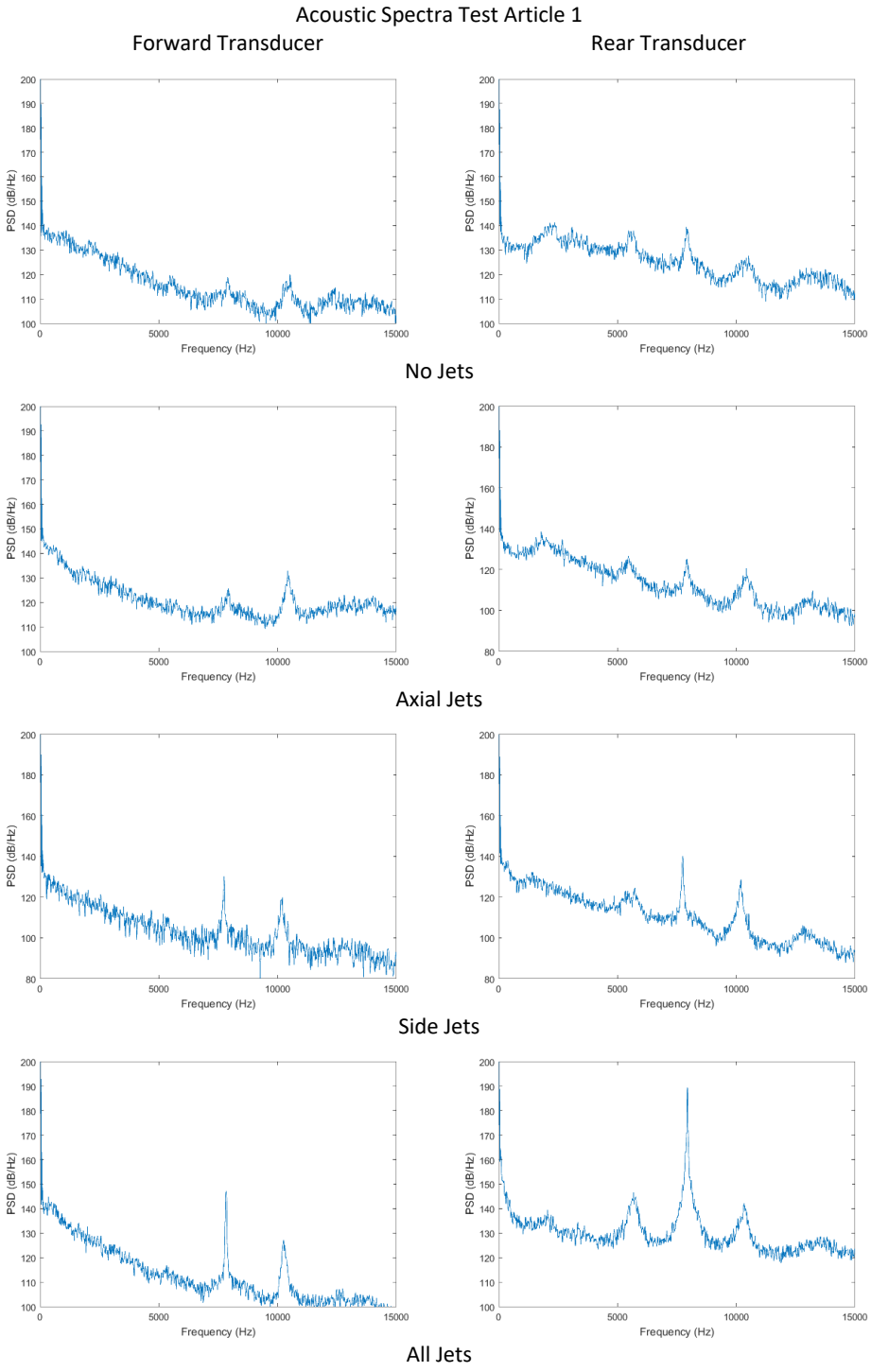

Figure 80. Acoustic Spectra Test Article 1, PSD (dB/Hz) vs Frequency (Hz).

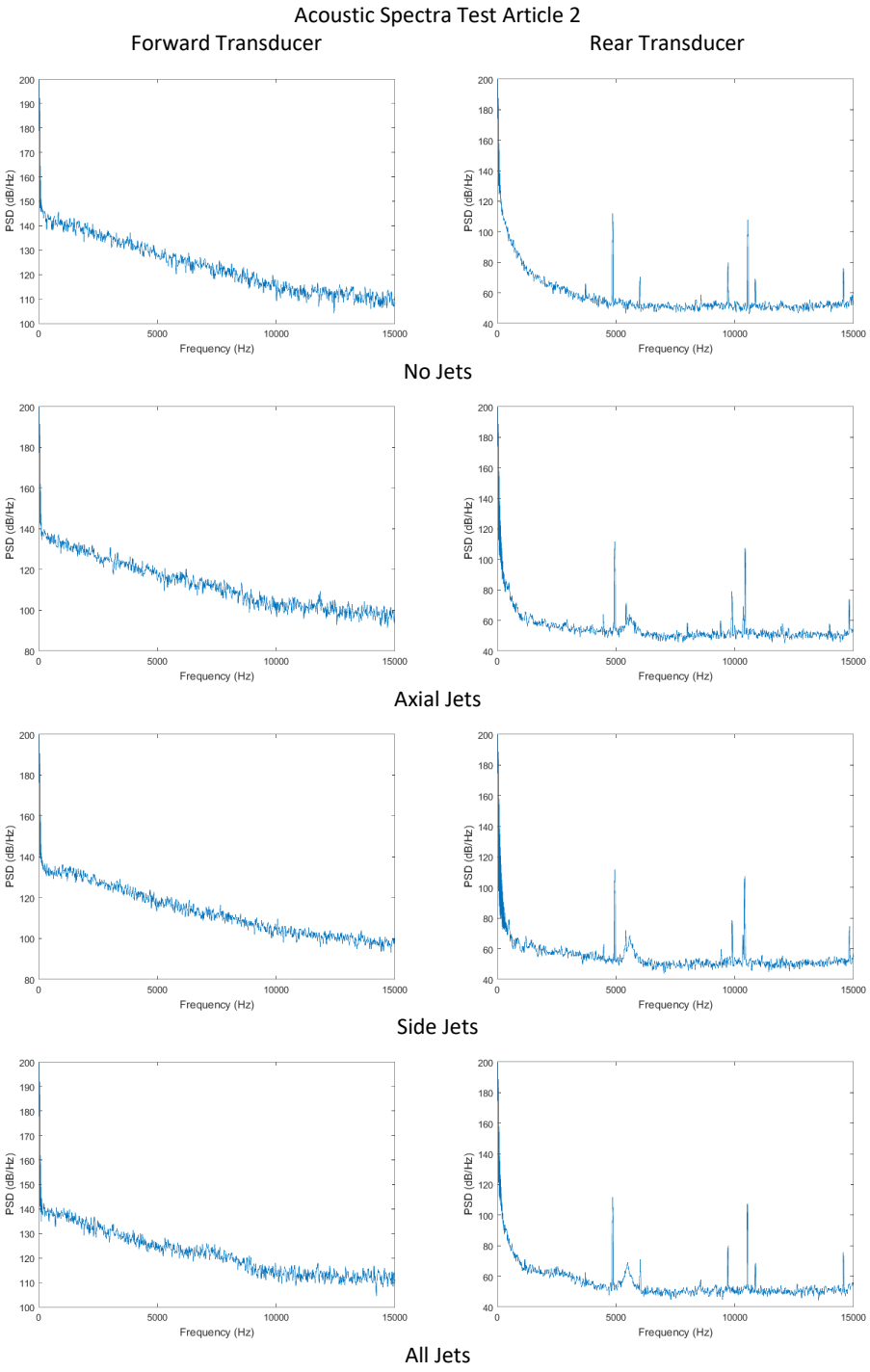

Figure 81. Acoustic Spectra Test Article 2, PSD (dB/Hz) vs Frequency (Hz).

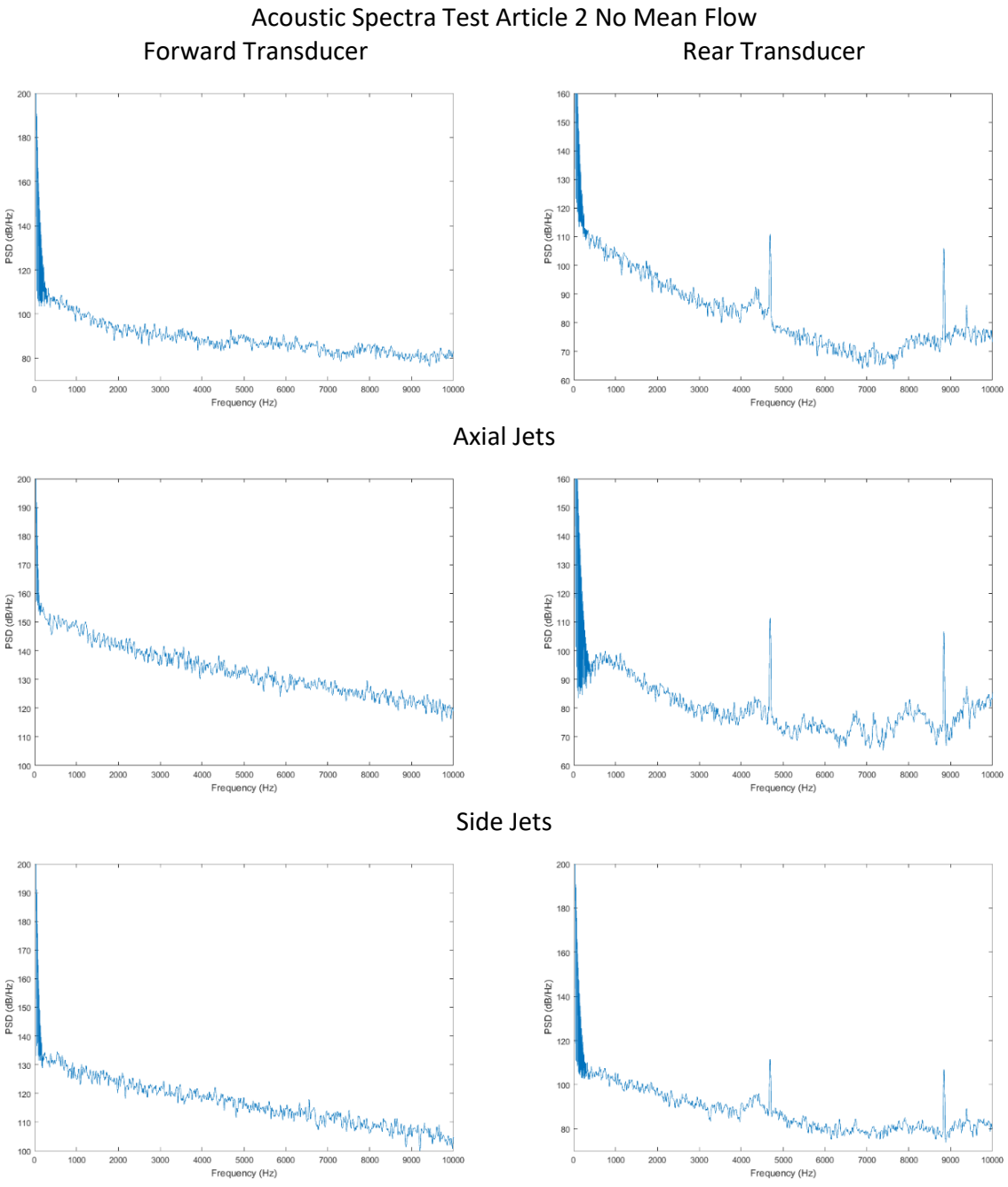

Figure 82. Acoustic Spectra Test Article 2, No Mean Flow, PSD (dB/Hz) vs Frequency (Hz).

Table 2. Oscillatory Modes of Cavity 2

	Mode 1	Mode 2	Mode 3	Mode 4
Rossiter Modes	2147	5010	7873	10735
Experimental	2000	5900	7700~7900	10290

The increases in high frequency fluctuations inside the cavity with injection will provide for increased turbulence and molecular mixing. The mixed flow is transported into the main flow, thereby increasing the fuel penetration into the flow for increased mixing and flame holding.

Summary

Based on contemporary literature, as noted in the cited literature, there are continuing efforts and needs to facilitate efficient fuel injection mixing in supersonic flows to be able to accomplish short practical supersonic combustors. Increased efficient fuel injection penetration into the cross flow has remained the strongest challenge. The present experimental study, compared with limited computational modeling, shows some success resulting from the passive configuration designed, based on fundamental flow physics, for a more efficient mixing methodology for high speed flows. Comparisons of the measured velocity, vorticity, turbulence, and Reynolds stress plots between the injection and non-injection cases illustrate the effectiveness of the mixing enhancement as determined by penetration into the freestream flow. The measurement results, contour

plots, indicate shear layer growth and flow penetration resulting in zones of high mixing over the cavity. This information along with the pressure data, showing increased high frequency oscillations inside the cavity with injection, indicate that these zones have the potential to create a very effective flame holding system.

The upstream boundary layer flow development/guiding passive designs and cavity combinations result in flows with counter rotating vortex pairs that are lofted into the main flow in the downstream. The result would be more effective combustion and hence shorter combustor lengths.

Chapter 5: Conclusions and Recommendations

Innovative passive flow path configurations were devised, integrating active fuel injection flow control methodology, and no moving parts, based on fundamental flow physics. The flow control paths included an upstream flow conditioning component positioned upstream of a cavity to provide enhanced local mixing. The cavities were fitted with flow injection jets (simulated fuel) to accommodate fuel injection as an integral aspect of flow control. The flow control path geometries were innovatively and integrally designed to generate relatively weak shock upstream structures and thus have relatively low shock losses when compared with other flame holding and mixing schemes. The upstream boundary layer flow control devices were designed to generate counter rotating vortices that would be lofted into the flow in the downstream. One was designed to concentrate the cavity vorticity in the center of the cavity and the second was to concentrate the vorticity near the sidewalls. One cavity was designed to maximize the pressure oscillations within the cavity and the second was designed to minimize them. The locations of the fuel injection ports were chosen to maximize interaction with the overall vortex flow structures. Independent CFD predictions, performed by collaborating researchers, were used in support of furthering physical understanding and refining of conceptual and potential designs and to predict the resulting flow fields.

Schlieren flow visualizations and preliminary numerical simulations were performed to identify dominant flow features for comparative analysis, redesign and refining two configurations for further study including detail experimental measurements.

The resulting flow fields were investigated experimentally in the University of Tennessee supersonic wind tunnel at a Mach number of approximately 1.84. Flow visualizations and measurements were conducted with Schlieren imaging, Particle Image Velocimetry and high frequency response dynamic pressure system. Independently performed, CFD simulations were helpful in the interpretation of the 2-D imaging and PIV results for comparative analysis of the various tested geometry and injection configuration measurements.

PIV results, with complementary information from CFD, show that both configurations generated streamwise flow vortices, which interact with the flow in and around the cavity, and are convected vertically away from the tunnel floor. The resulting streamwise swirling flow is coupled with strong cavity flow. Simulated fuel jets interactions with these flow features lead to increased shear layer thickness/vorticity and increased Reynolds stresses in the mixing region. These affect the vorticity spreading and help increased vorticity diffusion (mixing) regions.

The overall flow path configuration enhances the mixing into the freestream, in relatively shorter downstream distance, which could lead to enhanced combustion in short combustors. CFD results compared with experiments confirm that due to strong flow recirculation and swirl inside of the cavity, longer residence times is expected by the injected fuel inside of the cavity. The rotational and recirculating lower-speed flow region in the cavity is ideal for flame holding. Flow measurements, performed at a nominal supersonic free stream Mach number, indicate that this passive geometry design

is a relatively efficient and innovative approach for enhancing fuel injection, flame holding and mixing in a supersonic combustion environment.

Future Research

Due to the variety of issues with the Schlieren and PIV systems, in future experiments it would be beneficial to utilize 3D PIV and a higher quality Schlieren system to fully understand the flow structures.

A larger, more modular set of model/components would enable a parametric approach to understanding the most critical design criteria for sizing flow devices and cavities as well as locating fuel injection ports for optimum performance.

Experiments that include fuel injection with combustion are needed to fully understand the effectiveness of this concept as an operational flame holding and fuel injection technique, in high speed flows.

A more detailed CFD analysis and comparison with these new experiments would provide additional insight to the flow generated by this novel approach that utilizes passive flow control with cavities and flow devices and active flow control through fuel and/or oxidizer injection.

List of References

Abbitt III, J.D., Segal, C., McDaniel, J.C., Krauss, R.H., and Whitehurst, R.B., "Experimental Supersonic Hydrogen Combustion Employing Staged Injection Behind a Rearward-Facing Step," Journal of propulsion and Power, Vol. 9, No. 3, 1993.

Adrian, R.J., "Dynamic Ranges of Velocity and Spatial Resolution of Particle Image Velocimetry," Measurements Science & Technology, Vol. 8, No. 12, 1997, pp. 1393-1398.

Adrian, R.J., "Uses, Analysis and Interpretation of PIV Data," AIAA Paper 1999-3753.

Arai1, T., Sugano, S., Tsukazaki, Y., and Sakaue, S., "Interaction between Supersonic Cavity flow and Streamwise vortices for Mixing Enhancement," AIAA Paper 2015-3613.

Arunajatesan, S., Kamnepalli, C., Sinha, N., Sheehan, M., and Shumway, G., "Suppression of Cavity Loads Using Leading Edge Blowing Concepts," AIAA Paper 2008-44.

Barnes, F.W., Tu, Q., and Segal, C., “Mixing and Mass Exchange for Cavities in Supersonic Flows,” AIAA Paper 2014-2951.

Ben-Yakar, A. and Hanson, R.K., “Experimental Investigation of Flame-Holding Capability of Hydrogen Transverse Jet in Supersonic Cross-Flow”, Twenty-Seventh Symposium (International) on Combustion/The Combustion Institute, 1998, pp. 2173–2180.

Ben-Yakar, A. and Hanson, R.K., “Cavity Flame-Holders for Ignition and Flame Stabilization in Scramjets: An Overview”, Journal of Propulsion and Power, Vol. 17, No. 4, 2001.

Bilanin, A.J., and Covert, E.E., “Estimation of Possible Excitation Frequencies for Shallow Rectangular Cavities.”, AIAA Journal, Vol II, No. 3, March 1973, pp 347-351

Billig, F.S., “Research on Supersonic Combustion,” Journal of Propulsion and Power, Vol. 9, No. 4, 1993, pp. 499–514

Boles, J.A., Hagenmaier, M.A., and Hsu, K., “Hybrid LES/RANS Simulations of Shock-Distorted Injection Plumes,” AIAA Paper 2012-0480.

Boles , J.A., Milligan, R., Hagenmaier, M., Carter, C., and Donbar, J., “Effect of Flow Distortion on Cavity- Assisted Fuel Injection,” AIAA Paper 2012-4000.

Boudaghi, B., Fetterhoff, T.P., Vakili, A., Meganathan, A., “An Investigation of Modified Cavity Flow Generated Supersonic Mixing,” AIAA Paper 2018-1141.

Chang Y.K. and Vakili, A.D, “Dynamics of vortex rings in cross-flow,” Phys. Fluids Vol. 7, 1995, pp.1583-1597.

Curran, E.T., Heiser, W.H., and Pratt, D.T. “Fluid Phenomena in Scramjet Combustion Systems,” Annual Review of Fluid Mechanics Vol 28, 1996, pp 323-360.

Curran, E.T., “Scramjet Engines, The First Forty Years,” Journal of Propulsion and Power, Vol. 17, No. 6, 2001, pp 1138-1148.

Fowler, W.L., “Analysis and Comparison of Effects of an Airfoil or a Rod on Supersonic Cavity Flow”, M.S. Thesis, University of Tennessee, Knoxville, TN, Dec. 2010

Franke, M.E., and Carr, D.L., “Effect of Geometry on Open Cavity Flow-Induced Pressure Oscillations,” AIAA Paper 1975-492, 1975.

Franke, M., and Sarno, R., “Suppression of Flow-Induced Pressure Oscillations in Cavities,” AIAA Paper 1990-4018.

Fry, R. S. “A Century of Ramjet Propulsion Technology Evolution,” Journal of Propulsion and Power Vol. 20, No. 1, 2004: pp27-58.

Fuller, R.P., Wu, P.K., Nejad, A.S., and Schetz, J.A., “Comparison of Physical and Aerodynamic Ramps as Fuel Injectors in Supersonic Flow,” Journal of Propulsion and Power, Vol. 14, No. 2, 1998.

George, B., Ukeiley, L., Cattafesta, L.N., and Taira, K., “Control of Three-Dimensional Cavity Flow Using Leading-Edge Slot Blowing,” AIAA Paper 2015-1059.

Givogue, G.A., Fowler, F.L., and Vakili, A.D., “Control of Cavity Flow by Upstream Mass-Injection,” AIAA Paper 2011-3962.

Grady, N.R., Pitz, R.W., Carter, C.D., Hsu, K.-Y., Godke, C. and Menon, S., "Supersonic Flow over a Ramped-Wall Cavity Flame Holder with an Upstream Strut," Journal of Propulsion and Power Vol. 28, No. 5, 2012.

Gruber, M. R., Nejad, A. S., Chen, T. H., and Dutton, J. C., "Mixing and Penetration Studies of Sonic Jets in a Mach 2 Freestream", Journal of propulsion and Power, Vol. 11, No. 2, 1995, pp. 315-323.

Gruber, M.R., Donbar, J.M., Carter, C.D., and Hsu, K.-Y., "Mixing and Combustion Studies Using Cavity-Based Flameholders in a Supersonic Flow," Journal of Propulsion and Power Vol. 20, No. 5, 2004, pp 769-778.

Gruber, M.R., Hagenmaier, M.A., and Mathur, T., "Simulating Inlet Distortion Effects in a Direct -Connect Scramjet Combustor," AIAA Paper 2006-4680.

Hartfield Jr., R.J., Hollo, S.D., and McDaniel, J.C. "Experimental Investigation of a Supersonic Swept Ramp Injector Using Laser-Induced Iodine Fluorescence," Journal of propulsion and Power, Vol. 10, No. 1, 1994.

Heller, H.H. and Bliss, D.B., “The Physical Mechanism of Flow-Induced Pressure Fluctuations in Cavities and Concepts for their Suppression,” AIAA Paper 1975-491.

Heller, H.H., Holmes, D.G., and Covert, E.E., “Flow-Induced Pressure Oscillations in Shallow Cavities,” Journal of Sound and Vibration, Vol. 18, No. 4, 1971, pp. 545-553.

Houpt, A., Hedlund, H., Leonov, S., Ombrello, T., Carter, C., and Leiweke, R.J., “Cavity-Based Flow Control in a Supersonic Duct Utilizing a Q-DC Plasma Shock Wave Generator,” AIAA Paper 2018-1140

Huber, P. W., Schexnayder, C. J., and McClinton, C. R., “Criteria for Self-Ignition of Supersonic Hydrogen-Air Mixtures,” NASA TP 1457, 1979.

Im, H. G., Chen, J. H., and Law, C. K., “Ignition of Hydrogen-Air Mixing Layer in Turbulent Flows,” Proceedings of the Twenty-Seventh International Symposium on Combustion, Combustion Inst., Pittsburgh, PA, 1998, pp. 1047–1056.

Karamcheti, K., “Acoustic Radiation from Two-Dimensional Rectangular Cutouts in Aerodynamic Surfaces,” NACA TN-3478, 1955.

Kirik, J.W., Goyne, C.P., Peltier, S.J., Carter, C.D., and Hagenmaier, M.A., “Velocimetry Measurements of a Scramjet Cavity Flameholder with Inlet Distortion,” AIAA Paper 2013-3749.

Lamp, A. M., and Chokani, N., “Computation of Cavity Flows with Suppression Using Jet Blowing,” Journal of Aircraft, Vol. 34, No. 4, 1997, pp. 545–551.

Loewen, R.D., “Analysis of Cavity Flow and the Effects of a Rod in Crossflow,” M.Sc. Thesis, University of Tennessee, Knoxville, TN, Dec. 2008.

Meganathan, A.J., “Adaptive Control of Axisymmetric Jets by Cavities,” Ph.D. Dissertation, University of Tennessee, Knoxville, TN, May. 2005.

Milne, G.J., “An Experimental Investigation of Supersonic Cavity Flow Control Using Upstream Cylindrical Rods,” UTSI Report 12/17, University of Tennessee Space Institute, Tullahoma, TN, Aug. 2012.

National Advisory Committee for Aeronautics (NACA) Report 1135, “Equations, Tables, and Charts for compressible flow”, Ames Research Staff, Moffett Field California, 1953.

Nenmeni, V.A., and Wu, K., “Cavity-Induced Mixing Enhancement in Confined Supersonic Flows,” AIAA Paper 2002-1010.

Pandey, K. M., and Sivasakthivel, T., “Recent Advances in Scramjet Fuel Injection – A Review,” International Journal of Chemical Engineering and Applications, Vol. 1, No. 4, December 2010.

Paschal, K., Yao, C. and Ullrich, S., “Spatial Resolution Effects on PIV Measurements in a Turbulent Wake Flow”; AlAA Paper 1994-2297.

Peltier, S. J., Kirik, J. W., Goyne, C. P., and Carter, C. D., “Response of a Ramped Cavity to Shock-Induced Distortions in a Mach 3 Freestream,” AIAA Paper 2013-3699.

Perng, S. W., and Dolling, D. S., “Passive Control of Pressure Oscillations in Hypersonic Cavity Flow,” AIAA Paper 1996-0444,

Plentovich, E.B., Stallings Jr., R.L., and Tracy, M.B., "Experimental Cavity Pressure Measurements at Subsonic and Transonic Speeds," NASA TP-3358, 1993.

Riggins, D.W., McClinton, C. R., Rogers, R. C., and Bittner, R. D., "Investigation of Scramjet Injection Strategies for High Mach Number Flows," Journal of Propulsion and Power, Vol. 11, No. 3, 1995, pp. 409–418.

Riggins, D.W., and Vitt, P. H., "Vortex Generation and Mixing in Three-Dimensional Supersonic Combustors," Journal of Propulsion and Power, Vol. 11, No. 3, 1995, pp. 419–426.

Rockwell, D. and Naudascher, E. "Review – Self-Sustaining Oscillations of Flow Past Cavities," Journal of Fluid Engineering, Vol. 100, No. 2, pp. 152-155, 1978.

Roshko, A., "Some Measurements of Flow in a Rectangular Cutout," NACA TN-3488, 1955.

Rossiter, J.E., "Wind Tunnel Experiments on the Flow over Rectangular Cavities at Subsonic and Transonic Speeds," Aeronautical Research Council R&M No. 3438, 1966.

Sarno, R. L., and Franke, M. E., "Suppression of Flow-Induced Pressure Oscillations in Cavities," Journal of Aircraft, Vol. 31, No. 1, 1994, pp. 90–96.

Sato, N., Imamura, A., Shiba, S., Takahashi, S., Tsue, M., and Kono, M., "Advanced Mixing Control in Supersonic Airstream with a Wall-Mounted Cavity," Journal of Propulsion and Power, Vol. 15, No. 2, 1999, pp. 358–360.

Smith, R.A., Gutmark, E., and Schadow, "Mitigations of Pressure Oscillations Induced by Supersonic Flow Over Slender Cavities," AIAA Paper 1990-4019.

Sung, C. J., Li, J. G., Yu, G., and Law, C. K., "Influence of Chemical Kinetics on the Self-Ignition of a Model Supersonic Hydrogen-Air Combustor," AIAA Journal, Vol. 37, No. 2, 1999, pp. 208–214.

Tam, C., Hsu, K., Hagenmaier, M., and Raffoul, C., "Studies of Inlet Distortion in a Direct-Connect Axisymmetric Scramjet Isolator." AIAA Paper 2012-3224.

Tishkoff, J.M., Drummond, J. P., Edwards, T., and Nejad, A. S., "Future Direction of Supersonic Combustion Research: Air Force/NASA Workshop on Supersonic Combustion," AIAA Paper 1997-1017.

Thiemann, C.L. “Experimental Study of Supersonic Cavity Flow Control with Vertical Rods” M.S. Thesis, University of Tennessee, Knoxville, TN, May 2013.

Tuttle, S.G., Carter, C.D. and Hsu, K.-Y., “Particle Image Velocimetry in an Isothermal and Exothermic High-Speed Cavity,” AIAA Paper 2012-033.

Vakili A.D., J.M. Wu, Y.K. Chang, “Pulsed Jets In Cross--Flow,” International Symposium on Nonsteady Fluid Dynamics, FED-Vol. 92, pp. 465-475, edited by: J. A. Miller and D. P. Telionis, June 1990.

Vakili, A.D., and Gauthier, C., “Control of Cavity Flow by Upstream Mass-Injection,” Journal of Aircraft, Vol. 31, No. 1, 1994, pp. 169-174.

Vakili, A. D., Chang, Y. K., and Wu, J. M., “Supersonic Mixing Enhancement Using Pulsed Transverse Fuel Jets,” Proceedings of the 7th ONR Propulsion Meeting 1994. August 29-31, 1994, Edited by G.D. Roy and P. Givi.

VanLerberghe, W. M., Santiago, J. G., Dutton, J. C., Lucht, R.P. “Mixing of a Sonic Transverse Jet Injected into a Supersonic Flow”, AIAA Journal, 2000, Vol. 38, pp 470-479.

Westerweel, J. “Efficient Detection of Spurious Vectors in Particle Image Velocimetry Data,” Experiments in Fluids, Vol. 16, 1994, pp. 236-247.

Westerweel, J.; Dabiri, D.; Gharib, M., “The Effect of a Discrete Window Offset on the Accuracy of Cross-Correlation Analysis of Digital PIV Recordings,” Experiments in Fluids, Vol. 23, 1997, pp. 20-28.

Westerweel, J., “Fundamentals of Digital Particle Image Velocimetry,” Measurement Science and Technology, 1997, pp 1379-1392

Williams, N., Dissertation, University of Tennessee, “Numerical Investigations of a High Frequency Pulsed Gaseous Fuel Jet Injection into a Supersonic Crossflow”, 2016

Wolfe, R. C., Master’s Thesis, University of Tennessee, “An Investigation of the Effects of Upstream Mass Injection on Cavity Oscillations,” 1995

Yu, K. H., and Schadow, K. C., “Cavity-Actuated Supersonic Mixing and Combustion Control,” Combustion and Flame, Vol. 99, 1994, pp. 295– 301.

Zhang, X., Rona, A., and Edwards, J. A., “The Effect of Trailing Edge Geometry on Cavity Flow Oscillation Driven by a Supersonic Sear Layer,” Aeronautical Journal, March 1998, pp. 129–136.

Vita

Thomas “Tom” Paul Fetterhoff was born in Harrisburg Pennsylvania on 10 July 1962. He graduated from the Pennsylvania State University with a Bachelor of Science Degree in Aerospace Engineering in May of 1986. In May of 1998 Tom earned a Master of Science Degree in Mechanical Engineering. In May of 2017 Tom graduated from Air University with a Masters of Strategic Studies.

Tom has more than thirty years of acquisition experience in the Research, Development, Test, and Evaluation (RDT&E) of Department of Defense (DoD) and commercial aerospace systems. He possesses a breadth of experience as both a hands-on practitioner and program manager at all levels of the development process. He has been a project engineer, test engineer, plant operations engineer, flight test engineer, test capability development engineer, test technology developer, and test data analyst as well as branch chief, division chief, and technical director at the test branch, test division, and test wing level.